NTNU
Norwegian University of
Science and Technology

# Geometric and Qualimetric Modelling of the Hessjø deposit

Silje Marie Nørsett

Geotechnology
Submission date: July 2016
Supervisor: Steinar Løve Ellefmo, IGB

Norwegian University of Science and Technology
Department of Geology and Mineral Resources Engineering

Norges teknisk-
naturvitenskapelige universitet
NTNU

Fakultet for ingeniørvitenskap
og teknologi
Studieprogram Tekniske geofag

*MASTEROPPGAVEN*

| | |
|---|---|
| *Kandidatens navn* | Silje Nørsett |
| *Oppgavens tittel* | Geometrisk og kvalimetrisk modellering av Hessjøforekomsten |
| *English title* | Geometric and Qualimetric Modelling of the Hessjø deposit |
| *Utfyllende tekst* | Using the Leapfrog Geo software the student is expected to develop a geometric and a qualimetric 3D-model of the Hessjø deposit. The majority of available data associated with the Hessjø deposit were collected during the 1970's, and were further reviewed as a part of the student's project work. The available data are, however, scarce and partially incomplete, but will non-the-less be digitized and run through an evaluation of how to best implement the data into the modelling.<br><br>The master thesis shall account for and compare relevant methodologies for qualimetric modelling (geostatistics and implicit modelling).<br><br>Based on requirements regarding borehole spacing as they are presented in the literature, a qualitative resource classification shall be performed.<br><br>The deposit is deformed and as a part of the master thesis the geological history of the deposit (with particular regard to the ore-forming processes) shall be described and analyzed using relevant literature together with the geometric and qualimetric models. |
| *Studieretning* | Mineralproduksjon og teknisk ressursgeologi |
| *Hovedprofil* | Teknisk ressursgeologi |
| *Tidsrom* | 17.09.2015 til 01.07.2016 |

Steinar L. Ellefmo

Steinar L. Ellefmo, førsteamanuensis og hovedveileder

Skjemaet tas inn som side 1 i masteroppgaven

NTNU, 28/6-16

# Abstract

The main goal of this master thesis is to develop geometric and qualimetric 3D-models the Hessjø deposit, located in Holtålen, Norway, using data acquired in the 1970s. This includes a thorough evaluation of the data in terms of quality and applicability to 3D-modelling, a comparison between geostatistics and implicit modelling, in addition to performing a qualitative resource classification of the deposit with regards to drillhole spacing and data quality. The depositional and deformational history of the Hessjø deposit has also been reviewed. The modelling and data evaluation will focus on lens A of the deposit.

The 3D implicit modelling software Leapfrog Geo has been used to generate the geometric and qualimetric models of the deposit. When the geostatistical method of kriging is implemented as an interpolation, it is known as dual kriging, which is comparable to the Fast Radial Basis Functions used in implicit modelling.

Examples of drillhole spacing from feasibility studies that are JORC compliant are presented, together with the primary JORC Code principals.

By reviewing relevant literature, the Hessjø deposit is inferred to be a Cu-Zn-type VMS deposit, of a likely bimodal-mafic subclassification, and shows signs of characteristic zonation patterns inherent to VMS deposits. It is located within the Fundsjø Group, which has been proposed to have been deposited in an immature arc/marginal basin setting. Lens A in the Hessjø deposit has been subjected to deformation and upper greenschist-facies metamorphism.

The data inherent to the Hessjø deposit is partially incomplete, and of questionable quality. Through the evaluation of the data, necessary modifications and assumptions were made, prior to the generation of the geometric model of lens A together with the surrounding geology.

The results from the qualimetric modelling of lens A showed that, when applying various cut-off values, the output volumes of especially zinc, were significantly lowered. The block modelling provided mean grade estimates of copper and zinc at values of 0.92% and 1.19%, respectively, which is significantly lower than the historical estimates.

As the data from the Hessjø deposit is of questionable quality, it is unlikely that it could be classified as anything higher than an Exploration Target or Inferred Resource in terms of the JORC standards and classification scheme.

# Sammendrag

Hovedformålet med denne masteroppgaven er å generere geometriske og kvalimetriske 3D-modeller av Hessjøforekomsten, som ligger i Holtålen kommune, ved å bruke data som ble samlet inn på 1970-tallet. Dette inkluderer en grundig evaluering av dataene med hensyn på kvalitet og anvendbarhet i 3D-modellering, en sammenligning av geostatistiske metoder og implisitt modellering, og en utførelse av kvalitativ ressursklassifisering av forekomsten ut i fra borehullsavstand og datakvalitet. Avsetnings- og deformasjonshistorikken til Hessjøforekomsten har også blitt undersøkt. Hovedfokuset i denne oppgaven vil ligge på linse A i forekomsten.

Implisitt 3D-modelleringsprogrammet Leapfrog Geo has blitt brukt for å generere de geometriske og kvalimetriske modellene av forekomsten. Når kriging, en geostatistisk metode, blir anvendt som en interpolering, kalles det dual kriging. Dual kriging er sammenlignbart med Fast Radial Basis Functions som blir anvendt i implisitt modellering.

Eksempler på borehullsavstand fra forekomster som har blitt evaluert på grunnlag av JORC-koden, er presentert.

Gjennom litteraturstudier, Hessjøforekomsten er antatt å være en Cu-Zn-type VMS forekomst, med en bimodal-mafisk subklassifisering, og viser tegn til karakteristiske soneringsmønstre typisk for VMS forekomster. Forekomsten er lokalisert innunder Fundsjøgruppen, som er antatt å ha blitt dannet i en vulkansk øybue/marginalbasseng setting. Linse A i Hessjøforekomsten har blitt utsatt for deformasjon og øvre-grønnskifer-facies metamorfose.

Dataene tilhørende Hessjøforekomsten er delvis ufullstendige, og av en tvilsom kvalitet. Gjennom evalueringen av datene ble nødvendige antagelser og modifiseringer gjort, før selve genereringen av den geologiske modelleringen ble gjennomført.

Resultatene fra den kvalimetriske modelleringen av linse A viste at, ved å tilføre cut-off verdier, output-volumet av spesielt sink, ble betraktelig minsket. Gjennom blokkmodellering ble gjennomsnittsgehalter for sink (1,19%) og kobber (0,92%) estimert. Disse viste seg å være betraktelig mindre enn de historiske estimatene.

Fordi dataene fra Hessjøforekomsten er av en tvilsom kvalitet, er det usannsynlig at forekomsten kan klassifiseres som noe høyere enn Prospekteringsmål eller Antatt Ressurs ut i fra JORC klassifiseringssystemet.

*"Remember that all models are wrong; the practical question is how wrong do they have to be to not be useful."*

*George E. P. Box (1987, p.74)*

# Table of contents

# List of figures

# List of tables

# Abbreviations

| | |
|---|---|
| **CP** | Competent Person, as defined by JORC (2012) |
| **cpy** | Chalcopyrite |
| **HFS (HFSE)** | High Field Strength Elements |
| **IAT** | Island Arc Tholeiite |
| **IDW** | Inverse Distance Weighting |
| **LOD** | Limit of Detection |
| **LOQ** | Limit of Quantification |
| **LREE** | Light Rare Earth Elements |
| **MORB** | Mid-Ocean Ridge Basalt |
| **mt** | Magnetite |
| **ORS** | Old Red Sandstone |
| **po** | Pyrrhotite |
| **py** | Pyrite |
| **RBF** | Radial Basis Functions |
| **sl** | Sphalerite |
| **TNC** | Trondheim Nappe Complex |
| **VMS** | Volcanogenic massive sulphide |

# 1 Introduction

## 1.1 Objectives

The objective of this master thesis is as given by the thesis statement:

*Using the Leapfrog Geo software the student is expected to develop a geometric and a qualimetric 3D-model of the Hessjø deposit. The majority of available data associated with the Hessjø deposit were collected during the 1970's, and were further reviewed as a part of the student's project work. The available data are, however, scarce and partially incomplete, but will non-the-less be digitised and run through an evaluation of how to best implement the data into the modelling.*

*The master thesis shall account for and compare relevant methodologies for qualimetric modelling (geostatistics and implicit modelling).*

*Based on requirements regarding borehole spacing as they are presented in the literature, a qualitative resource classification shall be performed.*

*The deposit is deformed and as a part of the master thesis the geological history of the deposit (with particular regard to the ore-forming processes) shall be described and analysed using relevant literature together with the geometric and qualimetric models.*

## 1.2 Assumptions, limitations and delimitations

The objectives of the thesis statement are perceived to be clear, and no assumptions regarding the statement are made.

This work is limited to 30 ECTS, with no additional resources.

The data available for the Hessjø deposit is incomplete. Polished sections and a report regarding downhole survey measurements which is known to exist, have not been found, despite extensive searching within the time frame available. In addition, the validity of much of the data is questionable due to unknown methods of data acquisition.

Prior to this master thesis, a project thesis was written, which included a review of data required in 3D-modelling and resource classification, in addition to an initial evaluation of the data from the Hessjø deposit with respect to the JORC code. Anything previously reviewed in the project thesis will here only be presented shortly, with further referral to the project thesis (Nørsett, 2015), or other relevant literature. This includes the limitations related to the Leapfrog Geo software.

The Hessjø deposit consists of several mineralised lenses. However, for the purpose of this thesis, only lens A will be modelled, as it is the largest and richest of these lenses. All data described in this thesis is thus inherent to lens A, which includes any reference to *the mineralisation*, *the Hessjø deposit,* or *the lens*, unless stated otherwise. Evaluations of lens B-E are not within the

scope of this thesis, however, where it is found to be of purpose, data and descriptions of these other mineralised lenses are presented.

## 1.3 Thesis structure

Chapter 2.1: *The Hessjø deposit and Fundsjø Group* begins by giving an overview of the location, history and investigations conducted on the Hessjø deposit, before continuing on to describe the general geological characteristics of the deposit. The deposit is further set into a regional context, and a review of the geological and metallogenic history of the Fundsjø Group, in which the Hessjø deposit is situated, is presented.

Chapter 2.2: *Geostatistics and modelling* provides an insight into the general features of geostatistics and the processes that are inherent to Leapfrog Geo. This also includes a comparison between geostatistics and implicit modelling.

Chapter 2.3: *Resource classification* concludes the Background and theory chapter of the thesis by shortly presenting the JORC Code as well as providing examples of drillhole spacing used in JORC compliant copper deposits.

Chapter 3.1: *Evaluation and description of data* provides detailed insight into the data available for the Hessjø deposit, and continues on to evaluating the various data types in such a way that geometric and qualimetric modelling is made possible.

In chapter 3.2: *Geometric modelling,* the process of modelling lens A and its host rock geology is described.

Chapter 3.3: *Qualimetric modelling* gives an overview of the input parameters and Leapfrog Geo functions used in modelling of the drillhole assay data for zinc and copper.

In Chapter 4: *Results*, the visual and statistical results of the geometric and qualimetric modelling, along with a description of the drillhole spacing used in the Hessjø data, are presented.

In Chapter 5: *Discussion,* the results from the geometric and qualimetric modelling are discussed, along with a suggestion for the possible resource classification of lens A.

Conclusions and suggestions for further work are presented in chapter 6, while a complete bibliography is provided for in chapter 7.

# 2 Background and Theory

## 2.1 The Hessjø deposit and Fundsjø Group

### 2.1.1 The Hessjø deposit

The following subchapters present the main characteristics of the Hessjø deposit before continuing on to a more in depth discussion regarding the regional geological setting of the deposit in chapter 2.1.2 and onwards.

#### 2.1.1.1 Location and historical setting

The Hessjø deposit (written as *Hersjø* in older reports) is located approximately 17 km north-west of Røros in Holtålen municipality, Norway (Figure 1). The deposit is outcropping at about 1020 m.a.s.l. on the west side of the Kjurrudalen valley (Bjerkgård, 2007).

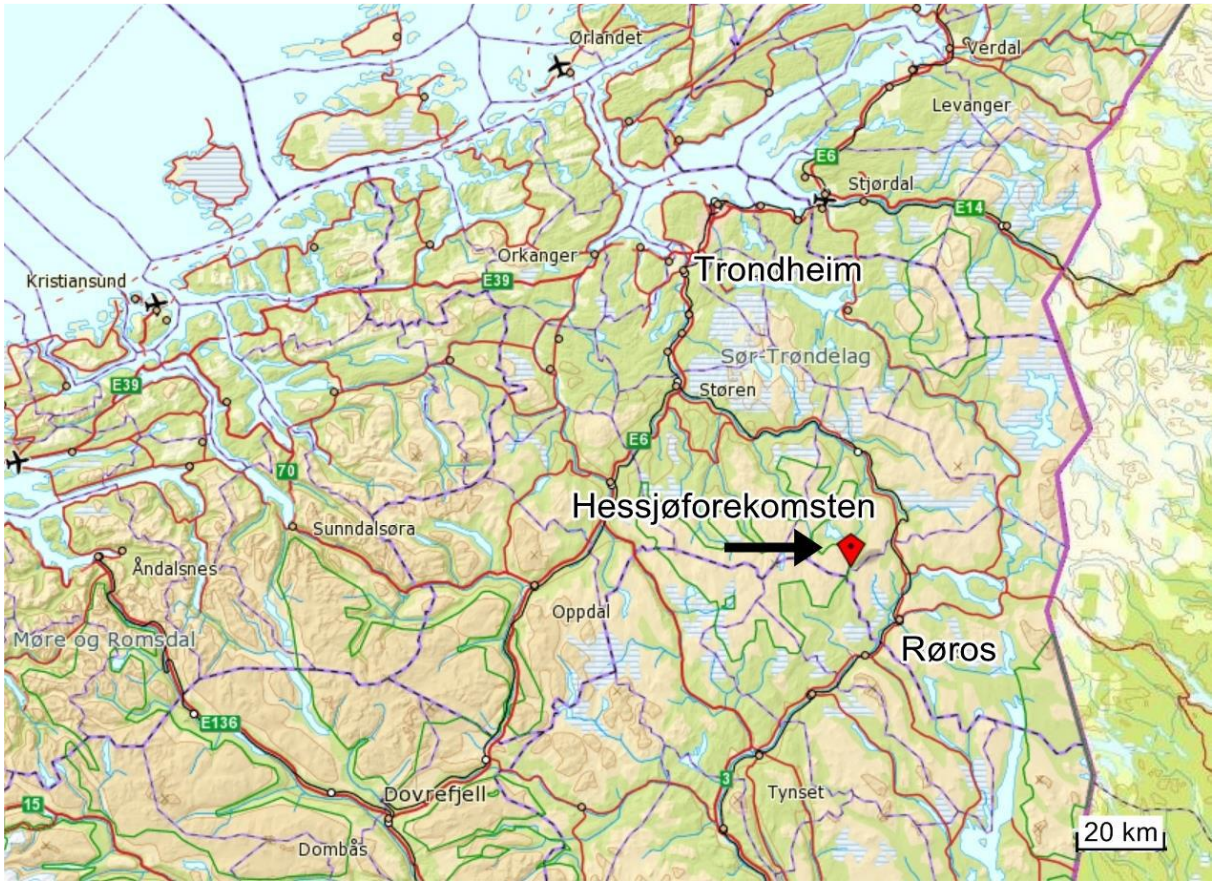


Figure 1: Location of the Hessjø deposit (Hessjøforekomsten). Map modified from (Kartverket, n.d.)

In 1948 and 1949, *Geofysisk Malmleting* conducted geophysical investigations using TURAM, an electromagnetic method (Singsaas & Brækken, 1949), revealing five separate sulfide lenses, noted lens A-E, where lens A, D, and F were previously unknown (NGU, 2007). The largest of these lenses, lens A, is the focal point of this thesis, and will be discussed further in the following chapters.

During the second half of the 17th century, lens B (often referred to as *Gammelgruva* 'the old mine') was subjected to mine workings, whereupon 4000 tons of copper was produced. The E-lens (often referred to as *Nygruva* 'the new mine') was mined around the year 1830, producing 70 tons of copper. In addition, sporadic extraction of pyrite from the B-lens took place towards the end of the 19th century (Bjerkgård, 2007).

Further investigations were initiated in 1969, and conducted throughout the 1970s by the mining companies A/S Røros Kobberverk, A/S Sydvaranger, and Killingdal Grubeselskap. Additionally, a master thesis concerning the deposit and surrounding geology was published in 1975 by Stig Bakke, then student at NTH (former Norwegian Institute of Technology). The most recent review of the data concerning the Hessjø deposit was published by Terje Bjerkgård in 2007.

Currently, Holtålen municipality, Norway, owns the rights to prospect and develop the Hessjø deposits until year 2022 (Hessjøgruva AS, 2013).

#### 2.1.1.1.1 Geophysical investigations

In addition to the TURAM measurements in 1948-49, several geophysical campaigns covering the Hessjø area were completed through the 1960s and 1970s, providing valuable information regarding the lateral and depth-wise extents of the mineralisations (Figure 2).

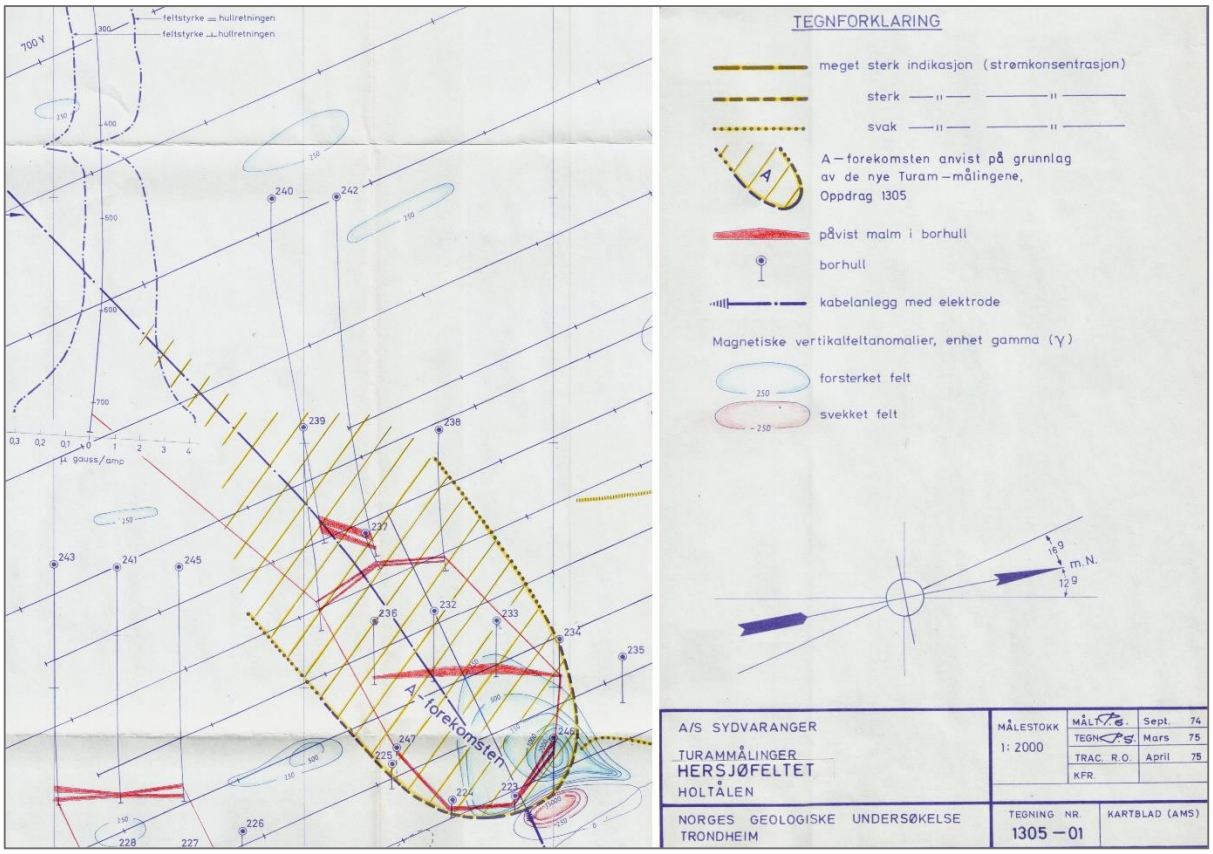


Figure 2: Extract of geophysical map given by Singsaas (1975). Yellow markings indicate the extent of lens A based on geophysical investigations, while red indicates where drillholes have intersected the mineralisation.

Further TURAM measurements were carried out in 1974-75, and the results gave the horizontal restrictions of lens A in the north and south direction to a depth of about 300 m, showing that the upper part of lens A has a width of approximately 200 m. These measurements also gave the direction of the main axis, and showed an indication that the lens exhibits a kink or fold c. 300 m from the outcrop (see Figure 3). Below this kink the lens turns slightly towards south and increases in dip (Singsaas, 1975; 1976). Using TURAM and VLF (Very Low Frequency Electromagnetics) it was not possible to delimit the mineralisation at depth due to shallow graphite horizons that overlie the deeper parts of the lens in the west (Singsaas, 1976; Logn, 1974, as cited in Bjerkgård, 2007).

Measurements using the mise-à-la-masse and SP (Self Potential) methods were carried out in nearly all drillholes in 1976 and 1977. These proved the continuity of the mineralisation and that there is no connection between the various mineralised lenses (NGU, 1980).

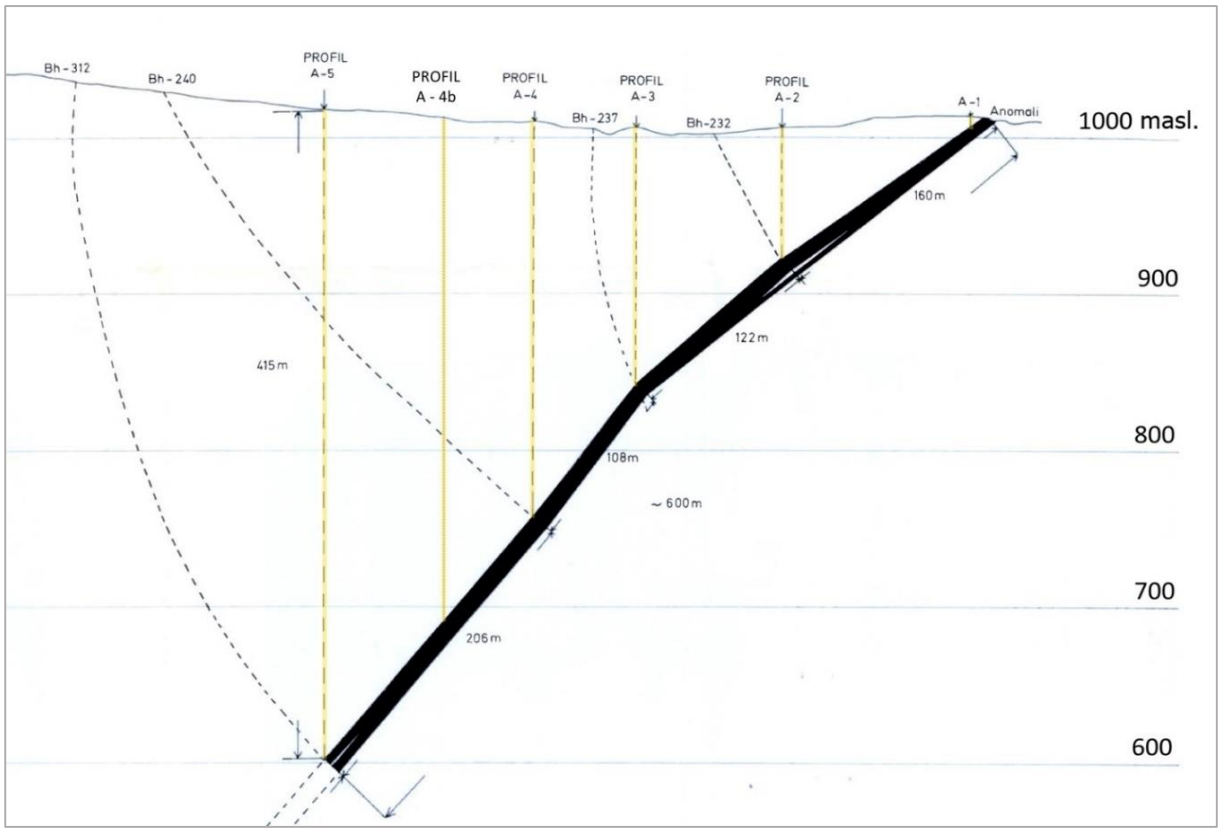


Figure 3: Simplified profile of lens A. 'Profil A-x' refers to the main cross-sections on which drilling was conducted. Image adapted from Gvein (1976).

#### 2.1.1.1.2 Drillhole campaigns

A total of 67 drillholes have been drilled in the Hessjø deposit area during the period 1970-1977, and 26 of these intersect lens A (see Table 1). Most of the cores still exist at the Norwegian Geological Society's storage facility at Løkken.

The deepest drillholes, 244 (Figure 4), 317 and 318, cut the mineralisation at a depths of 700-800 m (Bjerkgård, 2007). Samples from 317 and 318 only show a weak mineralisation, but according to Vokes (1983), this is due to the drillholes intersecting the outer edges of the lens. Lens A is not restricted by drilling, and has potential for additional ore at deeper levels (Bjerkgård, 2007), a conclusion also reached by Gvein (1976) as other sulfide deposits of similar shape in the Fundsjø Group and Røros area extends over several kilometres.

He further theorises that based on experience from other sulfide deposits in Fundsjø Group, it is likely that the mineralisation continues substantially further down.

A further review of the drillhole data is presented in chapter 3.1 and subsequent subchapters.

Table 1: Drillholes drilled on lens A, by year. Drillhole 238 is mentioned twice as it was begun in 1970 and finished in 1971. No drilling took place on lens A in 1974, but drilling campaigns on the other mineralised lenses did. Complete overview over drillholes on all lenses was presented in Nørsett (2015). Table based on data from Gvein (1976) and Rui (1990).

| Year | 1970 | 1971 | 1974 | 1975 | 1976/1977 |
|---|---|---|---|---|---|
| Drillhole number | 223 | 238 | | 312 | 317 |
| | 224 | 239 | | 313 | 318 |
| | 225 | 240 | | 314 | 319 |
| | 232 | 242 | | 315 | 320 |
| | 233 | 244 | | | 321 |
| | 234 | 246 | | | 322 |
| | 235 | 247 | | | |
| | 236 | | | | |
| | 237 | | | | |
| | 238 | | | | |

Figure 4: Drilling of the 745 m long drillhole 244. Picture taken in late summer of 1971 by Øystein Pettersen (Pettersen, 2011).

#### 2.1.1.1.3 Historical estimates

The grades and tonnages of the Hessjø deposit have been estimated and evaluated numerous times since the initial investigations were conducted. Different methods and assumptions have been applied, thus giving variations within the resulting estimates. In addition to the estimates given in Table 2, Vokes (1983), and others mentioned by Tessem (1985), have performed estimates where profiles A1 and A2 in Figure 3 have been excluded from the calculations. Their focus was solely on the copper rich parts of the lens, and thus disregarded the upper, more zinc-rich part.

Table 2: Historical estimates of the grades and tonnages of lens A. *Axial length* refers to the portion of the lens body, starting at ground level, used in the estimations.

| | % Cu | % Zn | Tonnage [Mt] | Axial length [m] |
|---|---|---|---|---|
| Bjerkgård (2007) | 1.40 | 1.70 | 2.99 | 1060 |
| Gvein (1976) | 1.28 | 1.91 | 2.4 | 746 |
| Bakke (1975) | 1.96 | 1.60 | 3.4 | 669 |

#### 2.1.1.2 Geology and mineralogy

The geology immediately surrounding and incorporating the Hessjø deposit is presented here as a preview for contextual purposes, before continuing on to the regional geological setting and possible geological history in chapter 2.1.2.

The majority of the geological information regarding the Hessjø sulfide deposit originates from thesis work published in 1975 by Stig Bakke, at the former NTH (The Norwegian Institute of Technology). This includes the geological map and geological profile given in Figure 6 and Figure 7. According to Gvein (1976), who was Bakke's supervisor, it should be emphasised that Bakke's maps are only an interpretation based on sparsely exposed geology and core material. He finds the interpretation to be somewhat simplified and questions the exaggeration of the porphyry zones (*porfyrisk metagabbro* and *porfyr* on map in Figure 6). Bakke (1975) also notes that the extent of the quartz keratophyres on the geological map in Figure 6 is exaggerated. The geology surrounding the Hessjø deposit as given by national bedrock maps is shown in Figure 5.

The Hessjø mineralisations are generally lens or ruler shaped, and lie conformably in massive greenstone, which consists mainly of dark green hornblende and feldspar with subordinate chlorite, epidote and calcite. Originally, the greenstone was probably basaltic meta-volcanites, but has been altered to dark chlorite schist or greenschist, commonly containing smaller lenses and layers enriched quartz ± feldspar, around the mineralisations. Subordinate lithologies in the proximal area include felsic volcanic rock (quartz keratophyre), gabbro, and pillow basalt (Bjerkgård, 2012; Bakke, 1975). In between the mineralised lenses (i.e. lens A-E), thin stripes or lenses of metagabbro and porphyritic layers occur (Bakke, 1975). Generally, the rocks surrounding the sulfide mineralisations have north-south strike, and a dip varying from $40^0$ to $65^0$, the main dip angle being $50^0$ towards west (Gvein, 1976).

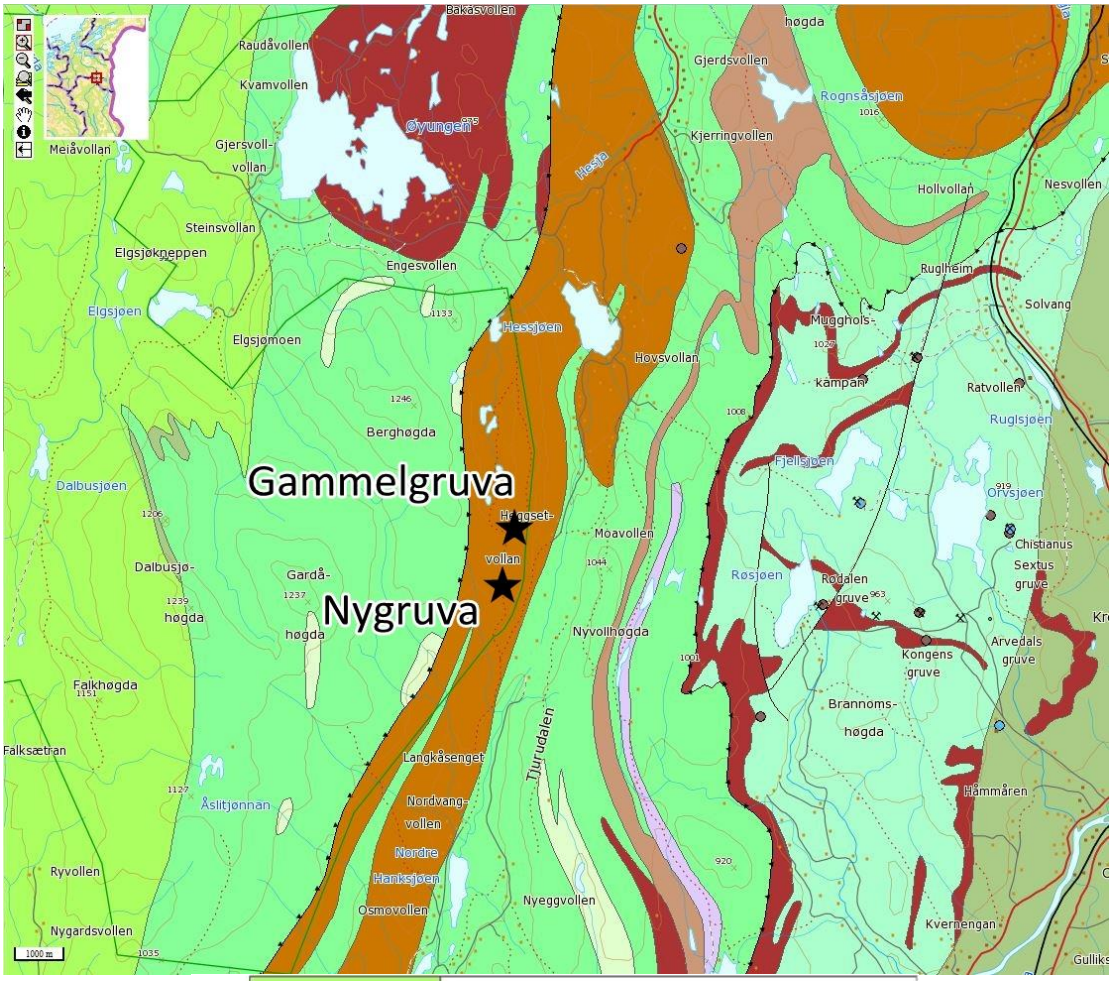


Figure 5: Regional geology surrounding the Hessjø deposit. Map from Norwegian Geological Society's online ore database (NGU, 2011), lithological names from Norwegian Geological Society's national bedrock database (NGU, 2009).

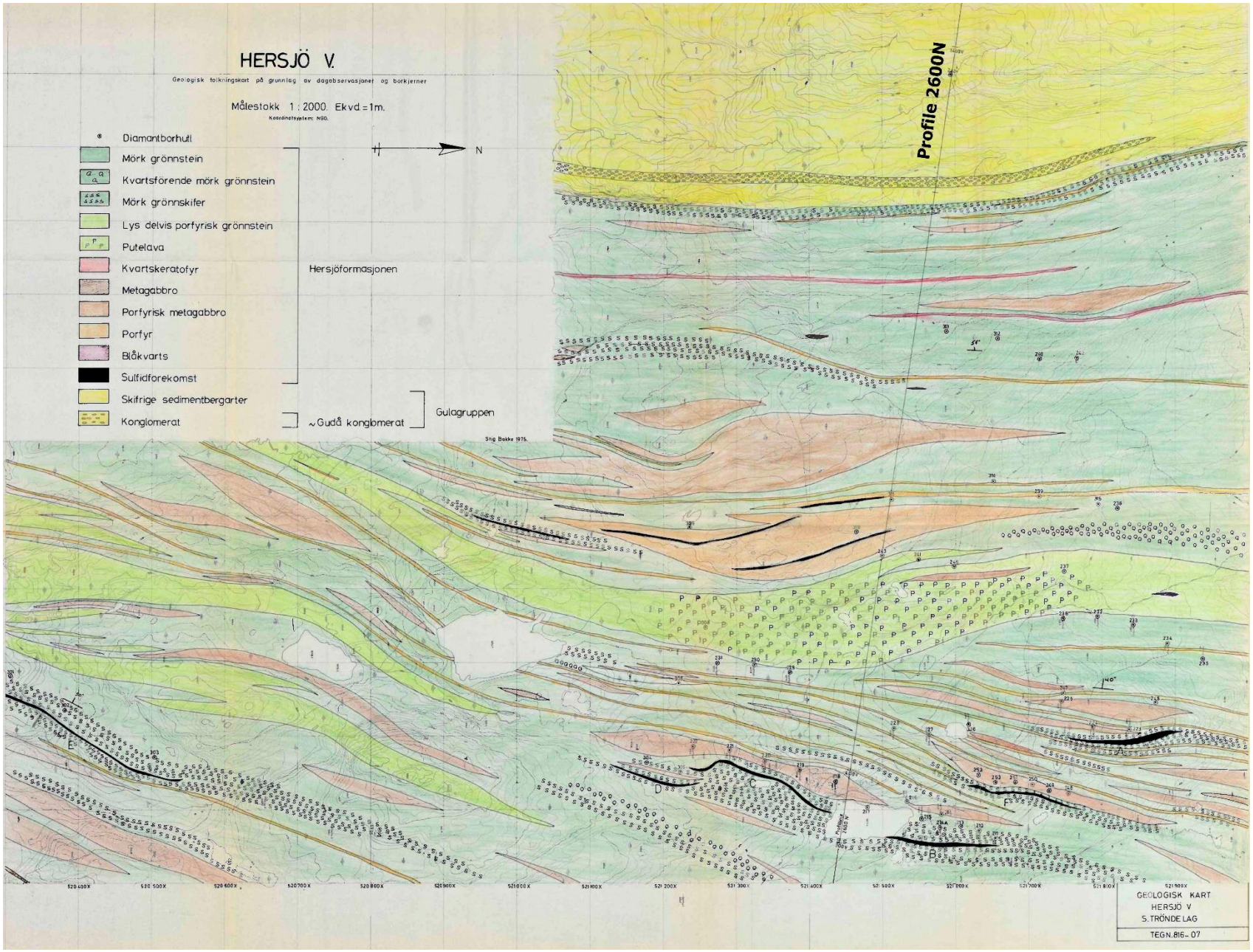


Figure 6: Geological map of the Hessjø deposit area. *Hersjøformasjonen* corresponds to the Fundsjø Group, while *Gulgruppen* denotes the Gula Group. The line adjacent to *Profile 2600N* refers to the placement of the geological profile shown in Figure 7. The outcrop of lens A is situated in the bottom right corner. Original format of the map is A1. (Bakke, 1975)

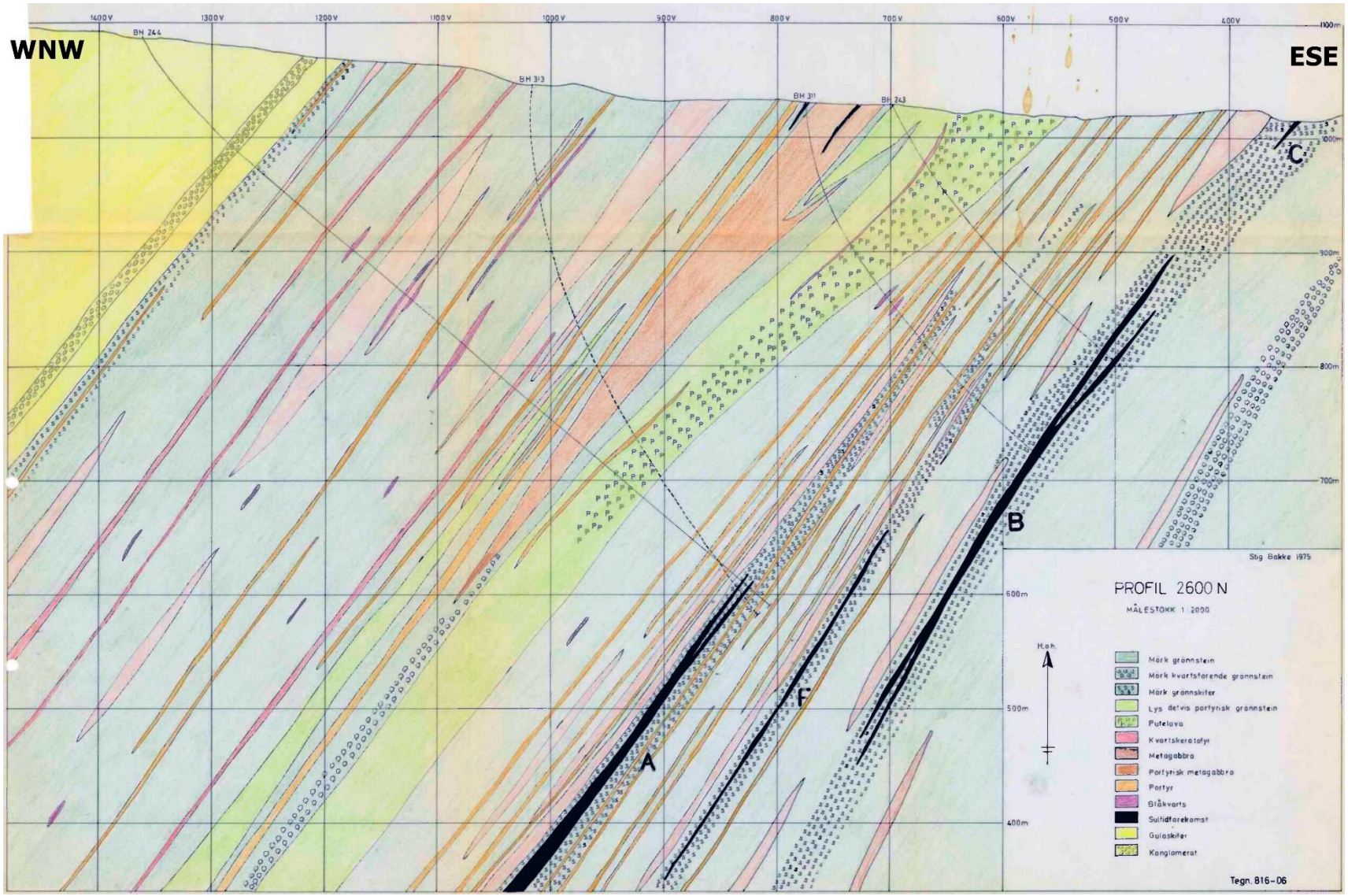


Figure 7: Geological profile of the Hessjø deposit area, looking from the south-west-south. Original format of map is A2. See Figure 6 for exact placement of profile. (Bakke, 1975).

The Hessjø area shows varying signs of tectonic deformation. According to Bakke (1975), the primary schistosity, S0, is weakly folded in an early folding phase F1, which occurs as macroscopic folds on the geological map in Figure 6. The associated axial plane schistosity S1, has a direction approximately east-west, with a probable dip towards south. A likely later folding phase, F2, has a wavelength of 2-4 m, and amplitude of 0.5-1 m. S2 has an approximate direction of north-north-west, with a dip 40°-50° towards east-north-east. Bakke further assumes that the mineralisations have been deformed during this folding phase, and states that aerial photos and maps show that S2 dominates the topography of the area. Finally, he remarks that some clay gouges are present in the drill cores, which would be indicative of faulting, though no faults are observed on the surface.

The sulfide lenses exhibit lengths from 100 to 160 m along strike (N-S direction), and the axes seem to coincide with the axis direction of the F1 folds, before further deformation by F2 folds. Bjerkgård (2007) also concludes that the trend of the lenses is controlled by folding, as shown by a strong lineation with a 250° WSW trend and a plunge of 46°.

#### 2.1.1.2.1 Geometry of lens A

Lens A of the Hessjø area is a likely VMS-type sulfide deposit (see chapter 2.1.5) of potential economic value with regards to copper and zinc concentrations. The outcropping of the lens is covered by soil. The lens is ruler-shaped with a strike length of up to 150 m in the N-S direction, and exhibits a dip of c. 35° in the upper part, and a dip of c. 45° in the lower part, below the kink mentioned in chapter 2.1.1.1.1 (Gvein, 1976). It is thickened in the central parts (along the main axis), where the lens has an average thickness of 10-12 m, but tapers and thins out towards the sides. The thickness varies from 1 cm to almost 15 m (Bakke, 1975; Vokes, 1983).

In connection with estimation of grades and tonnages, Bakke (1975) attempted to illustrate the variation of the geometry of lens A through cross-sections, as seen in Figure 8.

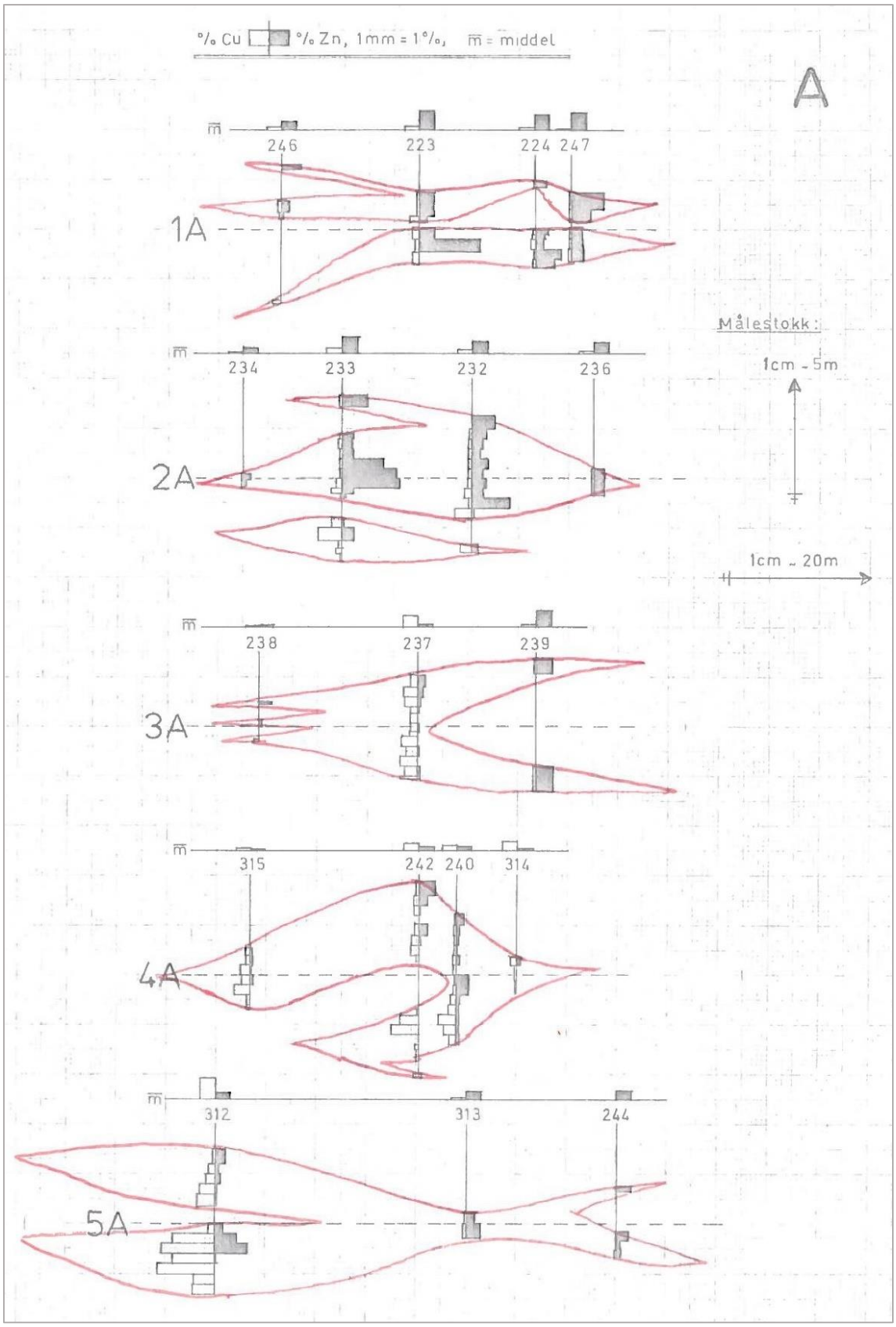


Figure 8: Cross-sections through lens A describing the geometry, as suggested by Bakke (1975, p.66). Numbers 1A-5A are equivalent to number of profiles A1-A5 in Figure 3. Note the vertical exaggeration of the cross-sections.

#### 2.1.1.2.2 Mineralogy of lens A

Gvein (1976) differentiates between two main types of potential ore in lens A:

- Type 1: Coarse grained pyrite, partly very rich in sphalerite and poor in chalcopyrite. Occurs along the south edge of the lens and is the main constituent of the hanging wall of the lens.
- Type 2: Pyrrhotite, partly very rich in chalcopyrite and poor in sphalerite. Magnetite can occur together with or instead of pyrrhotite. Main constituent of the footwall, and occurs along the north edge of the lens.

The two types of mineralisation also give way for a zonation pattern in lens A, with a zinc rich part in the upper 220 m of the lens, followed by a copper rich part of 380 m (Bjerkgård, 2007). The zonation pattern of lens A is discussed further in chapter 2.1.5.

In general, lens A is characterized by pyrite (py) as the dominant sulfide mineral, with additional chalcopyrite (cpy), sphalerite (sp), pyrrhotite (po), and quite some magnetite (mt). The mineralisation can be both massive and layered, and the grain size seems to become smaller towards the footwall. Veins and layers of compact pyrrhotite and magnetite also present towards the footwall, with magnetite enrichment towards northern part of the footwall. Rare, but present minerals are hematite and covellite (Bakke, 1975).

In his 1975 thesis, Bakke presents a considerable investigation of the mineralogy of lens A, B, and C. 46 polished sections of the mineralisations were made, and although he provides black and white photos of several of them, acquiring the polished sections has not been possible, if they even still exist. For lens A, Bakke has selected only photos of polished sections sampled from drillhole 312, for what reason is unknown. The following paragraphs summarise Bakke's descriptions of the ore minerals in lens A:

Pyrite occurs mainly as sub- and euhedral grains (0.01-5 mm) (Figure 9, Figure 10, Figure 11, Figure 12, Figure 15). The pyrite grains are very often fractured, occasionally with infillings of chalcopyrite and pyrrhotite (Figure 15, Figure 13). Observed inclusions in pyrite includes sphalerite, chalcopyrite, pyrrhotite, magnetite, and silicates. Inclusions are not very common, but those that are present are relatively large. In massive pyrite ore (Figure 9), it is possible to find mm-thick pyrite breccias. Layered changes in the grainsize might represent a form of foliation.

The pyrrhotite grains are always anhedral (Figure 14, Figure 15), and occur as infillings between pyrite grains, as veins, and as singular grains in chalcopyrite or sphalerite matrix (Figure 10). Pyrrhotite and chalcopyrite often occur together. Locally, pyrrhotite appears as myrmekitic intergrowth with sphalerite, and in cross polarized light, the pyrrhotite displays flame-like lamellae, that sometimes defines one or more directions of foliation.

Magnetite occurs as sub- to euhedral grains (0.01-1 mm) (Figure 11, Figure 15). The largest grains are found as euhedral crystals in the footwall chlorite schist. Magnetite is otherwise present as massive, fine-grained ore and massive veins (Figure 13). When occurring together with pyrite,

magnetite is often concentrated in stripes and layers (Figure 11). Large grains can have inclusions, particularly of chalcopyrite.

The sphalerite grains are always anhedral (Figure 10, Figure 12), and very often concentrated in cm to dm thick stripes and layers with more than 50% sphalerite. Can have small teardrop shaped inclusions of chalcopyrite. The sphalerite has few and brown internal reflections, indicating a low Fe-content.

The chalcopyrite grains are always anhedral, and occur as infillings between pyrite grains, as veins (Figure 15) in the mineralised lens and host rock, as fracture infillings in pyrite grains and breccias (Figure 13, Figure 14), and as matrix (Figure 10, Figure 11, Figure 12) and compact chalcopyrite. In cross polarized light, chalcopyrite displays unoriented twin lamellae.

The gangue minerals are hornblende, calcite, quartz, feldspar, biotite, chlorite, and epidote. As previously mentioned, lens A shows a distinct alteration pattern of the host rock around the lens. There is extensive chloritization of greenschist closest to the lens, especially in the footwall where chlorite is the dominating mineral. Less chlorite is present in the hanging wall, which can seem somewhat quartz rich. Sulfide impregnation of the host rock is deemed insignificant, though the footwall shows impregnation by chalcopyrite, pyrrhotite, and magnetite. The hanging wall is weakly impregnated by pyrite (Bakke, 1975).

The textures of the sulfide minerals present in the Hessjø deposit are discussed further in chapter 2.1.6.2.

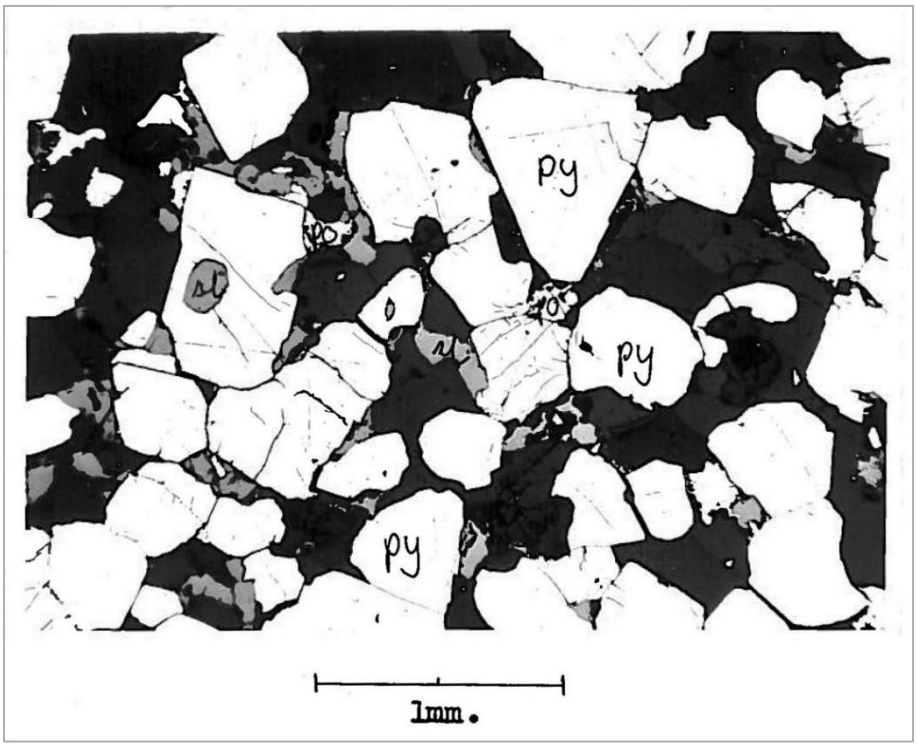


Figure 9: Drillhole 312, 455.5 m down, lens A. Massive, half-compact pyrite ore with some sphalerite and pyrrhotite (Bakke, 1975).

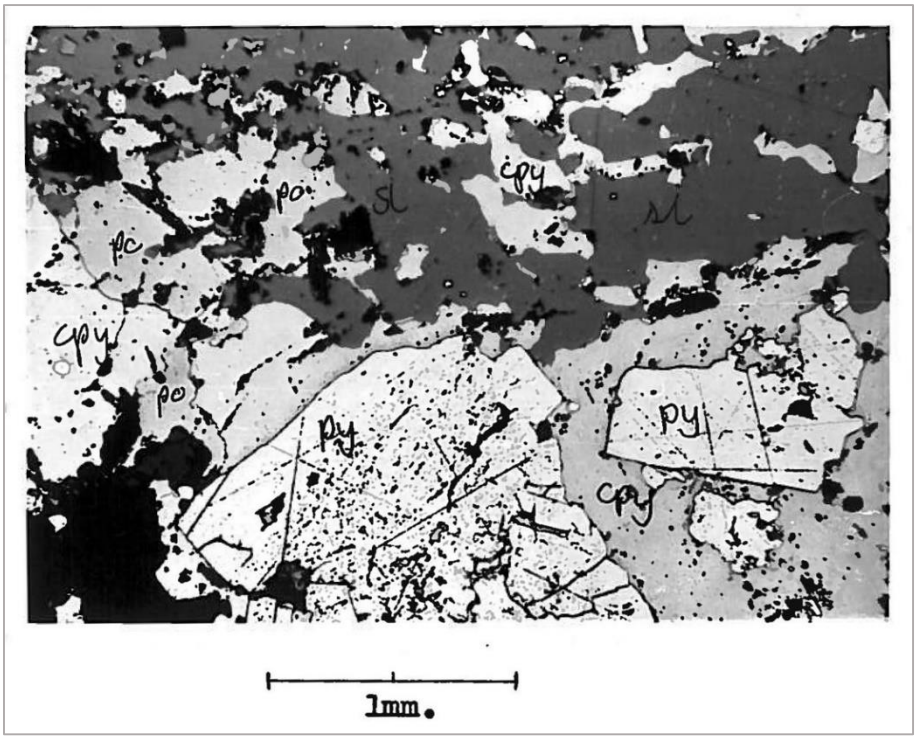


Figure 10: Drillhole 312, 460.0 m down, lens A. Pyrite porphyroblasts with inclusions of chalcopyrite in a chalcopyrite/sphalerite matrix (Bakke, 1975).

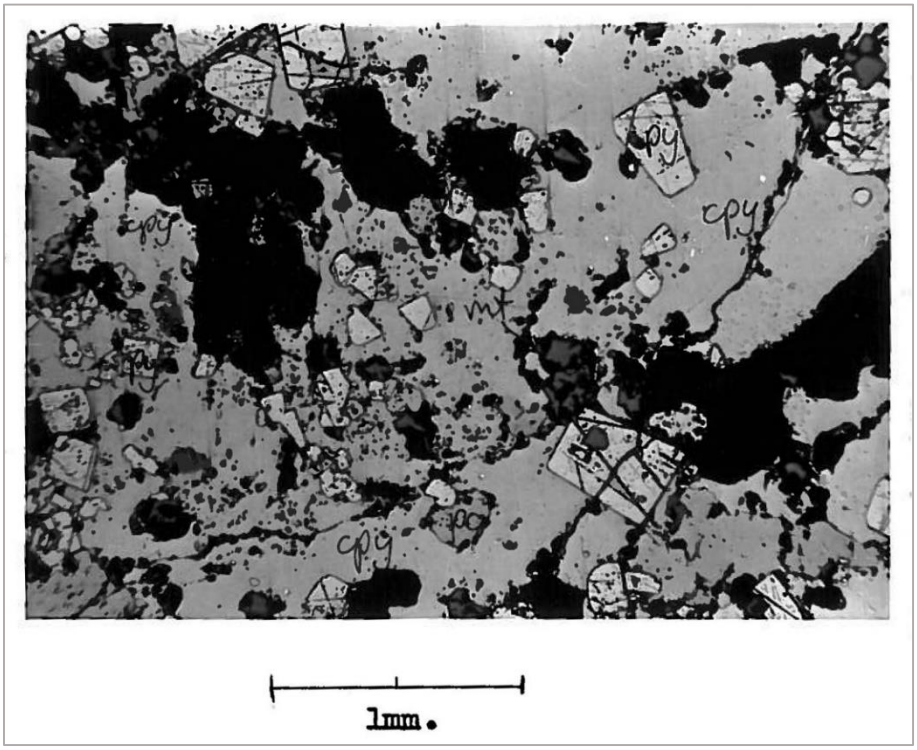


Figure 11: Drillhole 312, 460.0 m down, lens A. Pyrite, magnetite, and pyrrhotite in a chalcopyrite matrix (Bakke, 1975).

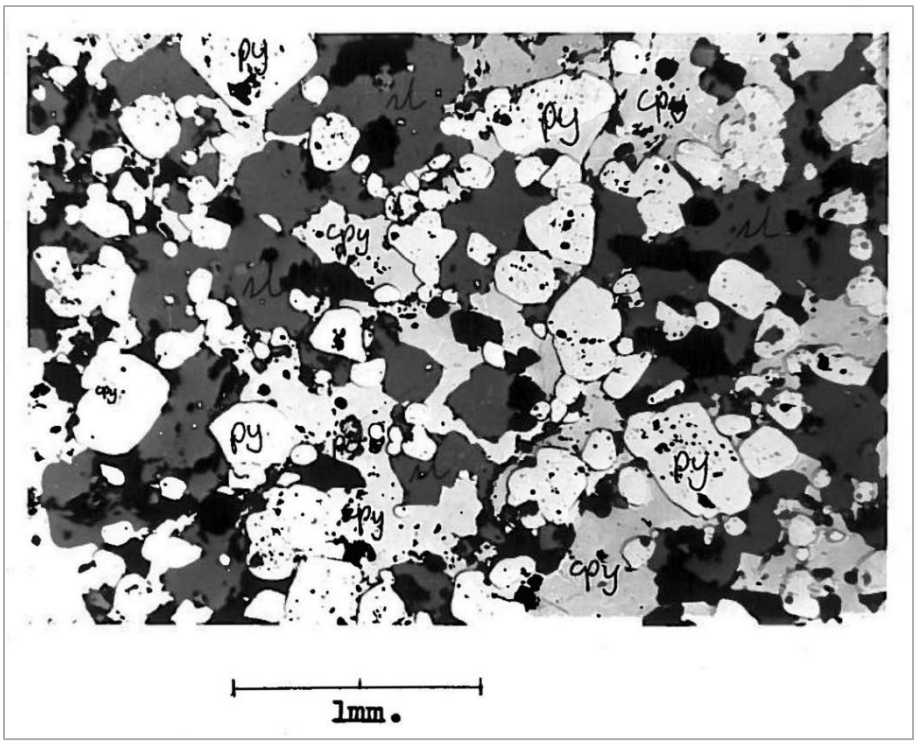


Figure 12: Drillhole 312, 465.4 m down, lens A. Rounded pyrite porphyroblasts in a chalcopyrite and sphalerite matrix (Bakke, 1975).

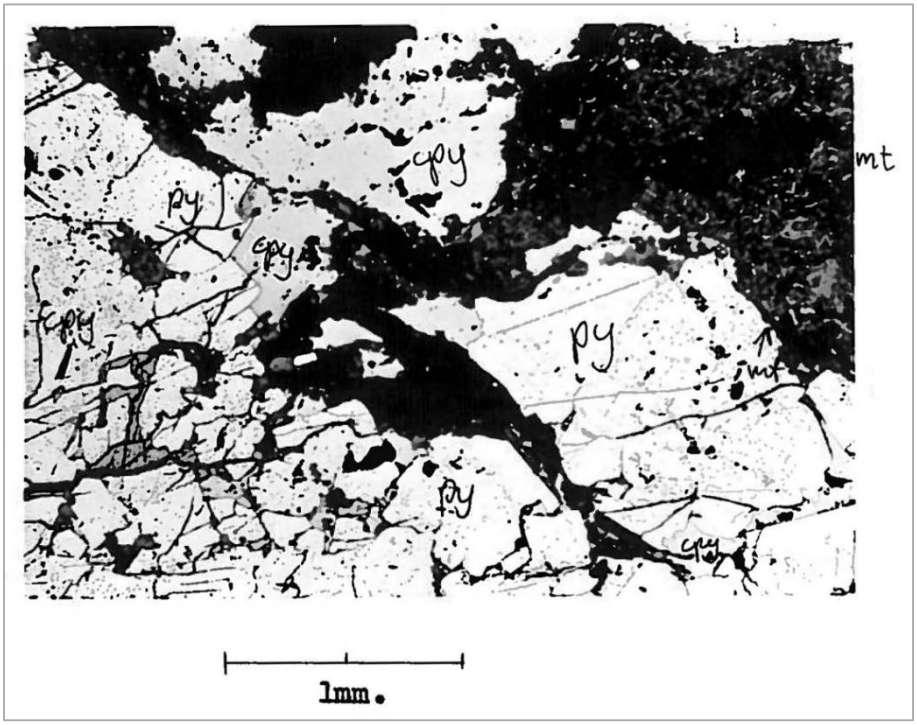


Figure 13: Drillhole 312, 466.7 m down, lens A. Crushed pyrite ore injected by chalcopyrite- and magnetite veins (Bakke, 1975).

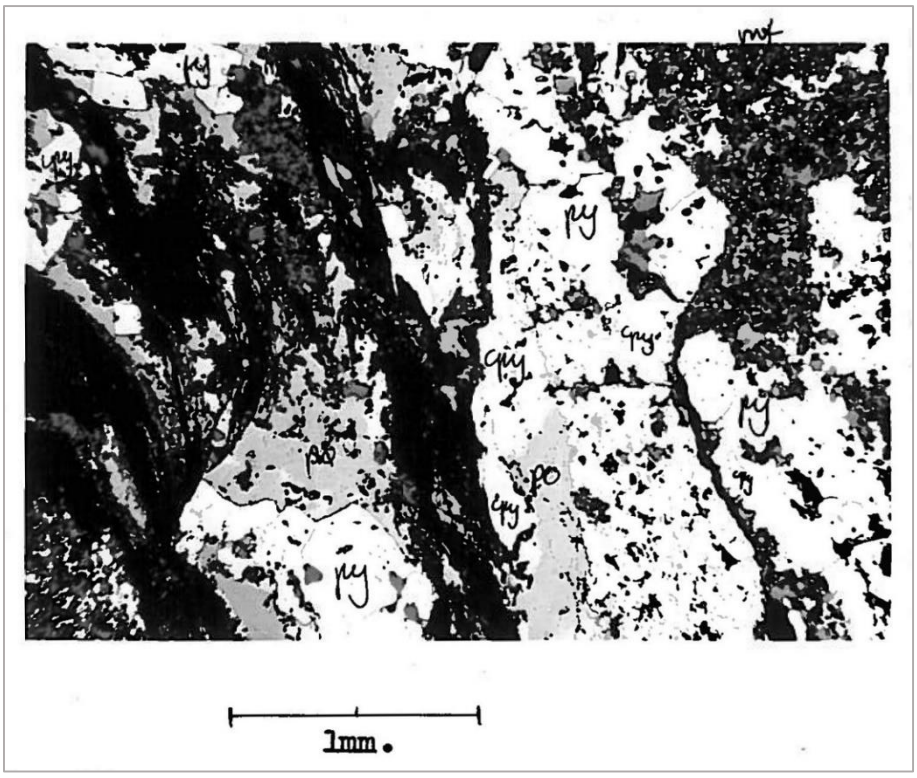


Figure 14: Drillhole 312, 467.1 m down, lens A. Crushed pyrite/magnetite ore injected by chalcopyrite, pyrrhotite, and magnetite (Bakke, 1975).

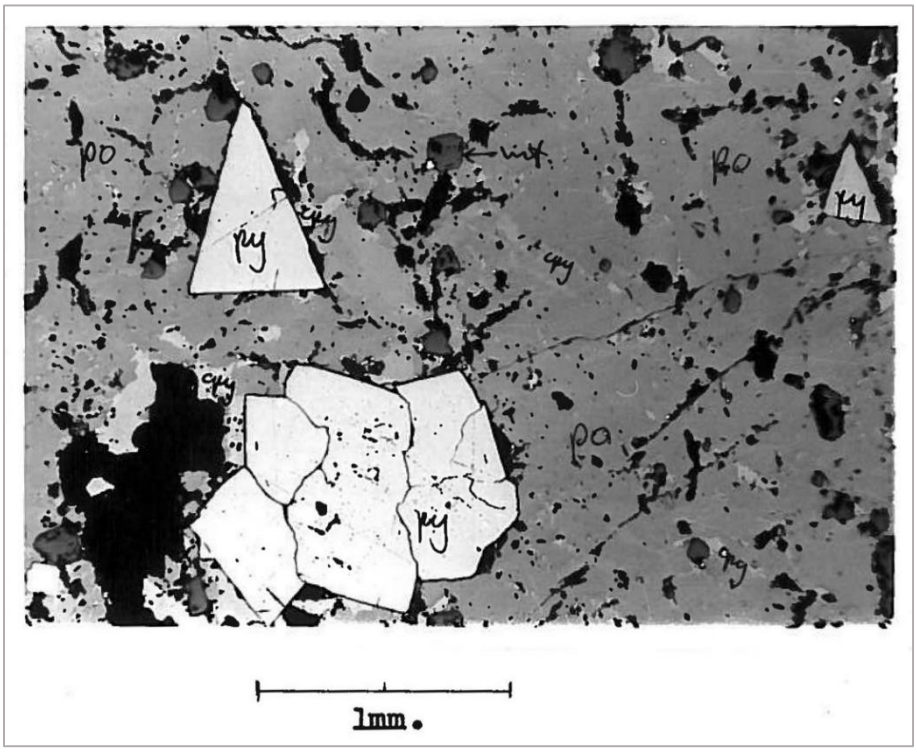


Figure 15: Drillhole 312, 469.4 m down, lens A. Massive pyrrhotite ore with chalcopyrite, pyrite, and magnetite (Bakke, 1975).

### 2.1.2 Caledonian orogeny

As a part of this thesis, a literature review on the possible geological and metallogenic history of the Hessjø deposit is to be performed, and will be presented in the following chapters.

There is a long history of exploration and exploitation of the various metallogenic deposits caused by the Caledonian metallogeny. Coupled with very good exposures, the Caldonian orogeny in Scandinavia can be used as an illustration of the relationship between metallogenic evolution and plate tectonics.

The Scandinavian Caledonides comprise of numerous nappes, or thrust sheets, of varying lithology and metamorphic grade, which have been thrust from west to east, with ages ranging from Precambrian to Devonian (Grenne et al., 1999). These nappe units have usually been divided into four allochthonous complexes: Lower, Middle, Upper, and Uppermost Allochthons (Roberts & Gee, 1985), where the Hessjø deposit belongs to the Upper Allochtons.

However, (Corfu et al., 2014) point out that there are several examples and indications that the simple tectonostratigraphic order of Lower-Middle-Upper-Uppermost Allochthons is too rigid and simplistic. While this may be the case, most of the source material regarding the Hessjø deposit and its surroundings uses the terminology defined within the four allochthonous complexes, and thus the same terminology will be used in this thesis.

(Grenne et al., 1999) divided the Caledonian orogeny into three main sequential stages:

- Stage 1: continental rifting and ocean floor spreading
- Stage 2: plate convergence and ocean closure
- Stage 3: continent collision

The Caledonian orogeny began with a period of plate movements about 700-600 Ma ago consisting of rifting and breaking up of the Proterozoic mega-continent Rodinia, followed by the opening of the Iapetus ocean (stage 1). There after followed plate convergence and closing of the Iapetus Ocean (stage 2). Lastly, stage 3 comprises the continental collision between Laurentia and Baltica (the Scandian phase) in Silurian times, where the passive margin of Baltica was subducted below the overriding margin of Laurentia. In total, the Caledonian orogenic belt results from a plate-tectonic cycle spanning ca. 300 Ma, where the Hessjø deposit originates from stage 2.

Furthermore, Grenne et al. (1999) grouped the Caledonian ore deposits into ten main types, where the Hersjø deposit goes under type number 5: “Stratabound, partly stratiform, massive, pyritic deposits of Cu-Zn (±Pb) sulphides in Cambro-Silurian metavolcanic or mixed metavolcanic-metasedimentary successions (VMS or volcex deposits)” (p.424).

The complexity of the Caledonian orogeny is high, and the subdivision into different units and the understanding of their relation to each other has varied greatly over the last decades. This is especially true for the units surrounding the Hessjø deposit, but a general consensus seems to place the deposit within the Fundsjø Group, a bimodal, though largely mafic, amphibolite-facies,

magmatic complex. The Fundsjø Group is situated at the base of the Meråker Nappe, which is part of the Caledonian Trondheim Nappe Complex (TNC), a major thrust complex (NGU, 2008). The TNC is contained in a major depression of the Precambrian basement, and comprises of the low-grade metamorphic Støren nappe in the west and the low-grade metamorphic Meråker nappe in the east, with the high-grade metamorphic Gula nappe forming a geographical central axis with an approximately N-S direction (Grenne & Lagerblad, 1985). The exact placement of the contact between the Fundsjø Group and the Gula nappe rocks (often just referred to as the Gula Group) is however, complex and not yet fully understood.

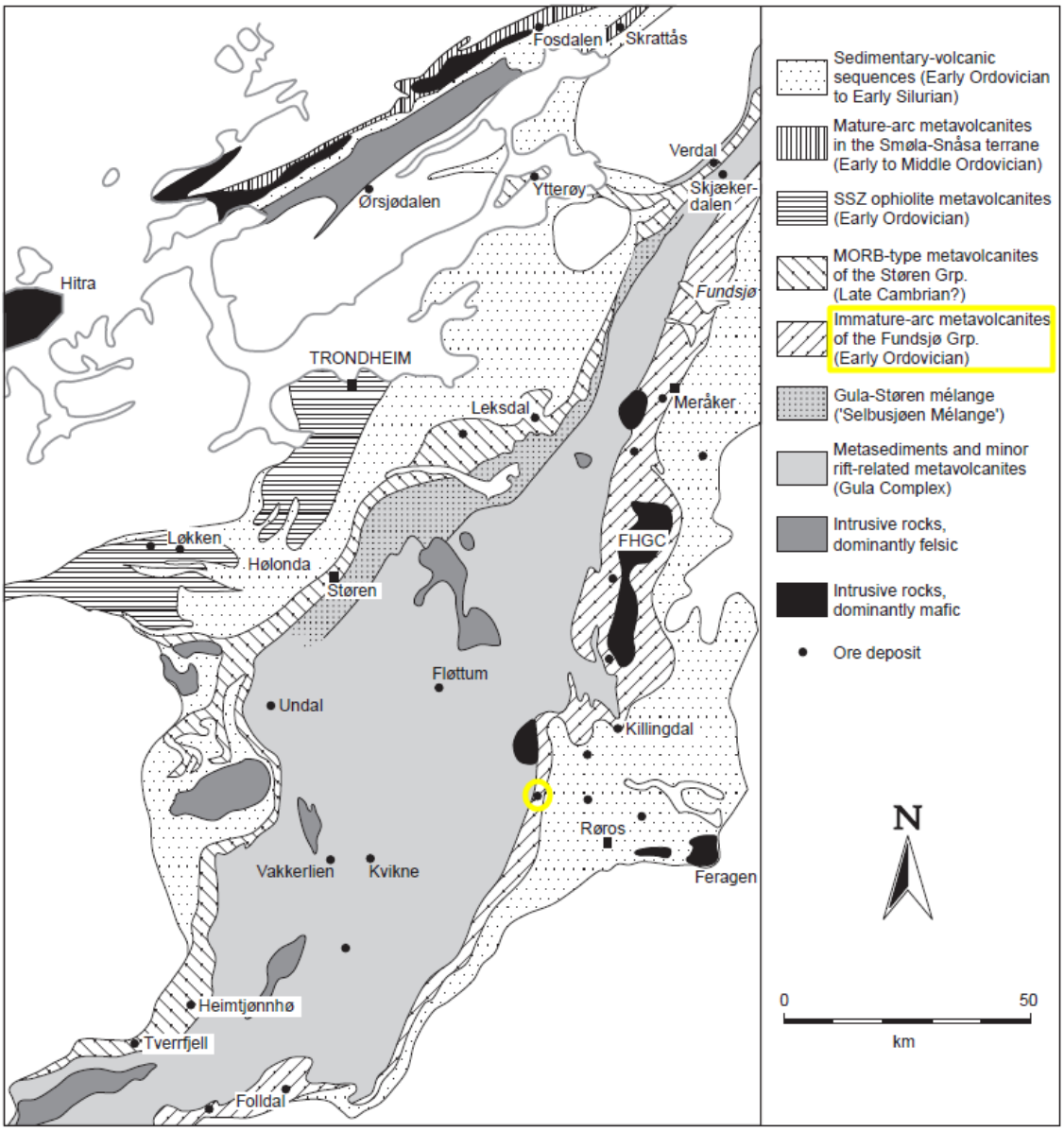


Figure 16: Location of the Hessjø deposit (yellow circle) in the Fundsjø Group. Modified from (Grenne et al., 1999)

### 2.1.3 The Fundsjø Group

Whereas the literature directly regarding the Hessjø deposit is sparse, information in conjunction with the Fundsjø Group and the Meråker nappe is more abundant. However, the details surrounding the depositional environment of these units are uncertain.

Geological surveys of Finland, Norway, Sweden and Russia have been working on a joint project dealing with the metallogeny of Fennoscandia, and have produced and published a metallogenic map of Fennoscandia (Figure 17) showing the various metallogenic domains or areas (Eilu, 2012). Here, the Hessjø deposit falls under the Folldal-Meråker Cu-Zn area, numbered N022. The extent of the Folldal-Meråker Cu-Zn area correlates approximately to the Fundsjø Group, and the Hessjø deposit is mentioned as one on the major deposits within this metallogenic area, the others being the deposits at Folldal, Sivilvangen, Vingelen, and Killingdal (Bjerkgård, 2012).

As mentioned in the previous chapter, the Fundsjø Group is situated next to the Gula Group in the west, and to the east it is mainly overlain by the Sulåmo Group (Bjerkgård & Bjørlykke, 1994).

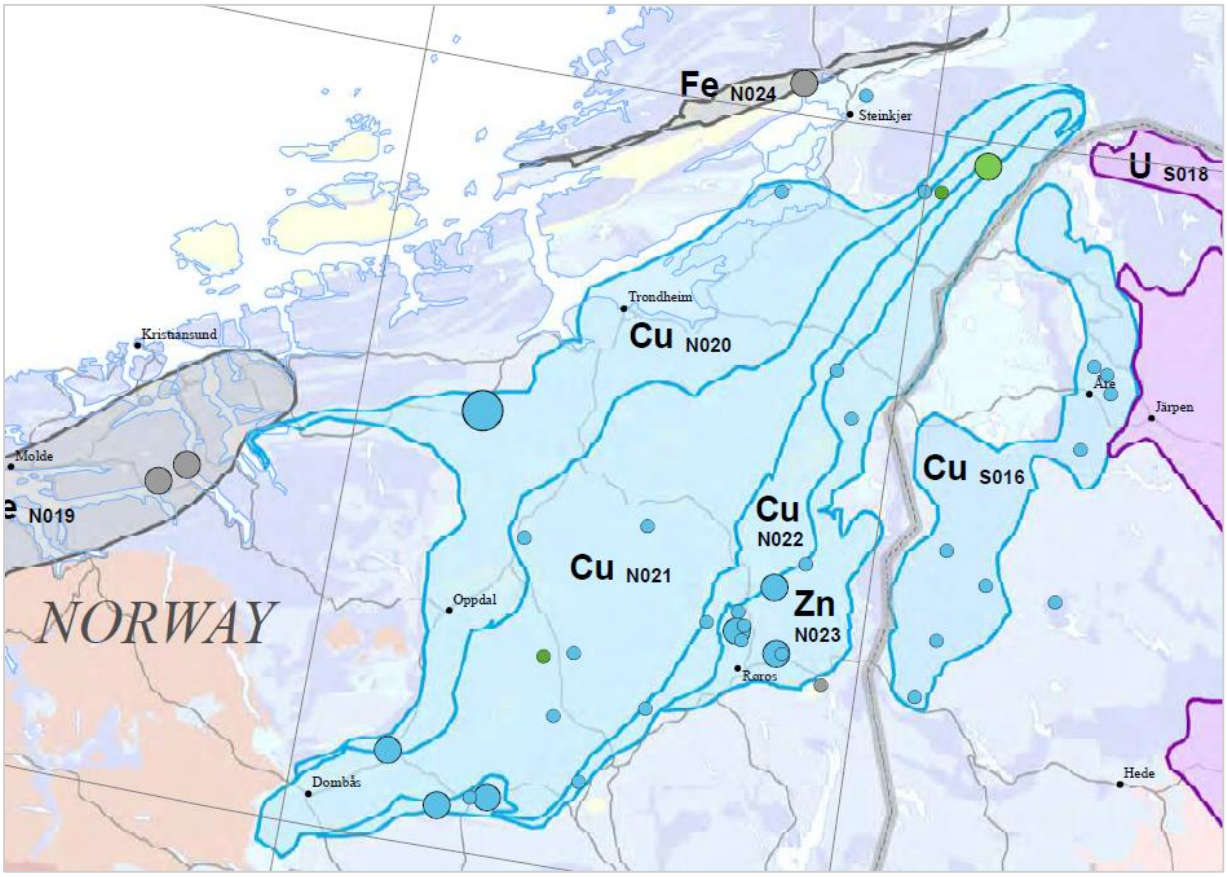


Figure 17: Excerpt from larger map showing metallogenic deposits in Fennoscandia. Blue circles mark base metal deposits. Figure modified from (Eilu et al., 2009).

The Fundsjø Group is characterized by a bimodal composition dominated by mafic rocks, with a few intermediate rock types. It has a high content of volcaniclastics with interlayered mafic and felsic units, as well as thick, relatively homogenous greenstone units, and locally tectonically elongated pillows. The group also contains amphibolites. The Fundsjø Group is intensely deformed, commonly finely banded with mm to dm thick individual layers, and shows a metamorphic grade varying from greenschist-facies to upper amphibolite-facies. At least parts of the Fundsjø Group rocks have been inverted, even though the Hessjø rocks have not (Grenne & Lagerblad, 1985).

Bjerkgård & Bjørlykke (1996) noted a further subdivision for the Fundsjø Group, with an upper and a lower part. The upper part contains volcaniclastics or tuffites with minor quartzites, greywackes, graphitic schists, and extensive felsic volcanics (rhyodacites) intercalated in the tuffites, whereas the lower part comprises of basalts. The group also contains sills and dykes of diorite, porphyry and trondhjemite, the latter representing shallow deposits (Røsholt & Wilberg, 2001), these being a possible source for the felsic volcanics (Bjerkgård & Bjørlykke, 1994). The Hessjø deposit is located in the lower part of the Fundsjø Group.

Massive sulfides frequent along the more than 300 km long Fundsjø volcanic unit, and there is a tendency to clustering of the sulfide deposits, e.g. in the Meråker, Ålen, Folldal districts. The deposits are generally Zn-rich, with the exception of the Hessjø deposit, having a comparably low Zn-content. In addition, the Pb-contents are low, while the gold and silver content is variable. The deposits occur as strongly deformed sheets or rulers, conformable to the layering of host rocks, and structurally controlled by tectonic deformation. It is common with sulfide disseminations in association with chlorite-quartz and quartz-sericite alteration in footwall volcanites (Grenne et al., 1999).

### 2.1.4 Depositional environment

Various theories have been put forward regarding the possible depositional origin of the Fundsjø Group. When comparing the available literature, it appears that the collective understanding is that the Fundsjø Group was deposited either in an immature island arc setting or in a marginal basin setting.

Grenne and Lagerblad (1985) suggested the following subdivision of the rocks in the Fundsjø Group, based on major and trace element content and trends (p.745):

1. A distinctive group of metabasalts to andesites with the geochemical signature of island arc tholeiites and characterised by very low $TiO_2$ and Zr abundances.
2. Amphibolites with element trends and abundances transitional between MORB and island arc tholeiites.
3. A group of metabasites showing similarities to MORB.

where the term *metabasite* refers to metamorphic mafic rocks that have recrystallized to the point where all traces of original texture and mineralogy is lost (Mineralogy Database, n.d.-a).

They further interpret the Fundsjø volcanites to have formed, at least partly, in a Tremadoc to late Cambrian immature, ensimatic island arc setting, and further suggest that incipient rifting of this arc caused the formation of the transitional and MORB-type magmas that occur intimately mixed with the tholeiitic basalts and andesites.

In connection to a study published by Grenne in 1988, metavolcanites in what he called the Hersjø Formation, were investigated. The Hersjø Formation is a name previously given to the part of the Fundsjø Group lying adjacent to the Røros and Tydal areas. Even though it is not explicitly defined in the article, it is apparent that several of the samples were taken either at or in close proximity to the old Hersjø minings. This is evident when comparing Figure 5 with Figure 18.

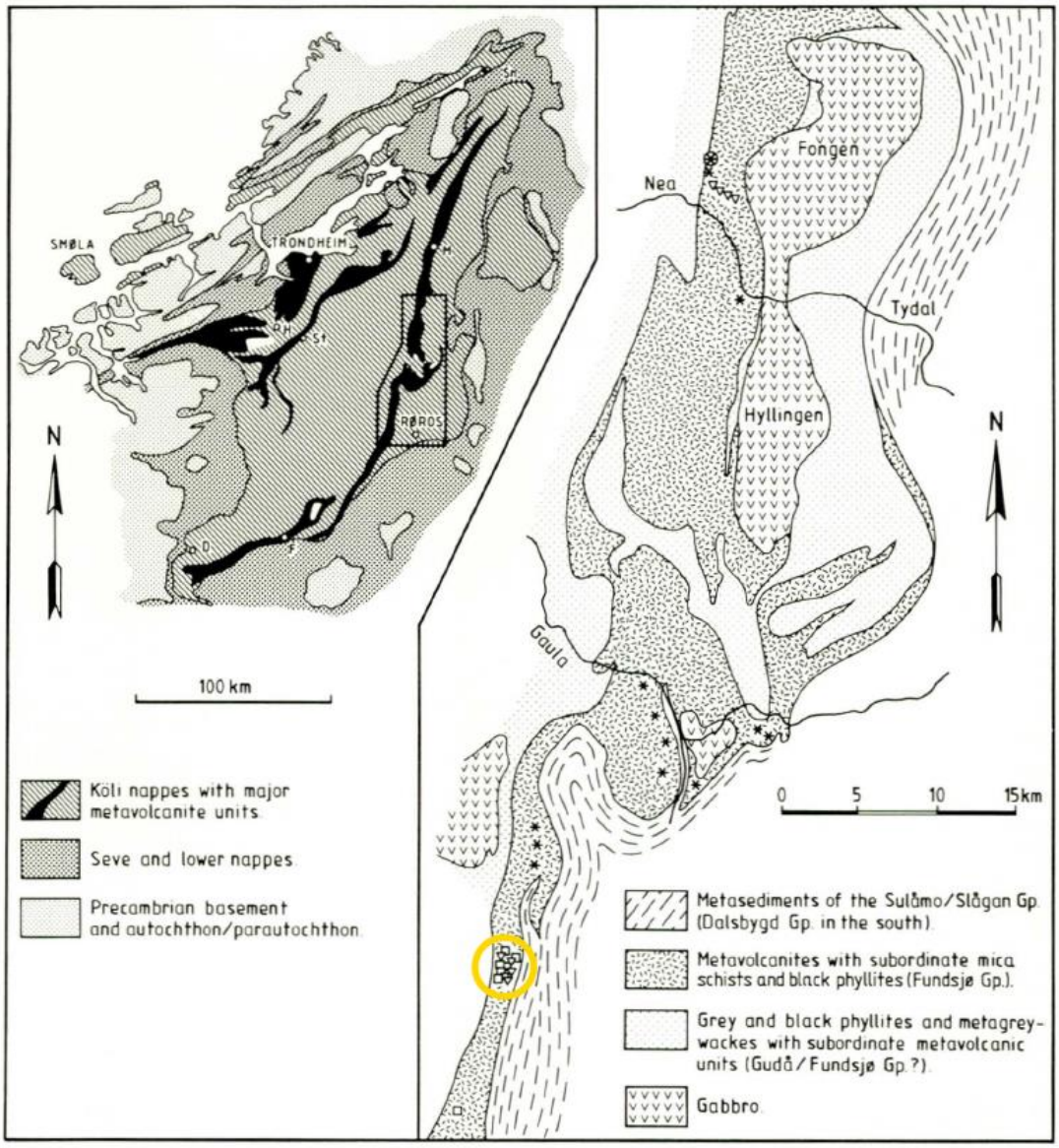


Geological map of the Røros-Tydal area. *Sample localities*: *squares* - type A; *triangles* - type B; *asterisks* - type C. *D* - Dombås; *F* - Folldal; *H* - Hølonda; *St* - Støren; *M* - Meråker; *Sn* - Snåsa.

Figure 18: From (Grenne, 1988), yellow circle marks the outcrop area of the Hessjø deposit.

Grenne (1988) suggested a tripartite subdivision of the samples based on their geochemical traits, dividing them into type A, B, and C (p.29):

- Type A: A group of HFS element-poor metabasalts to subordinate andesites with LREE-depleted to slightly enriched patterns.
- Type B: A group of metabasalts with compositions and trends comparable to somewhat fractioned MORBs, but with Th/Ta ratios suggesting a subduction zone affinity.
- Type C: A LREE-enriched, bimodal metabasalt rhyolite assemblage showing iron and titanium enrichment trends with inter-element ratios transitional between calc-alkaline and within-plate basalts.

Looking at Figure 18, one can see that samples associated with type A and type B are located around the old Hessjø mine locality. According to Grenne (1988) it is not evident if any of the analysed metavolcanites represent true island arc type magmas, or if they all formed in an arc-related marginal basin. The type A samples are those most similar to normal arc tholeiites, having a flat $TiO_2$ differentiation trend and a very low HFS-element content. However, many of the type A samples have a higher Cr content than what is typical for arc tholeiites. The type B samples display many geochemical traits similar to somewhat fractioned, normal MORB magmas, with clear iron-titanium enrichment trends and depleted LREE-pattern. As for the type C metavolcanites, Grenne denotes their geochemistry to be of a transitional character between calc-alkaline, within-plate, and mid-ocean ridge magmas, even though the high Th/Ta ratios infers their genetic relationship to subduction processes. In conclusion, Grenne (1988) finds it reasonable to assume that the Hersjø Formation metavolcanites "originated during the early stages of a marginal basin opening by rifting of a magmatic arc, with magma tapping from a heterogeneous mantle above a subduction zone" (p.29), and further that due to tectonic deformation, any primary stratigraphic relationships between the three types (type A, B, and C), have been erased. Contrary to later work by Bjørlykke et al. (1993) and Grenne et al. (1999), Grenne (1988) favours a deposition on the Laurentian side of the Iapetus Ocean rather than the Baltic side.

Two studies have been conducted where lead isotopic compositions from bulk sulfides and galena specimens from Norwegian Caledonian sulfide deposits have been determined to try to shed light upon the depositional environment, one by Fox et al. (1988) and one by Bjørlykke et al. (1993). Three different lead isotope ratios can be measured in sulfide deposits. Massive sulfide deposits usually have a local, rather immediate, metal source, often an underlying rocks sequence of 1-3 km thickness. In these cases, the lead isotope compositions mainly reflect the compositions of these sequences (Bjørlykke et al., 1993). Both studies included samples taken at and close to the old Hessjø minings.

Both studies revealed the isotope data to follow a linear trend interpreted to represent a mixing of two end members: a mantle source, and a continental basement source. According to Bjørlykke et al. (1993), the mantle source was Early Ordovician oceanic crust, whereas the sialic source

probably was the continental basement of the Baltic Shield. Bjørlykke et al. (1993) places the depositional environment of the Røros area and Fundsjø Group deposits in a mainly marginal basin setting, with the Folldal deposits possibly placed within an oceanic island arc setting. Fox et al. on the other hand, prefers a single, extensive epicratonic rifting environment for the Trondheim district massive sulfides, but does not rule out the possibility of an ensimatic primitive arc environment or an ensialic back-arc basin.

Looking specifically at the Hessjø deposit, both studies point out that the Hessjø samples are some of the least radiogenic (Figure 19). Bjørlykke et al. (1993) showed that the lead isotope compositions partly reflect the host-rock lithologies of the deposits, and Fox et al. (1988) also observed a crude correlation between the thickness of the host basalt and the sulfide $^{207}Pb/^{204}Pb$ ratios. Deposits within units of volcanic rocks contain less radiogenic lead than deposits within clastic sedimentary rocks or mixed units with tuffitic-sedimentary units. Bjørlykke et al. (1993, p.408) observes further that:

> This supports convection model for leaching metals from the underlying sequences and indicates that the clastic sedimentary component in the sequences serve as an important source of radiogenic lead during the formation of stratabound sulfide deposits.

Both Bjørlykke et al. and Fox et al. contribute the low radiogenic values of the Hessjø deposit to the fact that it is located directly on top of a more than 2 km thick mafic volcanic sequence (Grenne & Lagerblad, 1985), while all other deposits in Folldal and the Røros area of the Meråker nappe have a significant content of continentally derived lead. Bjørlykke et al. (1993) concludes that the lead compositions support the data of Mandeville (1988; as cited in Bjørlykke et al., 1993) that these deposits, including the Hessjø deposit, was formed in a rifted continental margin in the Early Ordovician.

A paper published in 1994 by Bjerkgård & Bjørlykke regarding the geology of the Folldal area, concluded that due to the bimodality, high content of volcaniclastics, intercalations of continental sediments, geochemical traits, and previous results from lead isotope investigations (Bjørlykke, et al., 1993; Fox, et al., 1988), the Fundsjø Group most likely represents an island arc accumulation close to a continent.

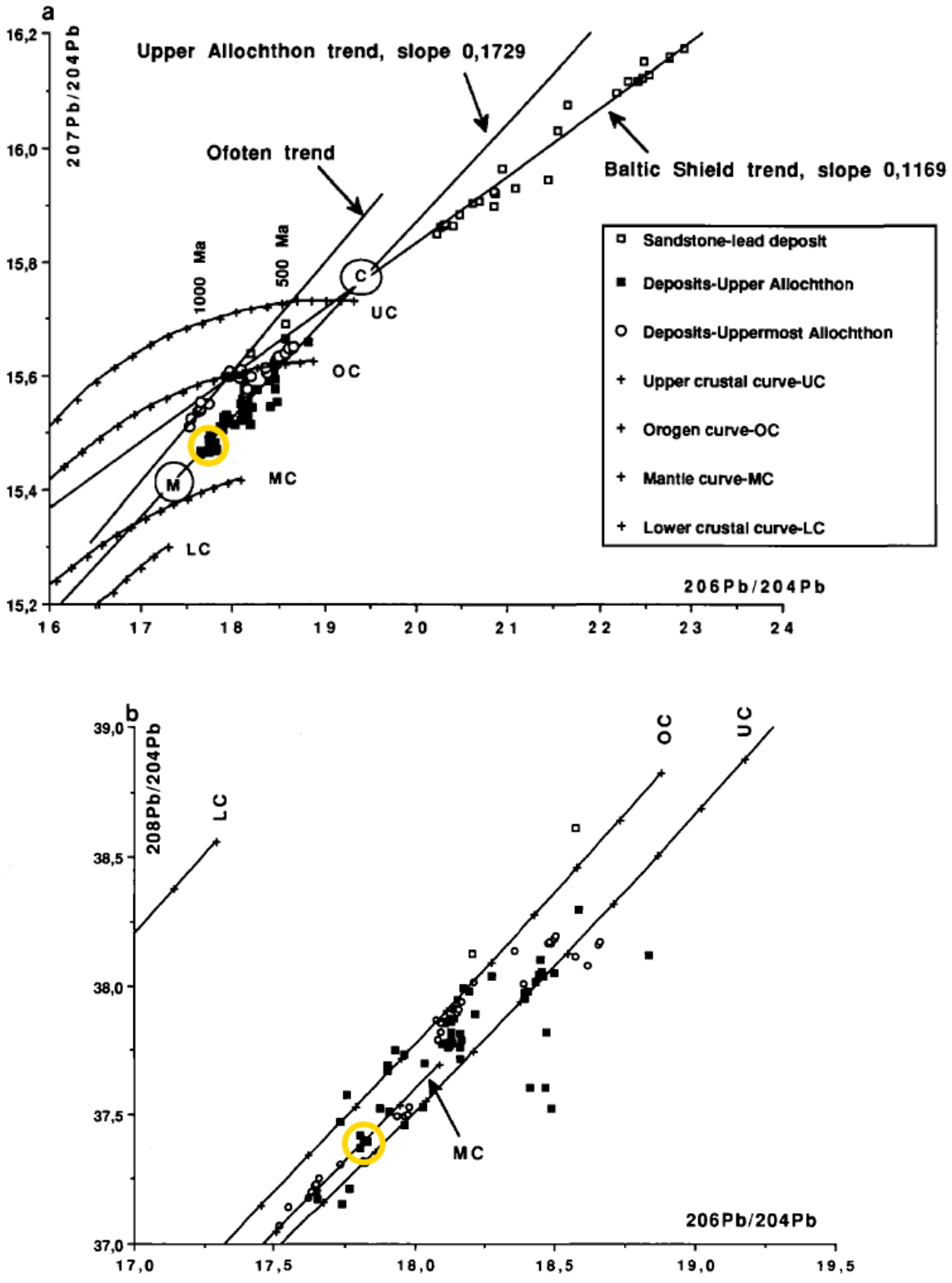


$^{207}Pb/^{204}Pb$ and $^{206}Pb/^{204}Pb$ ratios of ore deposits in relation to their tectono-stratigraphic position in the Norwegian Caledonides. M = the composition of the Lower Ordovician mantle, C = the average composition of the Baltic Shield (see text). b. $^{208}Pb/^{204}Pb$ and $^{206}Pb/^{204}Pb$ ratios of ore deposits in relation to their tectono-stratigraphic position in the Norwegian Caledonides.

Figure 19: results from lead isotope sampling of Norwegian Caledonian massive sulfide deposits by Bjørlykke et al. (1993). Yellow circle marks the results from the Hessjø deposit.

In an extensive article regarding the Scandinavian Caledonide metallogeny, Grenne et al. (1999) advocates a depositional model where immature, oceanic arc systems were present on both sides of the Iapetus Ocean, i.e. outboard of both the Laurentian and Baltica plate margins. The arc on the Baltic side probably had a short life span during the Early Ordovician, and by the end of the Ordovician, the Iapetus Ocean had narrowed considerably. In the remaining, narrow, ocean basin between Laurentia and Baltica, "thick, clastic sequences were deposited in fault-controlled basins with accompanying rift-related intrusive and volcanic activitiy" (p. 438), this in the Late Ordovician to Early Silurian. The immature, oceanic arc system on the Baltic side of the Iapetus Ocean in turn lead to numerous Zn-Cu type VMS deposits (and therein, the deposits in the Fundsjø Group) that are generally related to volumetrically significant felsic magmatism (Grenne et al., 1999). A schematic and interpreted figure of the Fundsjø Group is shown in Figure 20.

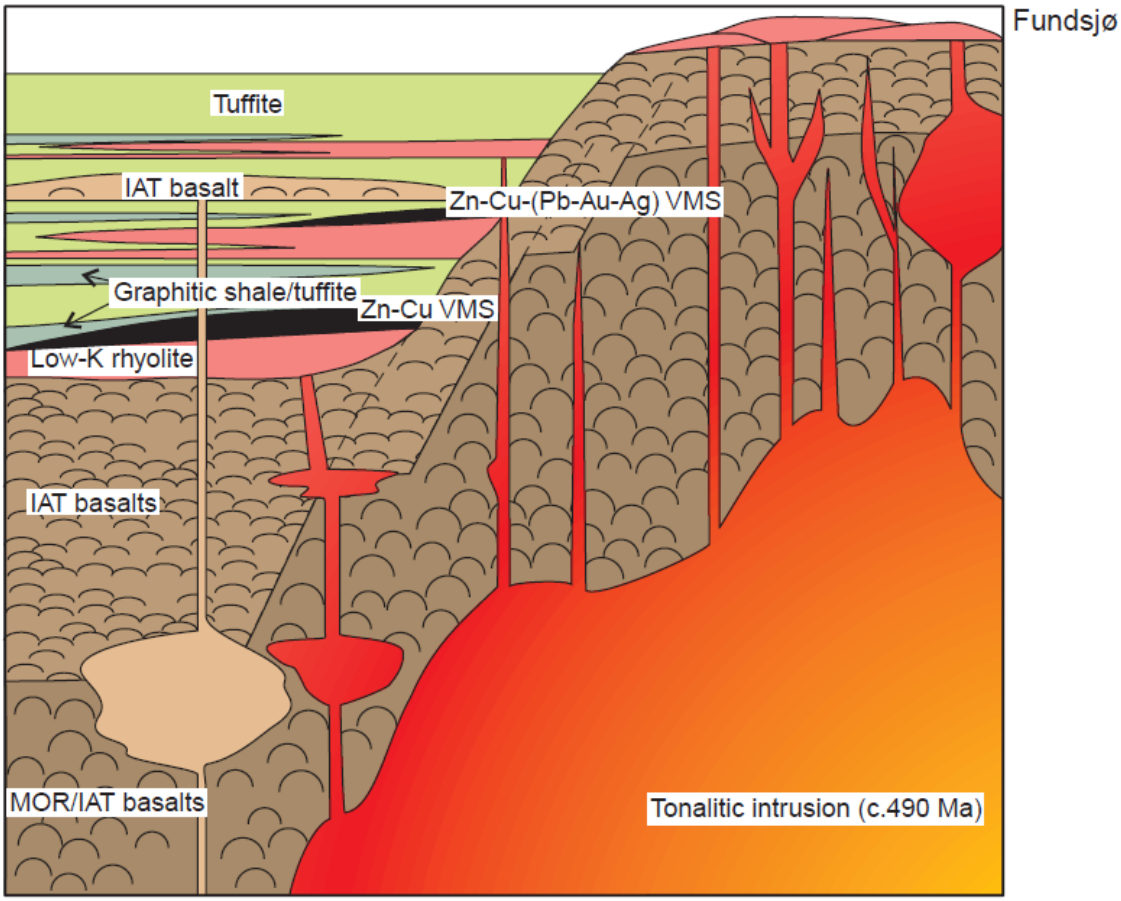


Figure 20: Schematic and interpreted section through the Fundsjø Group. (Grenne et al., 1999)

The following possible solution was proposed by Grenne & Lagerblad (1985, p.757) for the discussion regarding whether the Fundsjø group was deposited in an immature island arc or marginal basin setting:

> The MORB-like amphibolites may represent igneous activity following a shift in from a subduction to a tensional environment, i.e. incipient rifting of the arc and, eventually, the formation of an inter-arc marginal basin; a model comparable to the one proposed by Stephens (1981, as cited in Grenne & Lagerblad, 1985) for the Stekenjokk igneous rocks some 200 km to the NNE.

### 2.1.5 Ore deposition and morphology

The deposits and mineralisations in the Fundsjø Group constitute of massive stratabound sulfides occurring as highly deformed sheets/lenses or rulers conformable to the host rock layering, with the present morphology being mainly controlled by tectonic deformation. Pervasive wall-rock alteration is common and evident by the presence of chloritization, silicification, and sericitization, and subsequent sulfide disseminations (Grenne, et al., 1999; Nilsen, 1988). The mineralisations generally consist of pyrite with chalcopyrite, with pyrrhotite and sphalerite as minor constituent minerals. The copper content is usually between 0.5% and 2%, and the zinc content varies greatly from 1% - 5%, while the lead content is generally low, between zero and 1% (Nilsen, 1988). All of the above characteristics can be used to infer that the Fundsjø Group mineralisations are VMS-type deposits, as is further discussed in chapter 2.1.5.1.

As mentioned previously in chapter 2.1.3, the Fundsjø Group consists of mainly mixed mafic volcanic rocks, though there are uncertainties regarding the relative proportions between mafic and felsic volcanic rocks. There is however, a clear correlation between the type of volcanic host rock and metallic assemblage of the deposits, with a higher grade of Zn, Pb, and Ag where the dominating host rocks are felsic. The Hessjø deposit is surrounded by mainly mafic volcanic rocks and shows a metallic assemblage dominated by Cu and Zn with very little to no Pb and precious metals (Vokes, 1983).

The majority of the deposits can be regarded as being proximal relative to their hydrothermal feeder conduits (Grenne et al., 1999) even though any clear evidence of feeder channels has often been erased by subsequent deformation and metamorphism. This also makes it difficult to reconstruct the vertical zonation. However, many of the deposits display zonal relationships in which the pyrite/pyrrhotite ratio is lowest near the stratigraphic footwall and increases upward. This is also valid for the lens A in the Hessjø deposit (Vokes, 1983), and apparently reflects changes in ore fluid or depositional environment with time (Craig & Vokes, 1992). According to Craig & Vokes (1992), in composite orebodies that have only been subjected to minor deformation, it can be demonstrated that the pyrrhotite-rich areas often represent the stringer zones.

At Killingdal, Birkeland (1986; as cited in Nilsen, 1988) deduced a possible feeder zone by examining chalcopyrite and pyrrhotite disseminations stratigraphically underlying the massive, sphaleritic pyrite mineralisation which is capped by ferruginous cherts. Studies in the Meråker area (Grenne et al., 1995) indicate that the most important ore-forming event was the intrusion of large bodies of felsic magma into the pre-existing basalts. The mineralisations in the Meråker area are closely associated with felsic effusives, and it is inferred that intense hydrothermal activity was induced and driven by the large volumes of cooling felsic magma. In general, the formation of all Caledonian ore deposits seems related to a continuous process of tectonically induced fluid flow (Grenne et al., 1999).

An overview of some of the deposits in the Folldal-Meråker metallogenic area, which corresponds, at least partly, to the Fundsjø Group, is presented in Table 3.

Table 3: Deposits and occurrences in the Folldal-Meråker metallogenic area (N022, see Figure 17), with approximate tonnages and grade content. Adapted from Bjerkgård (2012, p.85).

| Deposit | Tonnage [Mt] | | Cu [%] | Zn [%] | When mined |
|---|---|---|---|---|---|
| | Total | Mined | | | |
| Nordre Geitryggen | 3 | 2.5 | 1.3 | 3.2 | 1920–1926, 1936–1970 |
| Søndre Geitryggen | >0.5 | 0.5 | 0.8 | 2.4 | 1770–1847, 1952–1965 |
| Folldal | 2 | 1.15 | 1.9 | 1.1 | 1748–1940 |
| Grimsdalen | 8.3 | - | 0.5 | 2.3 | Test mining |
| Sivilvangen | 0.4 | <0.01 | 0.69 | 4.31 | Test mining |
| Vingelen | 0.2 | 0.03 | 1.3 | 3.8 | 1723–1835 |
| Hessjø | 2.99 | <0.01 | 1.7 | 1.4 | 1670–1699 |
| Killingdal | 3 | 2.96 | 1.7 | 5.5 | 1677–1986 |
| Mannfjell | 0.1 | 0.1 | 1.8 | 5.3 | 1901–1918 |

#### 2.1.5.1 VMS-deposits

The Hessjø deposit, along with most of the other deposits located in the Fundsjø Group, are inferred to be *volcanogenic massive sulfide deposits* (VMS) (e.g. Vokes, 1983). An overview of the characteristics of VMS deposits, with a particular regard to classification types and the zonation patterns inherent to VMS deposits, will be presented in here.

Volcanogenic massive sulfide deposits are stratiform or strata-bound accumulations of sulfide minerals that formed on or near the seafloor by precipitation from hydrothermal fluids. The fluids are largely derived from modified seawater, and typically holds temperatures of 250 to 350 $^{0}$C. (Hannington, 2014). VMS deposits are spatially, temporally, and genetically associated with contemporaneous volcanism (Franklin et al., 2005), and the main source of metals is believed to

have been the volcanic rocks through which the seawater was percolating (Robb, 2005). Characteristic of VMS deposits is that they form early in the development of orogenic belts, where major peaks in deposit formation correlate with episodes of crustal growth and assembly of the continental landmasses, as well as with episodes of global ocean anoxia (Hannington, 2014).

All VMS deposits are polymetallic, with pyrite/pyrrhotite as the main sulfide minerals, while chalcopyrite, sphalerite, and galena, and to a lesser degree magnetite, constitutes the primary economic minerals. Mean gold content of VMS deposits is low, usually less than 1 ppm (Hannington, 2014).

The deposits consist of two main parts: a massive sulfide lens with more than 60% sulfides, underlain by a stockwork/stringer zone of disseminated or vein-type sulfide mineralisation in combination with intensely altered volcanic rock, i.e. the alteration pipe (Franklin et al., 2005; Robb, 2005), see Figure 21.

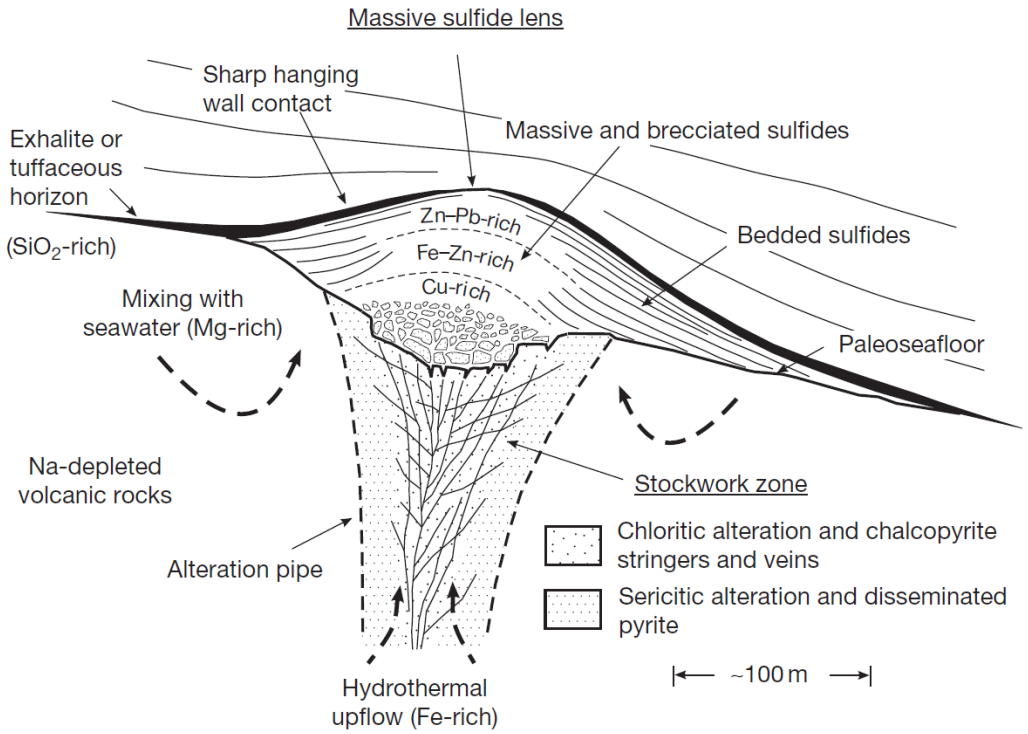


Figure 21: Schematic cross-section of a typical VMS deposit. From Hannington (2014, p.464), as adapted from Lydon (1984).

#### 2.1.5.1.1 Classification

There are several ways of classifying the various types of VMS deposits. At a governing level, deposits fall into one of two distinct groups based on metal content, a Cu-Zn group, and a Zn-Pb-Cu group (Hannington, 2014), where the Hessjø deposit would be classified as the former. This distinction mainly reflects the composition of the underlying rocks (Franklin et al., 1981;

Barrie & Hannington, 1999), where Cu-Zn deposits tend to occur above lithological successions dominated by mafic volcanic rocks (or their metamorphic equivalents), and Zn-Pb-Cu deposits occur above felsic volcanic and/or sedimentary successions (Hannington, 2014). This concurs with the Hessjø deposit being located directly on top of a more than 2 km thick mafic volcanic sequence (Grenne & Lagerblad, 1985). In addition, Cu-Zn deposits are commonly hosted by compositionally bimodal volcanic successions, and though they are dominated by mafic rocks, felsic volcanic rocks tend to occur in close association with the deposits (Hannington, 2014).

Franklin et al. (2005) advocate a further subdivision of VMS deposits and districts into five groups, using a "lithostratigraphic scheme based primarily on the principal volcanic and sedimentary lithological units that formed concurrently with the deposits in a given district" (p.525). This classification builds upon, and expands the lithological composition-based scheme of Barrie & Hannington (1999). The five lithostratigraphic types are: bimodal-mafic, mafic, pelitic-mafic, bimodal-felsic, and siliciclastic-felsic, where the first three are predominantly Cu-Zn types, while the last two also contain significant amounts of Pb. According to Franklin et al. (2005), deposits located in the Norwegian Caledonides are inherent to the mafic and bimodal-felsic types. However, the Fundsjø Group, and therein the Hessjø deposit, would appear to rather be classified as a bimodal mafic type. Franklin et al. (2005, p.529) defines the typical lithological units and tectonic setting inherent to bimodal-mafic type to be:

> Incipient-rifted bimodal volcanic arcs above intra-oceanic subduction (oceanic suprasubduction rifted arc); basalt dominated but up to 25% felsic volcanic strata; pillowed and massive basaltic flows, felsic flows, and domes predominate; subordinate felsic and mafic volcaniclastic rocks,

while the bimodal-felsic type (Franklin et al., 2005, p.529) is typified by:

> Continental margin arcs and related backarcs (continental suprasubduction rifted arc); felsic volcanic rocks constitute 35 to 70% of the volcanic strata, basalt 20-50%, and terrigenous sedimentary strata ~10%; submarine felsic volcaniclastic rocks are most common with basalt and/or basaltic andesite flows dikes and sills common.

That is not to say that some VMS districts may be classified as more than one type, and inevitably there are some that are transitional (Franklin et al., 2005). A summary of the geometric means for each subtype (Table 4) is given by Franklin et al. (2005, p.530), and from these values alone, the Hessjø deposit would fit in the bimodal-mafic type. However, Killingdal, which is also situated within the Fundsjø Group, has zinc content of 5.5% (Table 3), indicating that, at least parts of the Fundsjø Group could be bimodal-felsic.

Table 4: Geometric mean concentrations of metals in each of the five principal types of VMS deposits (Franklin et al., 2005, p.530)

| | Mafic | Bimodal-mafic | Pelitic-mafic | Bimodal-felsic | Siliciclastic-felsic |
|---|---|---|---|---|---|
| Cu [wt%] | 1.82 | 1.24 | 1.23 | 1.04 | 0.62 |
| Zn [wt%] | 0.84 | 2.32 | 1.58 | 4.36 | 2.7 |
| Pb [wt%] | 0.02 | 0.3 | 0.68 | 1.14 | 1.09 |
| Au [ppm] | 1.4 | 0.81 | 0.75 | 1.06 | 0.59 |
| Ag [ppm] | 11 | 21 | 19 | 56 | 39 |
| Total ore [tonnes] | 2699466 | 3421075 | 4721093 | 3320784 | 7139305 |
| Total metal [tonnes] | 63035 | 128515 | 132968 | 198461 | 324748 |
| N | 76 | 291 | 90 | 241 | 106 |

#### 2.1.5.1.2 Formation and deposition

VMS deposits are products of a hydrothermal convection of seawater, driven by oceanic crustal heat flow, with subvolcanic intrusions being the dominant heat source. Hydrothermal fluids are discharged either onto the seafloor or into permeable strata immediately below the seafloor. As the hydrothermal fluids approaches the seafloor, they are subjected to conductive cooling, mixing with seawater, boiling, and reaction with the wall rocks, which then causes precipitation of sulfides and gangue minerals (Hannington, 2014).

Initial precipitation occurs in the subsurface, typically forming a network of sulfide veins (stockwork zone), situated in highly altered wall rocks (alteration pipe). Alteration pipes situated beneath Cu-Zn deposits typically have a chloritic core and a sericitic outer zone, while beneath Zn-Pb-Cu deposits, the alteration is commonly dominated by quartz and muscovite.

At the seafloor, sulfide deposition occurs in response to cooling, pH changes, and oxidation, as hydrothermal fluids mix with seawater, resulting in the accumulation of a sulfide mound around the vent. Close to the vent, minerals that are soluble at high temperatures, e.g. chalcopyrite, will precipitate from the hydrothermal fluids. As the temperature lowers, the same fluid will eventually precipitate sphalerite and galena. However, many different discharge scenarios envisioned for different deposit types, depending on temperatures and salinities of ore-forming solutions (Hannington, 2014).

Typical ore-forming fluids in VMS deposits are acidic, reduced, 1-3 M chloride solutions. The chloride concentration is one of the most important factors concerning the total concentration of metal that can be present in the fluid, as metals are primarily transported as chloride complexes (Hannington, 2014). As the hydrothermal fluids evolve to higher temperatures, they are capable of containing and transporting significant amounts of Cu as a chloride complex. However, the temperatures at which this is possible is in excess of c. 350 $^{0}$C according to Hannington (2014), but in the range of 250-300 $^{0}$C according to Robb (2005).

The metals and sulfur are believed to have derived by leaching of volcanic rocks situated stratigraphically below the deposits. In addition, there is a potentially important contribution of metals from contemporaneous magmas (Hannington, 2014).

#### 2.1.5.1.3 Zonation

Most VMS deposits are characterised by well developed metal zonation patterns reflecting the temperature-dependent solubilities of the different ore minerals. The Cu- and Fe-rich sulfides are most abundant in the interiors and in the underlying stockwork zones, while Zn- and Pb-rich sulfides are deposited at the outer margins (Hannington, 2014; Robb, 2005). However, evidence of these patterns can become distorted or even obliterated by subsequent deformation and metamorphism.

The zonation patterns reflect a cooling path that sequentially crosses the stability fields of magnetite, pyrrhotite, and pyrite, first precipitating chalcopyrite and then sphalerite. The result is high-temperature Cu-rich areas in the core of the sulfide mound, as well as in the stringer zones, dominated by pyrrhotite ± magnetite, while the lower temperature Zn-rich massive sulfide zones are dominated by pyrite (Hannington, 2014). This zonation pattern, with Cu below Zn, is used as an indicator of stratigraphic facing direction, especially in deformed terranes (Sangster, 1972, as cited in Hannington, 2014), as was done by Vokes (1983) for lens A of the Hessjø deposit.

Equivalent zonation patterns can also be observed at a much larger scale. Deposits that formed close to their vent, where temperatures are high, commonly have a high Cu/Cu+Zn ratio, while deposits that formed at lower temperatures, i.e. further away from the discharge sites, have lower Cu/Cu+Zn ratios (Hannington, 2014). Figure 22 provides Cu/Cu+Zn ratios for the Noranda VMS district in Quebec, Canada. Using the Noranda values as an indicator, Cu/Cu+Zn ratios for lens A in the Hessjø deposit was calculated. However, Cu and Zn grades have been estimated several times since the first explorations of the Hessjø deposit, giving variations in the Cu/Cu+Zn ratio. Using grade estimates from Gvein (1976), Bjerkgård (2007), and Bakke (1975), gives a Cu/Cu+Zn ratio (multiplied by 100) of 40.1, 45.2, and 55.1, respectively, thus indicating that lens A was deposited relatively proximal to the vent. The historical estimates used are presented in chapter 2.1.1.1.3.

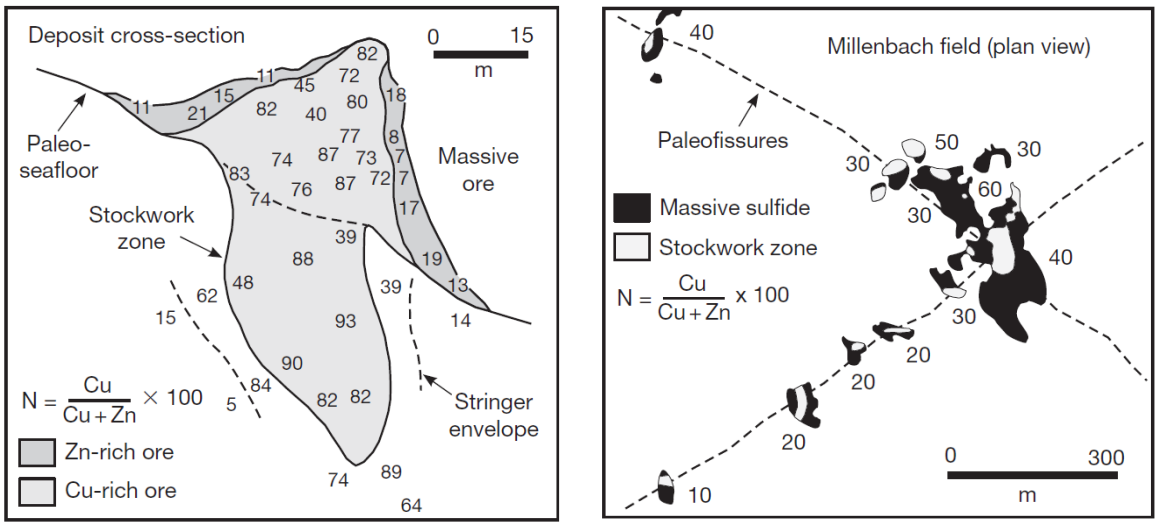


Figure 22: Schematic illustrations of metal zoning at different scales in a typical VMS district (Noranda, Quebec). The figure on the left shows Cu-Zn zoning (in terms of Cu/Cu+Zn ratios) in a small massive sulfide deposit, while the figure to the right shows higher Cu/Cu+Zn ratios in deposits at the center of a field and lower ratios in deposits farther away from the main upflow zone. From Hannington (2014, p.476) as adapted from Knuckey et al. (1982, as cited in Hannington, 2014).

It is important to bear in mind that this model of precipitation evolution, causing the zonation pattern, is a simplification where it is assumed that all of the minerals were precipitated from the same fluid in a uniform physiochemical gradient. More realistically, VMS deposits have highly variable and complex thermal histories, causing multiple replacement or overprinting events (Hannington, 2014). At the smallest scale, this can be seen as a texture termed 'chalcopyrite disesase' (Barton & Bethke, 1987), where higher temperature Cu-rich fluids have caused chalcopyrite to replace sphalerite in the form of intergrowths or disseminations. This texture is discussed further in chapter 2.1.6.2.

For further insight on the formation and characteristics of VMS deposits, the reader is referred to the works by Hannington (2014), Franklin et al. (2005), and Franklin et al. (1981).

### 2.1.6 Deformation and metamorphism

For many of the Caledonian ore deposits, metamorphism and deformation makes it challenging to identify the depositional environment, with the Hessjø deposit being no exception.

#### 2.1.6.1 Regional deformation

All the Caledonian tectonostratigraphic components have undergone polyphase deformation and metamorphism. Much of this reflects the Mid-Silurian to Early Devonian Scandian Orogeny, when the ultimate collision between Laurentia and Baltica occurred and the Iapetus Ocean finally closed. At this point, the accretionary prism with granitic batholiths was obducted onto the Baltic margin causing extensive thrust faulting (Fox, et al., 1988; Bjørlykke, et al., 1993). The obduction and subsequent uplift of the subducted edge of Baltica led to the formation of intramontane Old Red Sandstone (ORS) basins in the Early and Middle Devonian. The Caledonian orogeny terminated with the deformation of the ORS basins in the Late Devonian (Bjørlykke et al., 1993). It is also possible that the deformation and metamorphism was in part caused by the Finnmarkian Orogeny, a Late Cambrian to Early Ordovician tectonothermal event, corresponding to the early stages of oceanic contraction (Fox et al., 1988).

During the Scandian Orogeny, the entire TNC was subjected to deformation and metamorphism at grades of lower greenschist to lower amphibolite facies (Ihlen et al., 1997). The Fundsjø Group, together with the Gula Group/complex has been subjected to at least four phases of deformation (Lagerblad, 1983, as cited in Grenne & Lagerblad, 1985). Before the late Silurian thrusting of TNC, two phases of folding occurred, and therefore, the groups now show isoclinal, steeply dipping, mutually interfering folds. These are however, apparently not present in and around the Hessjø deposit, as pointed out by Vokes (1983). He finds it noteworthy that there are no obvious indications to any tight or isoclinal folding, as similar Caledonian deposits such as the Killingdal deposit, display complex internal folding. However, Vokes also points out the scarcity of information in which to base the interpretations on.

The Caledonian rocks of the Trondheim district display a regional schistosity caused by an intense deformation, which can probably be related to the thrusting of the TNC onto the Baltic shield. During the fourth deformational phase, the rocks were refolded into open folds with horizontal fold axes.

Metamorphic grade for the Fundsjø rocks vary from greenschist-facies to upper amphibolite-facies, with the Hessjø rocks at an upper greenschist-facies (Grenne & Lagerblad, 1985).

#### 2.1.6.2 Ore mineral textures

The study of mineral textures in ore deposits may provide evidence and clues regarding initial ore deposition, in addition to postdepositional metamorphism and deformation The textures observed in many polymetallic ores reflect the various stages in their development and postdepositional history, however, many textures are still inadequately understood and experienced ore microscopists still disagree on their precise origin (Craig & Vaughan, 1994).

The stratabound sulfide deposits in the Caledonian Orogen displays various signs of metamorphism and deformation, and while there has been little effect in altering of the mineral species of the deposits, significant effects on textures and on the distribution of minor elements can be observed. Probable changes of stratabound sulfide deposits due to thermal and dynamic metamorphism include an increase in grain size, homogenization of grains (loss of primary textures), and redistribution of minor elements (Craig & Vokes, 1992).

The following sections present the general behaviour and textures (both primary and secondary) of the relevant ore minerals with an attempt to recognise said behaviour in the Hessjø deposit, using microscopy pictures and descriptions from Bakke (1975). As only a few microscopy pictures from lens A exist, and assuming that all the mineralisations in the Hessjø deposit area have undergone approximately the same degree of deformation and metamorphism, pictures of polished sections from lens B and C will be provided where such is deemed relevant.

The degree to which individual mineral grains both respond to and preserve deformational effects vary greatly, depending on the mineral, the rate of strain, the nature of the deformation, the associated minerals, the temperature at the time of deformation, and the postdeformational history. The response threshold of minerals seems to be primarily a function of hardness, and thus, deformation textures in polymineralic ores are often evident in only some minerals. The more refractory minerals (pyrite, arsenopyrite, magnetite, and to some extent sphalerite) tend to retain their original compositions and, at least partly, their textures, while the softer sulfides (chalcopyrite, pyrrhotite, and galena) readily deform and recrystallize (Craig & Vaughan, 1994). Refractory minerals can be defined as "minerals or synthetic inorganic crystal phases that have high melting points. They should also be resistant to deformation and to softening at high temperatures" (Doman & Alper, 1983, p.441).

Pyrite, being one of the most refractory sulfides, is a suitable mineral for observation of the metamorphic and deformational history of deposits, as it offers an opportunity of preserving some evidence of pre- or synmetamorphic development (Craig & Vokes, 1993). It should be noted however, that pyrite still has the capability to deform plastically, though this is not readily observable using only optical microscopy (Barrie et al., 2010).

According to Craig & Vokes (1993, p.4), two characteristics dominate the physical behaviour of pyrite during metamorphism:

- Its bond strength, observable in pyrite's microhardness and resistance to ductile deformation.
- Its inclination to forming idiomorphic, most commonly cubic, crystals.

Despite its refractory nature, pyrite displays a tendency to recrystallize in response to metamorphism at greenschist grades and above, resulting in the development of annealed textures and changes in grain size (Craig & Vokes, 1993). Annealing due to the slow heating caused by metamorphism, usually results in recrystallization and an increase in grain size, and may also result in the growth of euhedral, sometimes porphyroblastic crystals, not only of pyrite, but also

of arsenopyrite, magnetite, and hematite (Craig & Vaughan, 1994). Pyrite porphyroblasts are present in all three of the major mineralised lenses (lens A, B, and C) of the Hessjø deposit, as can be seen in Figure 9, Figure 10, Figure 12, Figure 23, and Figure 24.

Porphyroblastic growth or overgrowth can complicate paragenetic interpretation, as it is often difficult to distinguish porphyroblasts from primary euhedral crystals. However, porphyroblasts frequently contain different amounts and types of inclusions compared to the corresponding primary minerals in the ore (Craig & Vaughan, 1994), e.g. sphalerite inclusions in pyrite in Figure 9, Figure 23, and Figure 24.

Pyrite porphyroblasts typically display only partly developed crystal faces, and can show considerable embayment of faces (Figure 23). Rounding of the sub- to euhedral shapes are apparent in many ores (Figure 9, Figure 12), which may be due to chemical resorption (corrosion) by the surrounding sulfides or, more commonly, to the mechanical effects (rolling, milling, or abrasion) caused by deformation subsequent to porphyroblastic growth (Craig & Vokes, 1993).

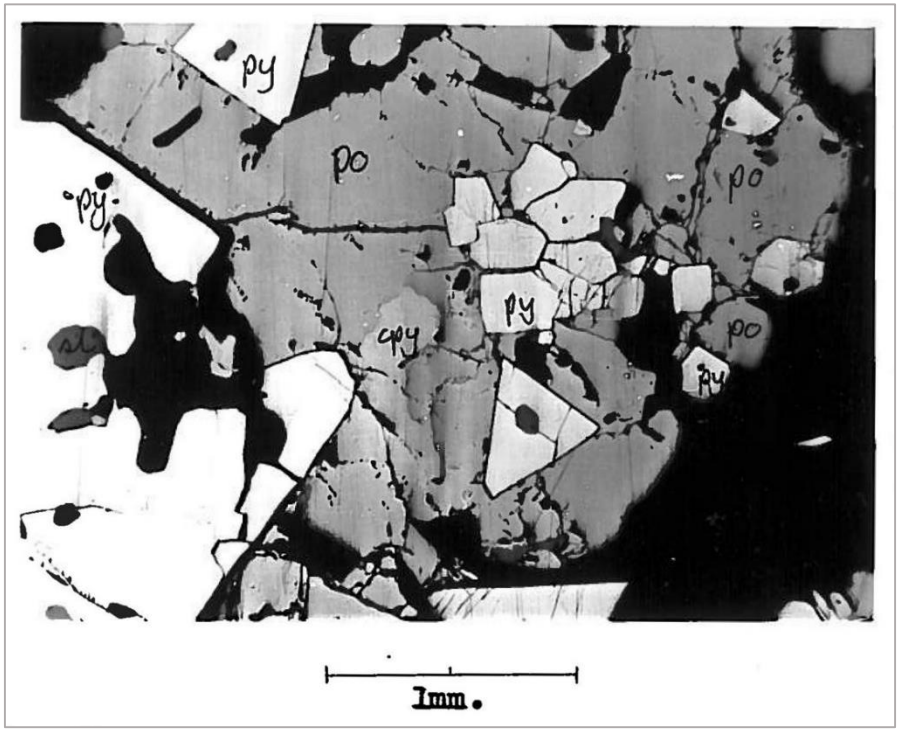


Figure 23: Drillhole 216, 42.8 m down, lens B. Pyrrhotite mineralisation with pyrite porphyroblasts and some chalcopyrite, magnetite and sphalerite. (Bakke, 1975)

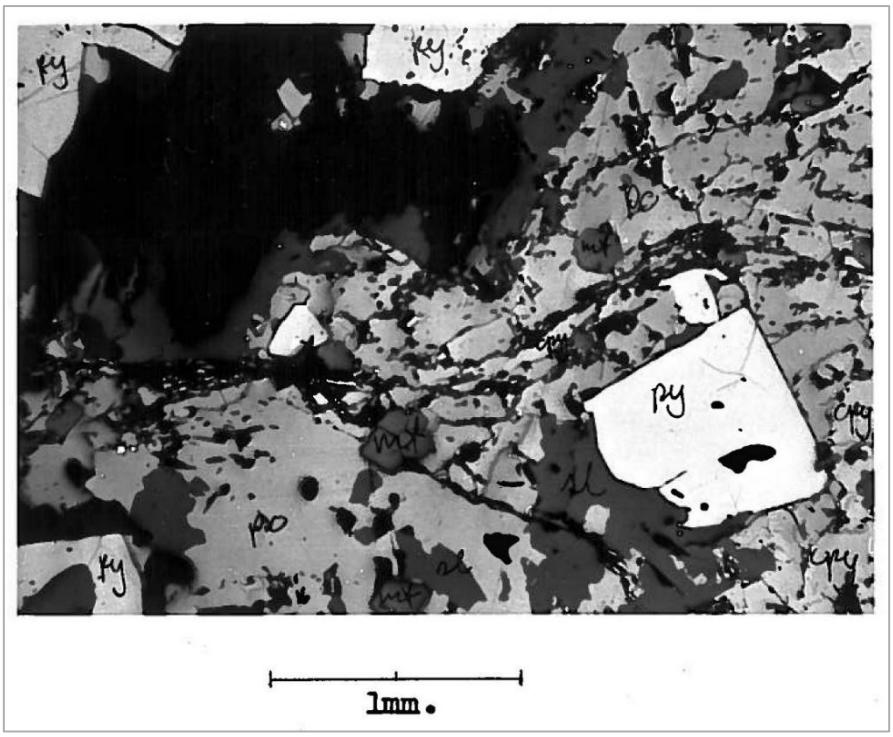


Figure 24: Drillhole 220, 15.25 m down, lens C. Foliated pyrrhotite mineralisation with pyrite porphyroblasts, chalcopyrite, sphalerite, and magnetite. (Bakke, 1975)

There is a general increase in pyrite grain size with increasing grades of metamorphism, and it assumes distinct grain shapes dependent on the volumetric proportions of pyrite in relation to other minerals present, both sulfides and gangue (Craig & Vokes, 1993). Where it occurs as monomineralic polycrystalline masses, pyrite tends to develop annealing textures characterised by 120º triple junctions, where recrystallization minimises the areas of grain surface and interfacial tension. However, with higher proportions of other minerals, as in heterogeneous iron-sulfide-bearing ores, pyrite tends to recrystallize as euhedral cubic porphyroblasts, whereas chalcopyrite, pyrrhotite, and sphalerite tend to develop equant anhedral forms (Craig & Vaughan, 1994), as seen in the Hessjø deposit. The increase in grain size or recrystallization of pyrite into annealed textures requires movement of iron and sulfur to permit nucleation or growth on pre-existing surfaces (Craig & Vokes, 1993).

Deformation in ores is often evidenced by fracturing or brecciation of ore and gangue minerals, especially of the more refractory minerals. Moderate deformation will result in considerable brecciation of massive pyrite or magnetite (Figure 26) where all the strain is relieved by brittle fracturing. In contrast, pyrite in combination with pyrrhotite or chalcopyrite usually shows little or no brecciation, even under extreme deformation, as the strain is absorbed by the softer minerals. Local brecciation of pyrite can occur where pyrite grains impinge upon one another (Craig & Vaughan, 1994), though fracturing of individual pyrite grains is also not uncommon in Caledonian sulfide deposits (Craig & Vokes, 1992). A particularly good example of this is present in lens B of the Hessjø deposit, and displayed in Figure 25. Here, the pyrite crystal shows tendencies of rotation. In fault zones and in ores that have suffered penetrative high-grade

metamorphism, softer ore minerals (galena, chalcopyrite, pyrrhotite, and sphalerite) are forced into the resulting relatively low pressure areas, or injected into fractures and cleavages in the more brittle ore and gangue minerals (Craig & Vaughan, 1994). Such signs of migration and remobilisation are common in metamorphosed sulfide deposits, and are also evident in the Hessjø deposit, as seen in Figure 13, Figure 14, Figure 26, and Figure 27, and mentioned by Bakke (1975) in the descriptions of the minerals in lens A (see chapter 2.1.1.2.1).

In zones of intense deformation, the mineralogical character of the ore may be a factor that contributes to the removal of premetamorphic features and to the development of chaotic textures. This is especially true of ores rich in pyrrhotite, chalcopyrite, and galena, all of which suffer dramatic loss of shearing strength as temperature rises (Craig & Vaughan, 1994). Even though the softer ore minerals do not preserve primary and secondary textures to the extent that pyrite does, several characteristics can still be discerned.

Chalcopyrite can show a variety of textural habits, which mainly depend on the degree of metamorphism. As in the case for most other sulfides, recrystallization and deformation leads to a coarsening of the grain size. Chalcopyrite can also develop deformation twin lamellae, though they may be destroyed at higher metamorphic grades (Craig & Vokes, 1992). As mentioned by Bakke (1975), chalcopyrite in lens A displays unoriented twin lamellae under cross-polarized light (chapter 2.1.1.2.1).

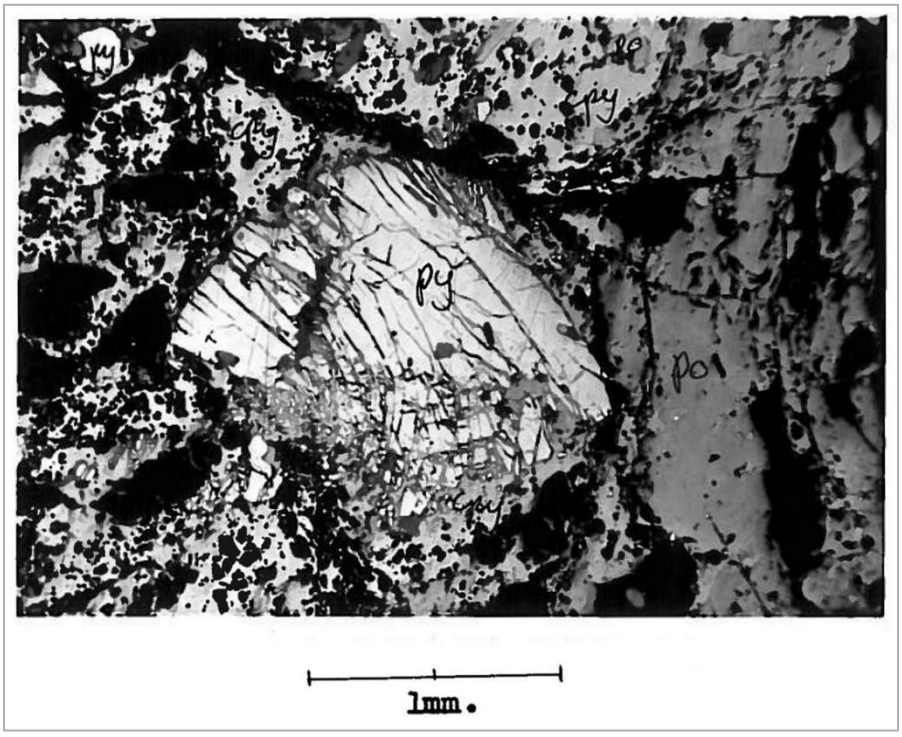


Figure 25: Drillhole 228, 114.2 m down, lens B. Fractured and folded pyrite crystal with chalcopyrite infillings, situated in pyrrhotite with additional magnetite and sphalerite. (Bakke, 1975)

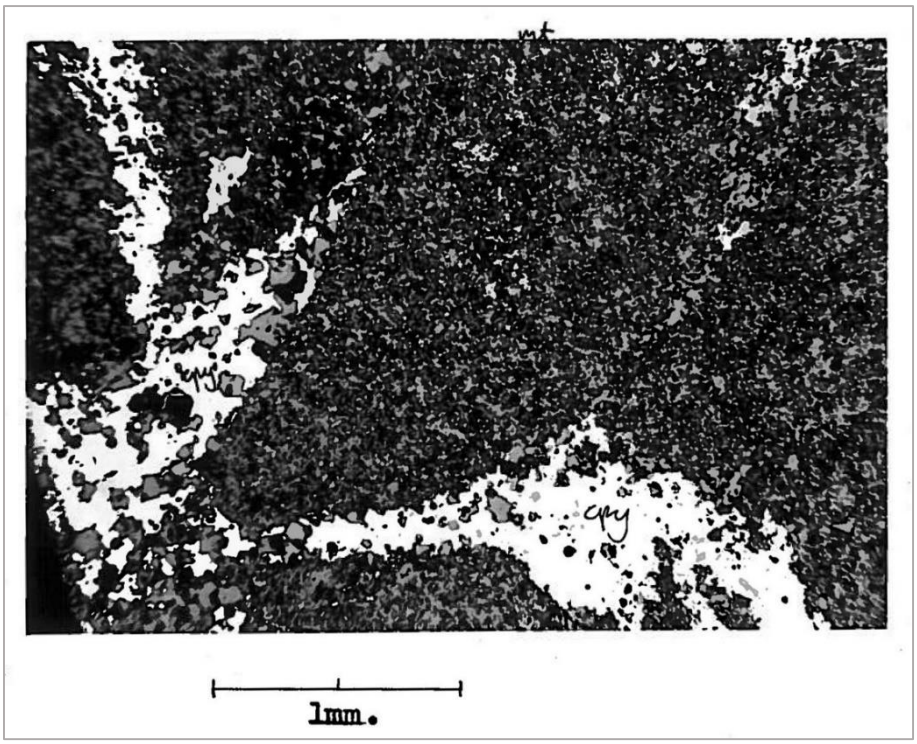


Figure 26: Drillhole 312, 468.5 m down, lens A. Brecciated magnetite with chalcopyrite infilling. (Bakke, 1975)

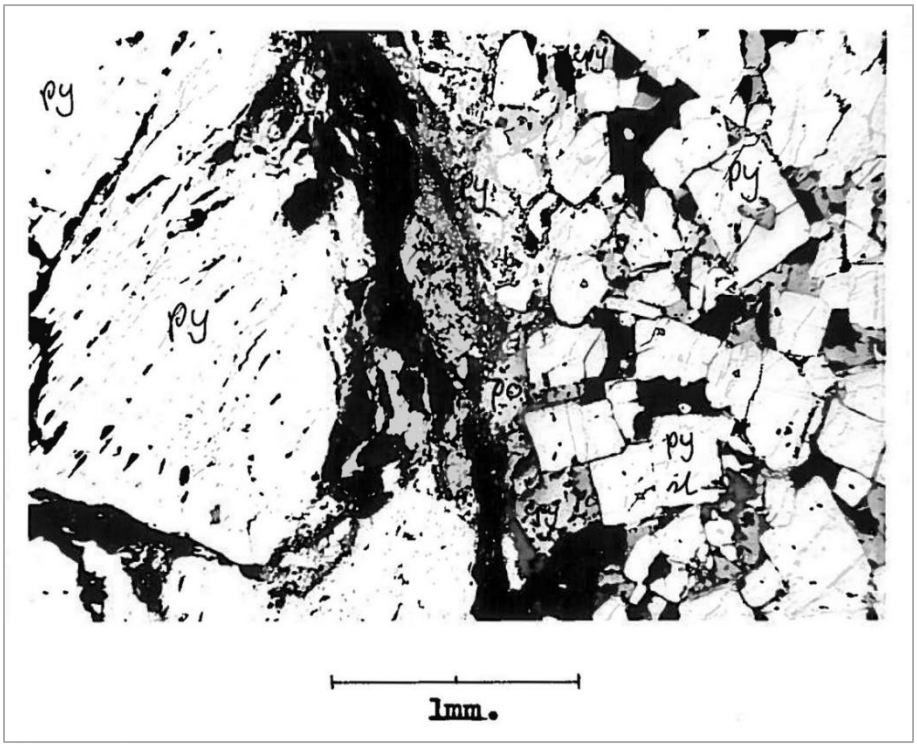


Figure 27: Drillhole 227, 101.6 m down, lens B. Tectonized border between coarse grained and medium grained pyrite, with chalcopyrite, pyrrhotite, and some magnetite and sphalerite. (Bakke, 1975)

In unmetamorphosed stratabound sulfide ores, sphalerite commonly contains micron-sized inclusions of chalcopyrite in the form of randomly dispersed or crystallographically oriented rows of blebs and rods, a texture termed *chalcopyrite disease* by Barton Bethke (1987) (example given in Figure 28). During metamorphism, the sphalerite is commonly recrystallized and homogenized, and the finely dispersed chalcopyrite is redistributed and concentrated as grains or rims along sphalerite grain boundaries (Craig & Vaughan, 1994). Though this texture was long interpreted to be a result of exsolution, Barton & Bethke (1987) concluded that it results from either epitaxial growth, or the replacement of sphalerite by copper-rich fluids, reacting with the sphalerite after initial formation. To greater or lesser extent, remnants of this texture can often be seen in metamorphosed sulfide deposits. In the upper right corner of Figure 10, within the sphalerite, it is possible to observe what might be signs of 'chalcopyrite disease'. This is further supported by Bakke's (1975) remark on droplet shaped inclusions of chalcopyrite in sphalerite (chapter 2.1.1.2.1). Zoomed in version of Figure 10 with higher contrast is given in Figure 29.

Bakke (1975, p.25) mentions that the pyrrhotite in lens A displays flame-like lamellae under cross-polarized light. One possible explanation of this texture, given by Craig & Vaughan (1994, p.136), is that "the removal of iron from hexagonal pyrrhotite results in an increase in the sulfur-to-metal ratio and the formation of monoclinic pyrrhotite", and this often results in what looks likes flames along the margins of fractures.

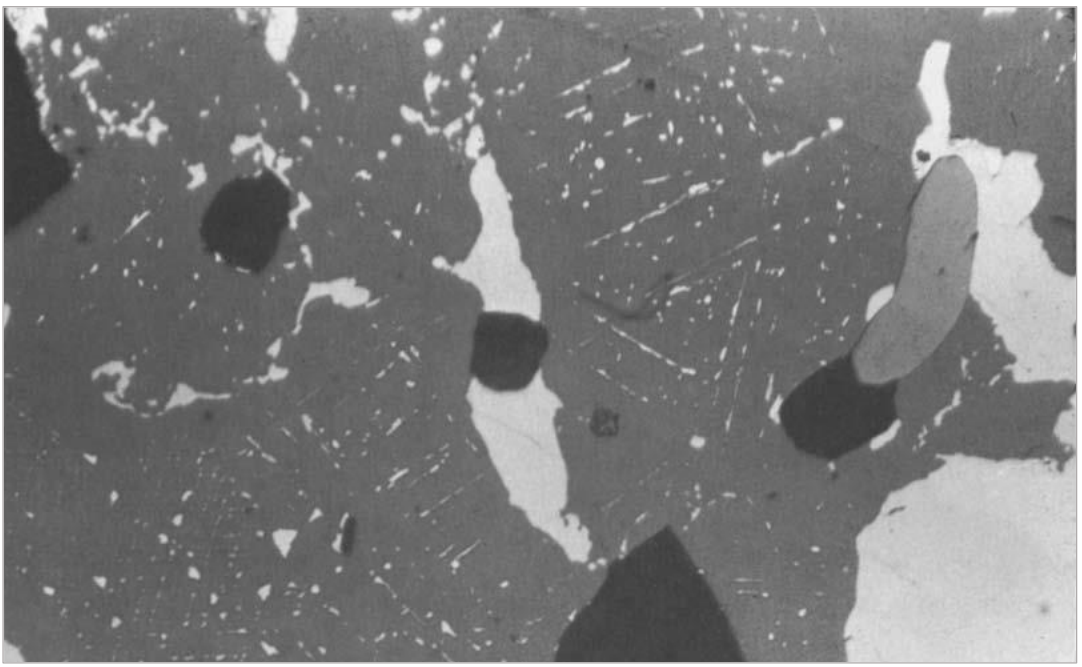

Figure 28: 'Chalcopyrite disease' texture with fine chalcopyrite blebs and rods in sphalerite (dark grey) intergrown with chalcopyrite (light) and gangue (black). Gossan Lead, Virginia. Width of field: 1.1 mm, ordinary reflected light. Figure from Craig & Vokes (1992, p.105).


Figure 29: Excerpt of Figure 10, modified with higher contrast. Indications of ‘chalcopyrite disease’ in sphalerite (sl), see text for further explanation. Figure modified from Bakke (1975).

## 2.2 Geostatistics and modelling

### 2.2.1 Geostatistics

*Geostatistics* is a collective term used for a group of estimation techniques used to estimate the value and distribution of spatial and spatiotemporal phenomena (Ellefmo & Larsen, 2013). The techniques were originally developed as a means to predict probability distributions or ore grades in the mining industry, but has evolved to be applied in essentially any discipline that exhibits spatial variability, e.g. hydrology, meteorology, and forestry, in addition to geology. While interpolation is a key aspect, geostatistical methodology extends far beyond simple interpolation problems.

Spatial data collection can never be complete, resulting in uncertainties regarding the non-sampled areas. Even if these uncertainties can be reduced with additional sampling, there is always the question of the cost/benefit balance, and thus, geostatistics offers a means to quantify the uncertainty, while leveraging the existing data to support sampling optimisation (Zhang, 2011).

While classical statistics only examines the statistical distribution of a set of sampled data, geostatistics also incorporates the spatial correlation among the sample data (Zhang, 2011). This is executed by the use of regionalised variables, which hold characteristics in between fully random and fully deterministic variables. They also have a spatial and sometimes structural dependency.

A complete geostatistical analysis would incorporate the following steps:

1. Initial analysis of data
2. Modelling/generation of a variogram
3. Estimation/simulation
   (Ellefmo & Larsen, 2013, p.14)

#### 2.2.1.1 Semivariogram modelling

Most interpolation techniques are built on the assumption that things that are close to one another are more alike than those farther away. In step two given in the list above, a variogram analysis is performed, resulting in a model, or an experimental variogram (also called a semivariogram), giving a characterisation of the spatial correlation between the regionalised variables. The experimental variogram is given by

$$\hat{\gamma}(h) = \frac{1}{2N(h)} \sum_{i=1}^{N(h)} [z(x_i + h) - z(x_i)]^2 \tag{2.1}$$

where:

- *N(h)* is the number of pairs separated by lag *h*
- *h* is the lag width or the distance between pairs of points
- *z* is the value in the given point
  (Ellefmo & Larsen, 2013, p.21)

As the experimental variogram only gives values correspondent to the sampled data points, it is necessary to fit a continuous function to the given variogram, resulting in a semivariogram model. This is then employed in step three: estimation and simulation.

There are numerous possibilities when choosing a model to fit the experimental variogram, but some are more often used than others. The following list provides the most commonly used semivariogram models:

- The linear model
- The generalised linear model
- The spherical model
- The exponential model
- The Gaussian model
- The Hole effect model
  (Edumine/Clark & Harper, 2014)

As Leapfrog Geo mainly uses two interpolation functions (see chapter 2.2.2), a linear interpolant function, equivalent to the linear semivariogram model, and a spheroidal interpolant function, closely resembling a spherical model, only the linear and spherical model will be presented here.

#### 2.2.1.1.1 The linear semivariogram model

The linear semivariogram is the simplest model applicable, being a straight line with a positive slope intercepting the γ-axis at either zero or a positive value. This intercept, dubbed the *nugget effect*, is common to many semivariogram models, especially in connection to ore deposits, but the effect can also be due to sampling errors (Edumine/Clark & Harper, 2014). In mining, the nugget effect can be defined as

> Anomalously high precious metal assays resulting from the analysis of samples that may not adequately represent the composition of the bulk material tested due to non-uniform distribution of high-grade nuggets in the material to be sampled. (Mineralogy Database, n.d.-b)

Figure 30 gives the shape and equations inherent to the linear semivariogram model.

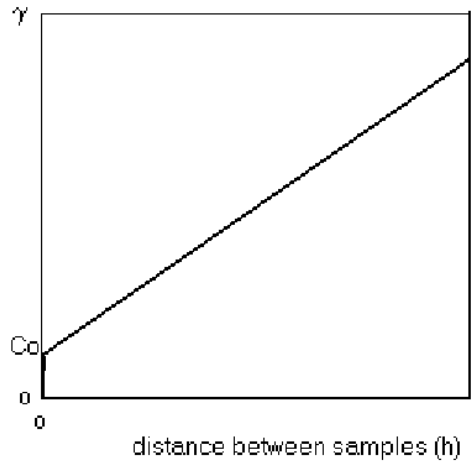


$$\gamma(0) = 0$$
$$\gamma(h) = C_0 + ph \quad when \;\; h > 0 \qquad (2.2)$$

where:
$h$ : the distance between two points of interest
$p$ : the slope of the line
$C_0$ : the nugget effect on the γ-axis

Figure 30: Linear semivariogram model. (Edumine/Clark & Harper, 2014)

#### 2.2.1.1.2 The spherical semivariogram model

The spherical semivariogram model represents the non-overlap of two spheres of influence. Its main equation is cubic as it expresses volumes, and depends on two parameters: the range of influence, (denoted as *a*), and the sill, or plateau ($C + C_0$), which is reached at the range. The range of influence is interpreted as the distance beyond which pairs of sample values are unrelated. A nugget effect ($C_0$), as for the linear model, can also be present here (Edumine/Clark & Harper, 2014).

Figure 31 gives the shape and equations inherent to the spherical semivariogram model.

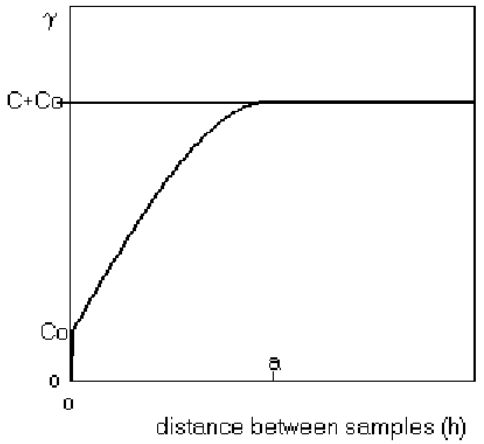


$$\gamma(0) = 0$$
$$\gamma(h) = C_0 + C\left(\frac{3}{2}\frac{h}{a} - \frac{1}{2}\frac{h^3}{a^3}\right) \; when \; 0 < h < a \qquad (2.3)$$
$$\gamma(h) = C_0 + C \quad when \;\; h > a$$

where:
$h$ : the distance between two points of interest
$a$ : the range of influence of the semivariogram
$C$ : the sill of the spherical component
$C_0$ : the nugget effect on the γ-axis

Figure 31: Spherical semivariogram model. (Edumine/Clark & Harper, 2014)

#### 2.2.1.2 Estimation and simulation

Two groups of methods within geostatistics are associated with the prediction of unknown values at points within a spatial demarcation: estimation, and simulation. While both forms of prediction use the semivariogram model as a basis, the resulting outcomes are different.

In estimation, a single, statistically "best" estimate of an unknown point is produced, and by estimating the value of all unknown points, it is possible to produce a map showing the overall spatial occurrence. The estimation is based on both the sample data and on the semivariogram model that most accurately describes the spatial correlation of the sample data (Zhang, 2011). However, this method does not guaranty that the estimated values concurs with the semivariogram and variance of the original data, as smoothing of the data is necessary when constructing the model, and thus the spread of the data is not conserved. This single estimate or map is usually produced using the kriging technique. Kriging is based on the regionalised variable theory which assumes that the spatial variation in the phenomenon represented by z-values is statistically homogeneous throughout a given surface (more on kriging in chapter 2.2.1.2.1).

Several other estimation techniques are also available, from the simplest form of arithmetic mean, to methods such as *natural neighbour* and *inverse distance weighting* (*IDW*, mentioned briefly in chapter 2.2.1.2.1) and other multivariate interpolation methods (Ellefmo & Larsen, 2013).

While estimation gives the most probable realisation, simulation produces several possible realisations, or maps/images, of the property distribution, all having approximately the same semivariogram and variance as the original data (Ellefmo & Larsen, 2013). Differences between the alternative realisations provide a measure of quantifying the uncertainty of estimates, be it oil volumes, grades above cut-off, or risk of pollution; this is an option not available when using only kriging estimation (Zhang, 2011). Theoretically, an average of the simulations should be close to the surface produced by kriging (Ellefmo & Larsen, 2013).

Figure 32 and Figure 33 provides an overview of the workflow associated with estimation and simulation, respectively.

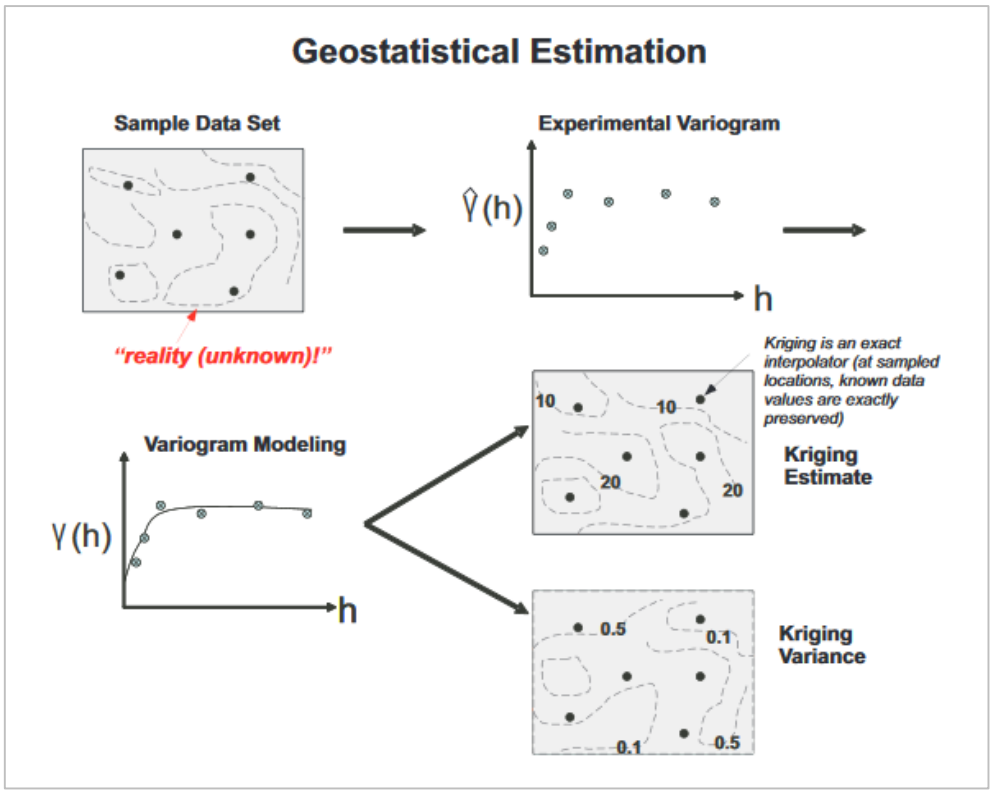


Figure 32: Geostatistical estimation workflow. (Zhang, 2011)

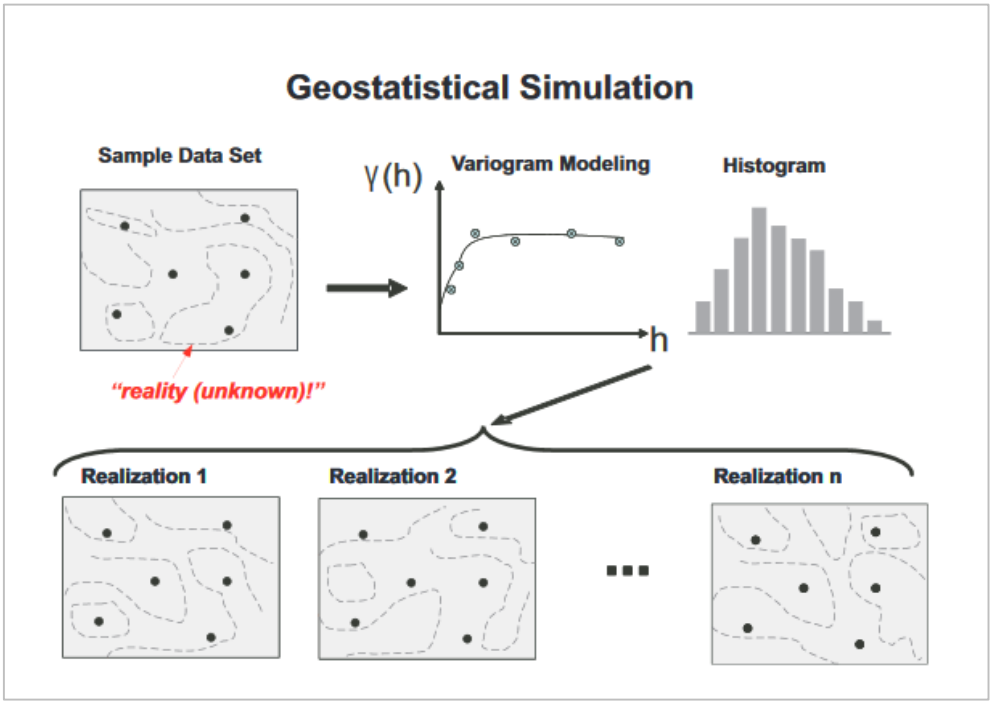


Figure 33: Geostatistical simulation workflow. (Zhang, 2011)

#### 2.2.1.2.1 Kriging

A general overview of the basic properties of kriging is presented here, so as to be able to review the differences between kriging and dual kriging, the latter representing the principal interpolation process used Leapfrog Geo (see chapter 2.2.2.3). The complete mathematics concerning kriging is beyond the scope of this thesis.

Kriging is an advanced geostatistical procedure that generates an estimated surface from a scattered set of data points. Many geological phenomena can be evaluated as regionalised variables, and as they often exhibit a certain degree of continuity, they can be assumed to be spatially correlated, at least over shorter distances. The further away two points of interest are, the higher the likelihood of statistical independence becomes. As previously mentioned, the degree of spatial correlation between regionalised variables can be expressed through a semivariogram. Kriging uses the information from the semivariogram to describe the correlation between known points, and further find an optimal set of weights used to estimate the value at an unknown point. As the semivariogram is a function of distance, the value of the weights changes according to the spatial distribution of the known data points (Ellefmo & Larsen, 2013). Kriging as presented in the mathematical framework of geostatistics is simply the *best linear unbiased estimator (BLUE)* of a random function (Trochu, 1993), i.e. that the estimated value is determined so as to minimize the estimation variance, and that differences between the estimated values and the real values are in average equal to zero, given the same point (Ellefmo & Larsen, 2013).

Kriging is similar to IDW in that it weights the surrounding measured values to derive a prediction for an unmeasured location. The general formula for both interpolators is formed as a weighted sum of the data:

$$\hat{Z}(x_0) = \sum_{i=1}^{N} \lambda_i \, Z(x_i) \tag{2.4}$$

where:

- $Z(x_i)$ : the measured value at the *i*-th location
- $\lambda_i$ : an unknown weight for the measured value at the *i*-th location
- $x_0$ : the prediction location
- $N$ : the number of measured values
  (ESRI, 2016)

Where with IDW, the weight $\lambda_i$ depends only on the distance to the prediction point, kriging weights are in addition determined from the overall spatial arrangement of the measured points. This is where the spatial autocorrelation portrayed through the semivariogram is applied (ESRI, 2016).

Kriging is essentially a family of generalised least-squares regression algorithms, giving rise to various kriging estimators. A very brief account of some of the more commonly used estimators is presented below, given by Goovaerts (1997, pp.126-27):

- *Simple kriging* considers the mean $m(x)$ of the regionalised variable to be known and constant throughout the study area:

$$m(x) = m, \quad known \tag{2.5}$$

- *Ordinary kriging* accounts for local fluctuations of the mean by limiting the domain of stationarity of the mean to a given local neighbourhood:

$$m(x') = constant\ but\ unknown \tag{2.6}$$

- *Universal kriging* considers that the unknown local mean $m(x')$ smoothly varies within each given local neighbourhood, hence over the entire study area. The component $m(x)$ is modelled as a linear combination of functions $f_k(x)$ of the coordinates:

$$m(x') = \sum_{k=0}^{K} a_k(x') f_k(x') \tag{2.7}$$
$$\text{where } a_k(x') \approx a_k \quad constant\ but\ unknown$$

  The coefficients $a_k(x')$ are unknown and deemed constant within each given local neighbourhood.

### 2.2.1.3 General limitations of geostatistics

Geostatistical models are mathematical objects, not geological objects, and mathematical functions cannot entirely describe the complexity of reality. It is therefore important to remember that geostatistics is a set of numerical tools, and does not replace professional geological insight and experience, i.e. geostatistics cannot produce good results from bad data (Zhang, 2011). There is also the question of which estimation method is best for a given situation, and kriging need not be the most appropriate estimation method.

A semivariogram model is only an approximation of the spatial variability of the available samples, and these are not necessarily always representative for the real conditions. It is possible to measure how well a model represents the spatial variability of the samples by cross-validation (EduMine, 2010a), but as there is no accepted universal algorithm for determining a semivariogram model, the cross-validation does not guarantee that an estimation procedure will produce good estimates at unsampled locations. The most consequential decisions of any geostatistical study are therefore made early in the exploratory data analysis (Journel, 1989).

### 2.2.2 Leapfrog Geo

Leapfrog Geo is a 3D geological modelling software developed and owned by ARANZ Geo Limited, and is furthermore the main software used in this thesis to evaluate the Hessjø deposit. The first version of Leapfrog was released in 2003. Leapfrog Geo implements implicit modelling by using Fast Radial Basis Functions as its primary computation engine, with drillhole data as the primary input factor.

The initial workflow and supported file formats used in Leapfrog Geo was reviewed in the project thesis preceding this master thesis, see Nørsett (2015).

#### 2.2.2.1 Implicit modelling and RBF

While traditional methods of explicitly defining 3D geological boundaries, where complex surface geometry is built up by digitising points that lie on a surface, is a time-consuming, manual process, the introduction of fast 3D interpolation methods has provided a practical alternative to explicit modelling. Such fast 3D interpolation methods are often referred to as *implicit modelling*, where volume functions are used to construct geological surfaces. Unlike explicit modelling, surfaces contained in volume functions are not explicitly defined, but rather as a continuous mathematical representation of an attribute across a volume, making it possible to define various surface criteria before extracting a tangible surface. The volume function is modelled from spatially interpolating sampled drillhole data (Cowan et al., 2003).

Imperative to implicit modelling is the use of a practical 3D interpolation method to construct the volume functions. Radial Basis Functions (RBF) has proven useful for this purpose, though they are not without their limitations.

Radial basis functions are a family of interpolation functions, and RBF interpolation represents the function as a sum of so-called basic functions, with linear weights in the same way as the dual formation of kriging (Cowan et al., 2003). When kriging is implemented as an interpolation, it is known as *dual kriging* (Lane/ARANZ Geo, 2013) (see chapter 2.2.2.3). While kriging uses the semivariogram model obtained from sampled data set, RBF uses a basic function that is chosen from a standard set. This set includes a function, called the biharmonic function, which corresponds to a linear variogram without a sill. RBF interpolation has proven to be a valuable technique, especially in situations where a semivariogram cannot be obtained, and it is suitable for modelling lithological boundaries, as there is no satisfactory mathematical description of how a geological surface must behave, other than the recognition of sample contacts.

As RBF interpolation is a global interpolation method, requiring all data points to be used in calculation of the coefficients, limitations arise in regards to large datasets and data storage problems. This, in turn, requires substantial computational power and time (Cowan et al., 2003).

Even though RBF was first introduced in the geological literature by Hardy (1971) in early 1970s, the severe limitation of RBF to process large datasets has limited the application of RBF when it comes to geological use. However, towards the end of the 1990s, a method for overcoming the limitations of direct RBF interpolation was developed, commonly known as a fast

form of RBF interpolation. Details regarding the mathematics behind this method is beyond the scope of this thesis, but it is based on the notion that infinite precision is neither required nor expected when performing RBF computations, allowing the use of approximation. The computation of the coefficients can therefore be simplified to within a predetermined accuracy, which, when assessing assay data, is set to a fraction of the detection limit. This fast numerical method eliminates the memory storage problem, as well as being able to globally interpolate very large datasets at high speeds (within minutes or hours). The fast RBF method is the first practical 3D interpolation method available to process large datasets, such as complete mine drillhole data sets (Beatson, et al., 1999; Cowan, et al., 2003).

Leapfrog uses their own version of fast RBF interpolation, a set of algorithms called *FastRBF™*, to produce dynamic implicit models (ARANZ Geo, n.d.).

#### 2.2.2.2 Interpolant functions in Leapfrog Geo

In Leapfrog Geo, the FastRBF™ algorithm employs interpolation functions to estimate values from known data, before producing dynamic implicit models for visualisation and further processing of ore grades from assay data, e.g. to produce grade shells. Values that can be interpolated include down-drillhole numeric data or points data. Leapfrog uses two main interpolant functions: the linear interpolant function, and the spheroidal interpolant function, to determine the weighting given to each sample value (ARANZ Geo, 2014).

The interpolant functions indicate how the function values are expected to vary as the distance between points increases, as sample values are expected to vary more at a greater distance from the estimation point than closer to it. The interpolant function in Leapfrog is equivalent to the semivariogram used in geostatistical modelling/estimation techniques (McLennan/ARANZ Geo, 2013).

When selecting *new interpolant* and applying it to the designated data set, Leapfrog generates a default model using the linear interpolant. This can later be changed.

##### 2.2.2.2.1 Linear interpolant

The basic principle of the linear interpolant (Figure 34) is that data closer to the chosen point of estimation, is deemed more important than data that is further away. This importance is therefore inversely proportional to the distance from the estimation point, making it equivalent to a linear semivariogram (Spragg/ARANZ Geo, 2013), see chapter 2.2.1.1.1: *The linear semivariogram* model.

A linear interpolant function will strongly reflect the sample values close to the estimation point, and it extrapolates aggressively out from the data (McLennan/ARANZ Geo, 2013). Therefore, extrapolation of the linear interpolant function at large distances will often give unrealistic results. It is, however, fast, making it adequate for an initial interpolant so as to be able to view trends (Spragg/ARANZ Geo, 2013).

The base linear interpolant function is multi-scale, therefore good for general purpose modelling, and it works well for lithology data, which typically has localised areas of high-resolution data. On the other side, it does not work well with values which have distinct finite range of influence, and most grade data does not interpolate well when using the linear function (McLennan/ARANZ Geo, 2013).

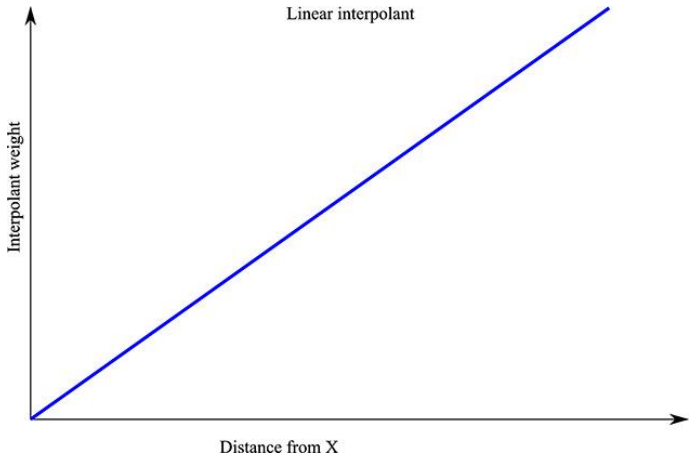


Figure 34: Principle of the linear interpolant used in Leapfrog Geo (Spragg/ARANZ Geo, 2013)

#### 2.2.2.2.2 Spheroidal interpolant

As mentioned in the previous subchapter, the extrapolation of the linear interpolant function at large distances is often unrealistic. When modelling most metallic ore deposits, there is a finite range beyond which the influence of the data on the estimation point should move towards zero, i.e. the sample values are nearing independence of each other, giving no influence (McLennan/ARANZ Geo, 2013). Using the spheroidal interpolant (Figure 35) in Leapfrog Geo, all sample values that lie beyond a set distance, called the range, from the estimation point, are given approximately the same weighting and therefore the same influence (Spragg/ARANZ Geo, 2013).

The spheroidal interpolant function in Leapfrog is an approximation of the finite range spherical semivariogram (see chapter 2.2.1.1.2), while still forming a smooth interpolant (McLennan/ARANZ Geo, 2013).

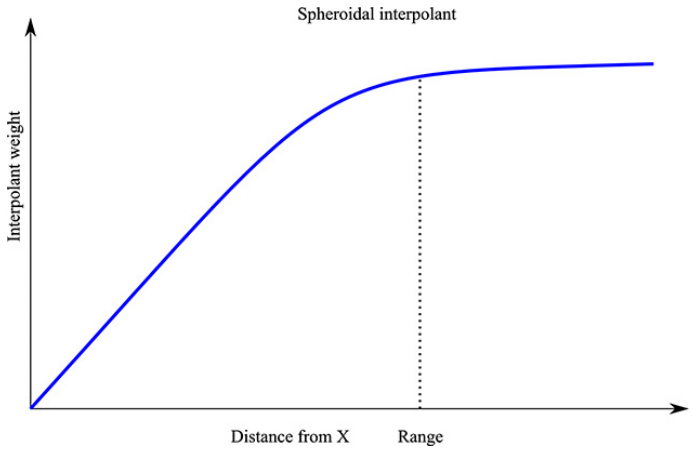


Figure 35: Principle of the spheroidal interpolant used in Leapfrog Geo (Spragg/ARANZ Geo, 2013)

#### 2.2.2.2.3 Parameters

In Leapfrog Geo, the shape of the interpolant function determines how it affects the interpolant, rather than the actual value. If you scale the interpolant function by a constant value, then the interpolant and any evaluations of it will be unchanged (McLennan/ARANZ Geo, 2013).

Both interpolant functions use the same key parameters, making it easy to switch between the two functions. However, unlike the spheroidal interpolant function, the linear interpolant function does not have a *range* in a traditional geostatistical manner. Furthermore, if there is no *nugget* value added, the function is multi-scale, effectively making the linear interpolant non-sensitive to the scale of the input data (McLennan/ARANZ Geo, 2013). An example of the editing window used for adjusting the main parameters in Leapfrog is shown in Figure 36. The following subsections describe the main interpolant parameters available for adjustment in Leapfrog Geo.

##### *Sill*

For the spheroidal interpolant function, the sill defines the upper limit where the correlation between values is minimized. While a spherical semivariogram reaches the sill at the range and does not increase any further beyond this, the spheroidal interpolant approaches the sill near the range and continues asymptotically beyond the range (ARANZ Geo, 2014). During a course on Leapfrog Geo given by Niklas Sääv, it was noted that it is good practice to set the sill value to the variance calculated by Leapfrog (N. Sääv, personal communication, April 21st 2016).

##### *Base range*

The base range is the distance where the interpolant value is 96% of the sill value, given there is no nugget value set. As a rule of thumb, it may be set approximately twice the average distance between the drillholes (ARANZ Geo, 2014), though ideally a variogram analysis prior to modelling should be performed, thus indicating the correct base range value.

A linear semivariogram is defined by the slope and has no sill or range to speak of. The same is true for the linear interpolant, but in Leapfrog Geo the sill and base range values are instead used to set the slope, where the base range is the distance at which the interpolant value is at the sill.

The use of these two parameters instead of a single gradient permits easy switching between a linear and a spheroidal interpolant (ARANZ Geo, 2014).

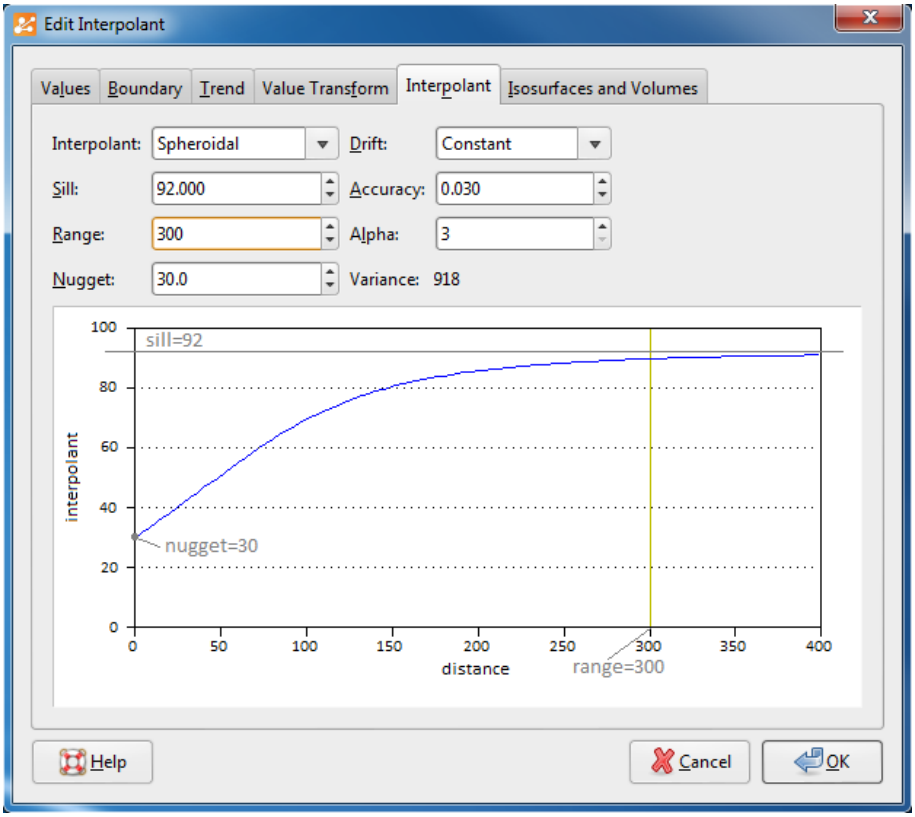


Figure 36: Example of interpolant editing window in Leapfrog Geo (McLennan/ARANZ Geo, 2013)

### *Nugget*

For both the linear and the spheroidal interpolant, the nugget represents a local anomaly that is substantially different from the otherwise predicted value at the given point, based on the surrounding data. When increasing the nugget value, more emphasis is placed on the surrounding sample values than on the actual values at the given point. This can be used to reduce noise caused by, for example, inaccurately measured samples (ARANZ Geo, 2014). As a rule of thumb, the nugget value can be set to 5-15% of the sill value (N. Sääv, personal communication, April 21st 2016).

### *Alpha*

The alpha is a constant that is only available for the spheroidal interpolant, and determines how steeply the interpolant rises towards the sill. The available alpha values are 3, 5, 7, and 9, where a low alpha will produce a more steeply rising curve than a high alpha value. An alpha of 9 generates the curve closest in shape to a spherical semivariogram, which in most cases will provide the most accurate results. However, a high alpha value requires more time and computational processing power as a more complex approximation function is used, and for large datasets, a lower alpha value is often chosen for practical reasons.

*Drift*

The drift evaluates how the values distributes away from the data, and for a spheroidal interpolant function, it can be set to *constant*, *linear*, or *none*.

- Constant: the interpolant will go to the approximated declustered mean of the data.
- Linear: the interpolant will behave linearly away from the data; this may result in negative values.
- None: the interpolant will pull down to zero away from the data.
  (ARANZ Geo, 2014, p.257)

For a linear interpolant function, it is possible to choose either the constant or the linear drift model.

*Accuracy*

The accuracy determines how tightly the interpolating process adheres to the data. Ideally this value should not be set finer than the errors in the data (McLennan/ARANZ Geo, 2013). For example, if values are specified to two decimal places, setting the accuracy to 0.001 is more than adequate. Any lower values would cause the interpolation to process more slowly and degrade the interpolation results. This is valid for both the linear and the spheroidal interpolant function.

In addition, it is possible to apply a trend to an interpolant, either using a global trend set from a moving plane, or a structural trend set from e.g. meshes (ARANZ Geo, 2014).

#### 2.2.2.3 Dual kriging

When kriging is implemented as an interpolation it is known as *dual kriging*, and RBFs, which are used as the primary computation engine in Leapfrog Geo, are effectively a way of implementing dual kriging (Lane/ARANZ Geo, 2013). The dual kriging method was first developed in 1985 by Trochu (Trochu, 1993).

While classical kriging is usually implemented as a local estimation method, i.e. the procedure requires the solution of a new system of equations for each interpolated value, dual kriging can be regarded as another representation of kriging through which the estimates are expressed as linear combinations of covariance values instead of data values (Journel, 1989). One distinct advantage of dual kriging when contouring very large data sets, is that it is a global estimation kriging method, where the kriging system is evaluated only once for the whole domain by simultaneously using the information provided by all data points (Trochu, 1993). Effectively, the dual kriging weights are equivalent to a variogram model, and rather than solve the equations directly which is slow, Leapfrog Geo uses advanced algorithms to find the dual Kriging weights and evaluate the estimates quickly (Lane/ARANZ Geo, 2013).

For a more in depth review of dual kriging and its applicable equations, the reader is referred to the works of, for example, Trochu (1993) and Goovaerts (1997).

## 2.3 Resource classification

Mineral resource classification concerns the classification of mineral deposits by evaluation of their geologic certainty and economic value. An overview of codes for the reporting of mineral resources and reserves, with a particular focus on the JORC code, was presented in the project thesis preceding this master thesis. As for the scope of this thesis, a qualitative resource classification will be performed based on the evaluation of the drillhole spacing used in the Hessjø deposit, compared to that which has been used in other deposits, along with the guidelines given by the 2012 JORC code. Key points of the JORC Code is presented in the subsequent chapter, for further insight and details, the reader is referred to the JORC Code, 2012 edition.

### 2.3.1 The JORC Code

The *Australasian Code for Reporting of Exploration Results, Mineral Resources and Ore Reserves* (the JORC Code) sets out "minimum standards, recommendations and guidelines for Public Reporting in Australasia of Exploration Results, Mineral Resources and Ore Reserves" (JORC, 2012, p.3), and is prepared and published by the Joint Ore Reserves Committee of The Australasian Institute of Mining and Metallurgy, Australian Institute of Geoscientists and Minerals Council of Australia (JORC). The classification system is organised as shown in Figure 37, where mineral deposits, or sections of, can be classified as either an *Exploration Result*, *Mineral Resource* (inferred, indicated, or measured), or *Ore Reserve* (probable or proven). The JORC Code is grounded in three governing principals: *Transparency, Materiality*, and *Competence.*

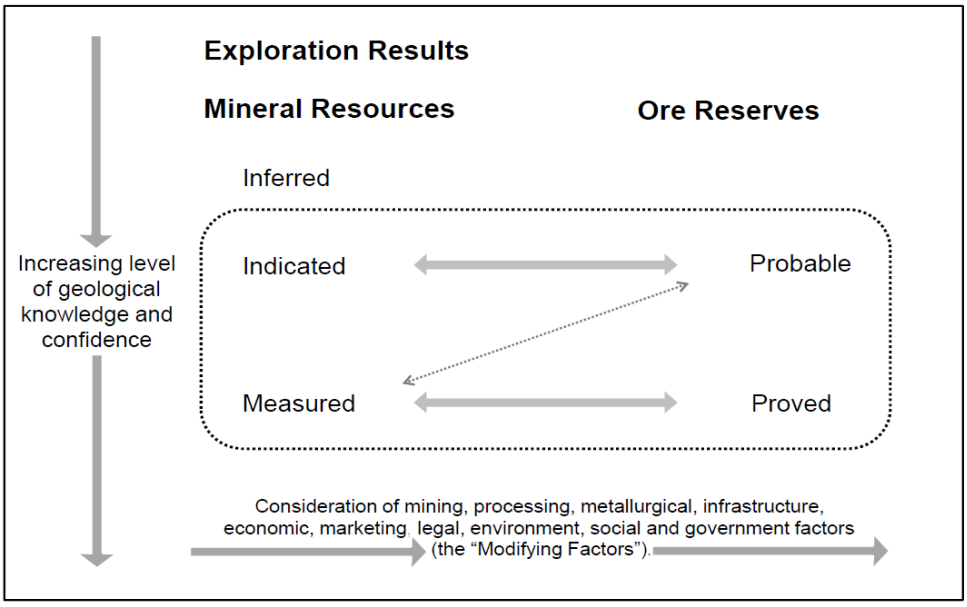


Figure 37: General relationship between exploration results, mineral resources and ore reserves, as defined by JORC (2012, p.9).

Public reports concerning the classification of mineral deposits in accordance with the JORC code, must be prepared by, or under the direction of, a *Competent Person* (CP). A Competent Person must meet certain pre-defined requirements. According to JORC (2012, p.7), a CP must

- have minimum five years of relevant experience in the style of mineralisation or type of deposit under consideration and in the activity which that person is undertaking,
- be a minerals industry professional,
- be a member or fellow of The Australasian Institute of Mining and Metallurgy, or of the Australian Institute of Geoscientists, or of a 'Recognised Professional Organisation'.

A *Mineral Resource* is a mineralisation of potential economic interestof such form, quality, and quantity that there are reasonable prospects for eventual economic extraction. The Mineral Resource is presented as an estimate of tonnage and grade for the mineralised body, and represents a realistic inventory that, under assumed and justifiable technical and economic conditions, possesses the possibility to become economically extractable, wither wholly or partially. Resource estimates are, in fact, *estimates*, not calculations. The requirements for estimating Mineral Resources would be:

- Confident geological interpretation
- High quality, representative samples and assays
- Application of appropriate estimation technique

These requirements are met by:

- Mapping and sampling of the mineralisation
- Ensuring the highest standards of sampling and assaying integrity
- Employing experienced, qualified professionals, i.e. *Competent Persons*

The main factors affecting Mineral Resource estimates are the reliability of the geological interpretation, and the amount, distribution, and quality of the resource data.

An Ore Reserve is an estimate of the tonnage and grade that is expected to be delivered to the mill or treatment plant. It is the economically mineable part of a Mineral Resource, including additional material and losses which may occur when the material is mined. Realistically assumed Modifying Factors, i.e. mining, metallurgical, economic, marketing, legal, environmental, social and governmental factors, must be taken into consideration (Stephenson, 2005; JORC, 2012).

### 2.3.2 Drillhole spacing

Examples of drillhole spacing from feasibility studies of copper deposits that are compliant with the JORC code, are presented here. It is important to bear in mind that these are only examples, and that every deposit is unique. Results from these studies cannot be inferred to be correlatable to the Hessjø deposit, but are helpful in giving an indication as to what drillhole spacing is

commonly used for different deposits. The drillhole spacing used in the Hessjø deposit is presented in chapter 4.3.

*The Calingiri Project* (Caravel Minerals, 2016):

The Calingiri Project in Western Australia consists of three prospects: Bindi, Dasher, and Opie, which are sulfide mineralisations of a porphyry and/or skarn deposit style. The mineralisations consist of typically chalcopyrite ± molybdenite ± magnetite. Highlights of the results include:

- Over 74% of the Mineral Resource is in the Indicated category
- 143 Mt @ 0.38% for 549,800 tonnes copper at a higher cut-off grade of 0.30%
- 530 Mt @ 0.27% for 1,407,900 tonnes copper at a lower cut-off grade of 0.15%
- Resources remain open along strike and at depth, and include higher grade zones from near surface

Drill spacing supporting Indicated Resource is:

- Bindi: 80 m across strike x 200 m along strike
- Dasher: 100 m across strike x 200 m along strike
- Opie: 100 m across strike x 80 m along strike

Drill spacing supporting Inferred Resource is:

- Bindi: 160 m across strike x 200 m along strike
- Dasher: 100 m across strike x 200 m along strike
- Opie: 100 m across strike x 80 m along strike

The following statement was made regarding the classification of the deposit (Caravel Minerals, 2016, p.24):

> The volume of the Mineral Resource models classified as Inferred are based upon limited geological evidence, derived from widely spaced drill hole samples. The geological evidence is sufficient to imply but not verify the geological and grade continuity between drill holes. The majority of the Inferred volumes are located down dip or along strike of the last drill hole intercept of mineralisation, and therefore where drill support is more limited than in the Indicated volumes.

*The Little Eva Deposit* (Altona Mining, 2014):

The Little Eva Deposit is located in Queensland, Australia, and is an iron-oxide-copper-gold style deposit. Highlights include (Altona Mining, 2014, p.21):

- Measured Mineral Resources have been defined in areas of 50 m x 40 m drill spacing with low variance in grade and good grade and geological continuity.

- Indicated Mineral Resources have been defined in areas of 50 m x 40 m drill spacing where grade variance is moderate.
- Inferred Mineral Resources have defined generally in areas of 100 m x 100 m drill spacing.

*The Wee McGregor Project* (Argosy Minerals, 2015):

The Wee MacGregor project is located in Queensland, Australia, and is a shear hosted copper-gold-silver-cobalt mineralisation within amphibolite schist and quartz feldspar porphyry/quartzite host rocks. Highlights include:

- Inferred Resource estimate of 1.65 Mt at 1.6% Cu, containing 25,818t of copper.
- Exploration Target range of 1.0 – 1.5 Mt at 2.5 – 3.7% Cu
- Drillhole data spacing 40 m along strike, 20 m across strike, data spacing sufficient for at least an inferred level resource estimate.

*The Pilbara VMS copper project* (Venture X Resources, 2010):

The Pilbara volcanogenic massive sulfide copper project, in Western Australia, comprises of the Mons Cupri, Whim Creek, and Salt Creek deposits. The deposits are Archean polymetallic (Cu, Zn, Pb, Ag, Au) VMS deposits hosted by volcanogenic sediments. There are two principal styles of mineralisation: stratabound massive sulphide, and stringer/feeder. Highlights include:

- Ore Reserve of 4.5 million tonnes at 2.7% Cu Eq.
- At Mons Cupri and Whim Creek the drillhole spacing within the ore body is generally 15-30 m, with the majority less than 20 m.
- At Salt Creek the drillhole spacing within the ore body is generally 20-50 m.

*The Nussir Project:*

The Nussir project in Northern Norway is a sedimentary copper deposit with possible additional gold and silver, where the Ulveryggen deposit is the most promising mineralisation (Nussir, n.d.). Only extracts of the feasibility study performed by Adam Wheeler was available (Sletten, 2015). Highlights for Ulveryggen include:

- 3.7 million tonnes of indicated resources
- 3.9 million tonnes of measured resources
  (Nussir, n.d.)
- The measured resources are based on a drill grid of 125 m.
- The indicated resources are based on a drill grid of 225 m.
  (Sletten, 2015)

# 3 Methods and data

## 3.1 Evaluation and description of data

The evaluation of the data associated with the Hessjø deposit was commenced during the work with the project thesis written in 2015 (see Nørsett (2015). Further evaluations of the specific datasets have been deemed necessary to be able to apply the data to the geometric and qualimetric 3D-modelling of the Hessjø deposit.

### 3.1.1 Available material

The majority of the data material from the Hessjø deposit is collected in two reports, one by Gvein (1976) and one by Rui (1990). These compilations include analysis tables, core logs, geological and geophysical maps, tonnage calculations, downhole survey tables, and rock strength index tables. The two reports also overlap at times with respect to the material. They are, however, not complete with regards to all data types. This is particularly valid for the downhole surveys, as only four of the total 26 drillholes intersecting lens A have available survey measurements. The survey data is discussed further in chapter 3.1.4.

Another aspect of the data from the Hessjø deposit is the lack of metadata, especially concerning the chemical analysis (chapter 3.1.5) and geographical positioning (chapter 3.1.2).

In addition to the reports mentioned above, several short geophysical reports are available, giving valuable information regarding the continuity of the mineralisation. Also, Bakke's thesis work from 1975 comprises the main geological framework.

In connection with a report on the Hessjø deposit published in 2007, Terje Bjerkgård digitised the majority of the available data into an excel-file, with the exception of lithological data. This file has been the basis for the geometric and qualimetric modelling of the Hessjø deposit. However, adjustments of this file have been necessary, as discussed in the following chapters. The file and its contents will be further referred to as *Bjerkgård's excel-file*, or simply the *excel-file.* For further description of the data for all mineralised lenses in the Hessjø deposit area, see Nørsett (2015) and Bjerkgård (2007).

As Leapfrog Geo expects input drillhole data to be sorted into minimum three tables sorted in separate .csv-files (comma separated values file), a *collar table, survey table,* and *interval tables*, the evaluation of the data follows this same format. Two interval tables have been imported to Leapfrog Geo, containing *lithological data* and *assay data*, respectively.

### 3.1.2 Collar data

The original tables containing analysis data (in Gvein (1976) and Rui (1990)) are also where the data concerning positioning of the drillholes are registered. The geographical positions are given in a local coordinate system that is determined from a grid defined by the magnetic north. The magnetic north is not a constant, and while the direction of the grid was N 12º E in 1948, it had changed to N 9º E in 1976. While it is not impossible to convert the positions to UTM coordinates, it is however, difficult and time consuming. The geological map in Figure 6 contains placements of most of the drillholes, as does several of the geophysical maps (in e.g. Singsaas (1976); Anon. (1985)), and Bjerkgård used this is as a basis in ArcGIS to extract UTM coordinates and elevation data for the drillholes. For the remainder of the drillholes he calculated the coordinates from the original positional data (Bjerkgård, 2015). These are the coordinates for the collar positions provided in the excel-file from Bjerkgård.

Due to apparent difficulties between switching from ArcGIS and Leapfrog Geo, the positions given by Bjerkgård do not concur with the Bakke's geological map when imported into Leapfrog Geo. Among other things, the elevation of the collar positions is generally located below the topographical map. By further inspection of source material, some elevation data was found, from Bakke's 1975 thesis work, and from some of the core logs in Rui (1990). The elevation data in the collar file used in Leapfrog was then changed to include the more accurate positions, for those drillholes where such was found. As can be seen in

Table 5, the difference between Bjerkgård's elevation data and that found in Bakke (1975) and Rui (1990) vary from nil and up to 6.1 m. These adjustments did move the collar positions further toward the topography, but much deviation is still present.

Even though the collar positions do not concur with the geological map, nothing further was done to readjust this. The main reason for this is that no records concerning the procedures and equipment used in the registration of the collar positions have been found, and hence there is no way of knowing the error and uncertainties pertaining the collar coordinates. It is also worth noting that the geological map given in Figure 6 covers an area of 1700 x 1200 m with a scale of 1:2000, so the manual placement of the drillholes on the map would probably cause errors in itself.

However, adjustments have been made to the position of one particular drillhole. When the data was imported into Leapfrog Geo, it was inferred that the position of drillhole 319 was incorrect. It was placed just a couple of meters next to drillhole 320, which is illogical compared to the relative placement of all the other drillholes. The drilling was conducted with a goal of covering the mineralisation in section profiles, as seen in Figure 3; for example, drillholes 232-236 all lie nicely on line with 45-55 m spacing in between. Drillholes 319-322 also lie on a line, with 30-40 m spacing between holes 320-322. Due to a slight difference in onset angle of drillhole 319 and 320, the downhole paths almost cross, and when adding the lithology, it is obvious that adjacent

lithologies do not match. It is also worth noting that the cores from drillhole 319 and 320 were logged by the same person, and should therefore be comparable (see chapter 3.1.3). The collar of drillhole 319 was therefore moved to the position given in Table 6. This places hole 319 approximately on the same line as 320-322, but slightly further west, as even with this adjustment, the mineralised zone of drillhole 319 still does not coincide with the level at which the mineralised zones of other drillholes lie, making a distinct and rather extreme 'dip' shape in the geometric model of the lens (see Figure 38).

It is possible that the placement of the mineralisation in the core log of drillhole 319 is incorrect, or that the drillhole path deviates much more than what is estimated (see chapter 3.1.4.2.1). In any case, this drillhole causes rather large errors in the modelling of lens A.

Table 5: Corrected elevation data. Where elevation data exists from both Bakke (1975) and Rui (1990), numbers from Bakke have been used to calculate the difference in elevation from Bjerkgård's excel-file.

| Drillhole number | Elevation [m] | | | Difference [m] |
|---|---|---|---|---|
| | From Bakke (1975, p.48) | From Rui (1990), core log tables | From excel-file Bjerkgård | |
| 237 | 1006 | | 1007 | -1 |
| 238 | 997.9 | | 1000 | -2.1 |
| 239 | 1011.5 | | 1010 | 1.5 |
| 240 | 1024.4 | | 1025 | -0.6 |
| 242 | 1018.1 | | 1020 | -1.9 |
| 244 | 1086.1 | | 1080 | 6.1 |
| 312 | 1034.1 | 1034 | 1035 | -0.9 |
| 313 | 1040.9 | 1041 | 1040 | 0.9 |
| 314 | 1017.5 | 1017 | 1015 | 2.5 |
| 315 | 1000.1 | 1000 | 1000 | 0.1 |
| 317 | | 1076 | 1070 | 6 |
| 319 | | 1020 | 1020 | 0 |
| 320 | | 1020 | 1020 | 0 |
| 321 | | 1015 | 1017 | -2 |
| 322 | | 1012 | 1016 | -4 |

Table 6: Position of drillholes 319 and 320, with adjusted coordinates for drillhole 319.

| | Drillhole number | |
|---|---|---|
| | 319 | 320 |
| Coordinates in local grid system | 2337 N – 912 V | 2740 N – 913 V |
| Coordinates from Bjerkgård's excel-file | 608388 East<br>6951980 North | 608389 East<br>6951985 North |
| Adjusted coordinates | 608377 East | - |

| | | |
|---|---|---|
| | 6951947 North | |

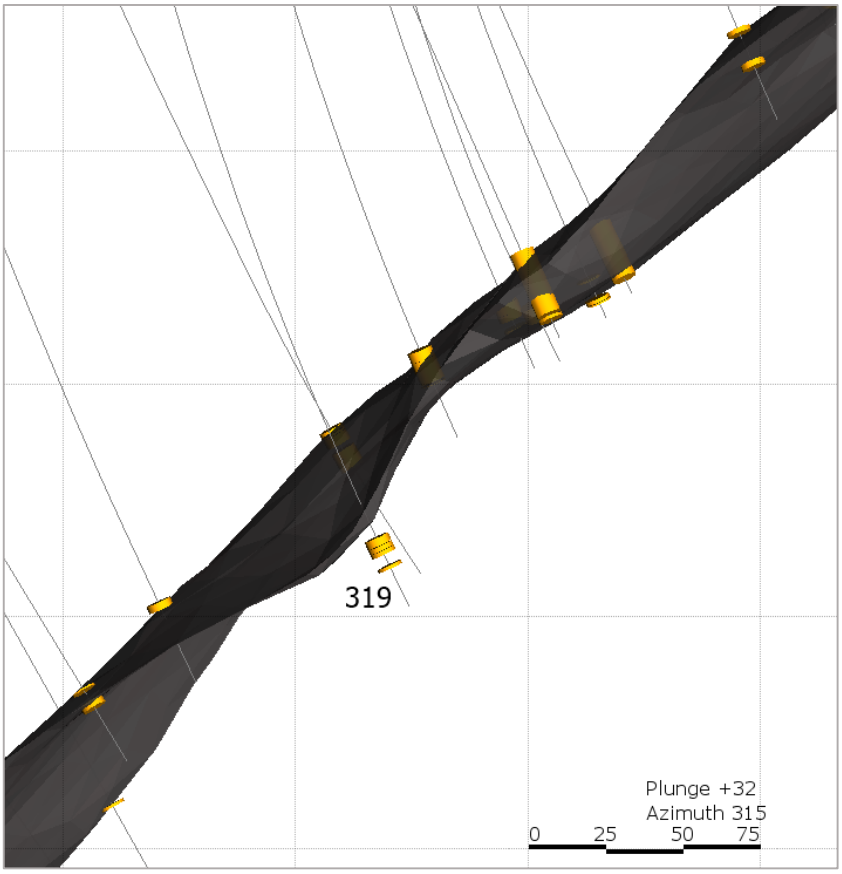


Figure 38: Drillhole 319 with mineralised zone (yellow) relative to model of lens A, after adjustment of collar position.

### 3.1.3 Lithological data

For lens A, nine of the drillholes have complete core logs (no. 312-315 and 317-321). In addition, drillhole 322 has been logged just around the mineralisation (Rui, 1990). There are no core logs available for drillings conducted on any of the mineralised lenses prior to 1974. As the logs had not been added to the excel-file from Bjerkgård, digitisation of the core logs was necessary and thus performed in connection to this thesis work.

Bakke (1975) notes that core logging was performed by A. Skordal, Ø. Gvein, G. A. Johannessen, and Ø. Pettersen, in addition to himself. Several of the core logs available in the report by Rui (1990) are signed by the logger, though some are not. However, it is possible to deduce from the style of the logging that cores from drillholes 317-321 were likely logged by the same person (hereby denoted as *NN-1*), especially as these logs all contain a summary of the lithology at the end of the log. In addition, as none of the core logs belonging to any of the mineralised lenses are signed by Ø. Pettersen, it is not unlikely that he logged cores 317-321, as both A. Skordal and Ø. Gvein have signed other core logs on lenses B-F. The short log of drillhole 322 does not match the style of core logs 317-322, and the logger is hereby denoted as *NN-2*.

An overview of who logged which drillhole is presented in Table 7, and an example of the layout of the original core logs is given in Figure 39.

Table 7: Overview of who logged the various drill cores in lens A. NN-1 is most likely Ø. Pettersen (see text for reasoning). Table based on data from Rui (1990).

| Drillhole number | Logged by |
|---|---|
| 312 | S. Bakke |
| 313, 314, 315 | G. A. Johannessen |
| 317, 318, 319, 320, 321 | NN-1 |
| 322 | NN-2 |

As the cores have been logged by four people, difficulties arise concerning their different interpretations regarding the lithology, for example, Bakke (1975) mentions that the various core loggers have very different interpretations of the amphibolitic rocks. This proved to be a substantial problem in modelling of the host rock lithology of the Hessjø deposit (see chapter 3.2.2).

DIAMANTBORING Hersjø v. 19 75

**Kjerneobservasjoner.**

Borhull nr. 313 Profil

Koordinator: N 2643 V 1015

Påsatt i høyde 1041 m.

" i retning N 84°Ø

" med helning 85°

Borhullets lengde 514,40

G.A. Johannessen

| Boret meter | Bergart | Kjerne-mangel | Skifrighet | Bergart prøve |
|---|---|---|---|---|
| 1.75 | Jord | | | |
| 10.00 | Grønnstein, lys, skifrig, oppknust, med tette bånd av kvarts-feltspatisk materiale, linser, etc., klorittbånd. | 25% | 25g | |
| 11.75 | Kvartskeratofyr, finstripet. | | | |
| 13.05 | Grønnstein, småstripet, mørk. | | | |
| 13.65 | Kvartsnyre med klorittårer. | | | |
| 15.75 | Grønnstein, lys, småstripete med ~1 cm bånd av kvarts-feltspatisk materiale, og kloritt, foldet. | | | |

Figure 39: Example of the layout of the original core logs as given in the report by Rui (1990). The example is taken from drillhole 313 logged by G.A. Johannessen. Translations from Norwegian:

*Borhullets lengde = drillhole length, Boret meter = meters drilled, Bergart = Rock type, Kjernemangel = core loss, Skifrighet = schistosity.*

The summaries made by NN-1 for core logs 317-321 have not been incorporated into the digital file containing the core logs, but are presented here none-the-less as they provide valuable information concerning the general geology (Table 8).

Table 8: Summaries of lithologies in drillholes 317-321 logged by NN-1, as given in the report by Rui (1990), translated from Norwegian.

Drillhole 317

| from [m] | to [m] | Lithology |
|---|---|---|
| 0 | 3.4 | Soil |
| 3.4 | 128.0 | Phyllite |
| 128.0 | 266.4 | Mainly green phyllite (or chlorite rich schist) with calcium carbonate, locally highly calcareous. |
| 266.4 | 548.9 | Varying greenstones, keratophyre resembling areas, metagabbro, porphyry. Distinct light coloured greenstone towards the end. |
| 548.9 | 721.05 | Dark green greenstone with some schistose sections. Areas of porphyry. Formations of agglomerate in the lower part. |
| 721.05 | 722.0 | Half compact ore, pyrrhotite, pyrite, chalcopyrite. |
| 722.0 | 736.5 | Mainly chlorite schist. |
| 736.5 | 760.0 | Varying greenstones, relatively light in colour, locally garnets. |

Drillhole 318

| from [m] | to [m] | lithology |
|---|---|---|
| 0 | 3.0 | Soil |
| 3.0 | 126.0 | Mainly grey phyllite. |
| 126.0 | 242.5 | Green chlorite schist, highly calcareous |
| 242.5 | 560.0 | Alternating between greenstone, keratophyrelike sections, metagabbro, and porphyry |
| 560.0 | 588.4 | Light coloured, massive greenstone. |
| 588.4 | 733.0 | Dark greenstone with some schistose sections. Porphyritic and agglomeratic sections in lower part. |
| 733.0 | 736.6 | “Ore zone”. Weak impregnation of pyrrhotite and chalcopyrite. |
| 736.6 | 739.65 | Chlorite schist |
| 739.65 | 769.0 | Relatively light coloured greenstone with lesser chlorite sections. Garnet common. |

Drillhole 319

| from [m] | to [m] | lithology |
|---|---|---|
| 0 | 2.5 | soil* |
| 2.5 | 117.0 | Mainly light coloured, calcitic greenstone, often schistose. |

| | | |
|---|---|---|
| 117.0 | 163.1 | Mainly light and dark greenstones and porphyrys. |
| 163.1 | 324.1 | Mainly dark coloured, fine grained, homogenous greenstone. Locally areas of agglomerate. |
| 324.1 | 412.2 | Alternating between light and dark greenstones, gabbro, and porphyry. |
| 412.2 | 413.0 | Chlorite schist |
| 413.0 | 418.9 | Pyrite ore with zinc stripes and little chalcopyrite. Pyrrhotite and magnetite ore towards the footwall. |
| 418.9 | 422.8 | Chlorite schist |
| 422.8 | 423.9 | Pyrrhotite and magnetite with areas of chalcopyrite. |
| 423.9 | 427.0 | Chlorite schist |
| 427.0 | 437.7 | Partly massive and firm rocks, but still some chloritized areas. |

*original summary does not include *soil*, but is added here to maintain correspondence to the other summaries.

Drillhole 320

| from [m] | to [m] | lithology |
|---|---|---|
| 0 | 3.7 | soil* |
| 3.7 | 98.1 | Mainly light coloured calcitic greenstone, partly schistose. |
| 98.1 | 149.1 | Alternating light and dark greenstones and porphyrys. |
| 149.1 | 354.97 | Initially dark greenstone, onwards alternatingly light and dark greenstones, gabbro, and porphyry. The rocks are firm up until the ore zone. |
| 354.97 | 366.0 | Ore zone, initially with zinc stripes, poor in copper. Midsection is copper rich within pyrite and pyrrhotite. Pyrrhotite and magnetite dominate towards the footwall, not much copper. |
| 366.0 | 373.5 | Chlorite schist with mainly pyrrhotite impregnation and some chalcopyrite. |
| 373.5 | 386.3 | Partly massive and firm rocks. Lesser chloritized areas. |

*original summary does not include *soil*, but is added here to maintain correspondence to the other summaries.

Drillhole 321

| from [m] | to [m] | lithology |
|---|---|---|
| 0 | 5.1 | soil* |
| 5.1 | 90.6 | Mainly light coloured greenstone, partly schistose. Calcite. Ending with a gabbroic section, as in drillhole 320. |
| 90.6 | 144.0 | Dominated by light greenstone. Some dark sections and benches of porphyry. Calcite in veins and cracks. |
| 144.0 | 349.86 | Initially dark greenstone. Continuing with alternatingly light and dark greenstone, gabbro, and porphyry. Some quartzitic sections. |
| 349.86 | 358.5 | Ore zone in the usual pattern. Pyrite with zinc stripes in hanging wall, pyrrhotite and chalcopyrite in central section and magnetite in footwall. The magnetite makes up the last three meters where the first (upper) meter is chalcopyrite bearing in the crack. “Economical” ore zone is limited to 356.65 meters. |
| 358.5 | 361.8 | Chlorite schist |

| | | |
|---|---|---|
| 361.8 | 363.8 | Secondary ore zone. Pyrrhotite, magnetite dominated with some chalcopyrite. Sections of chlorite schist. |
| 363.8 | 376.7 | Alternating sections of chlorite schist and massive rocks. |

*original summary does not include *soil*, but is added here to maintain correspondence between the drillhole summaries.

The core logs were translated from Norwegian to English before being digitised and sorted into an excel file. As much detail as possible was incorporated into the file, before necessary simplifications were made in a new column. Even so, it is not always clear what is meant in the log entries, and assumptions have had to be made in the digitisation process. The following sections provide an overview of the assumptions and simplifications that were deemed necessary during the digitisation work.

#### 3.1.3.1 Initial digitisation

When digitising the core logs, the input information was divided into the following columns:

- *Hole ID*: drillhole number
- *From*: starting depth indication for given section
- *To*: ending depth indication for given section
- *Original entry information*: rock type entry as given in core logs
- *Colour:* colour of rock, where available
- *Grain size:* grain size of rock, where available, given as fine/medium/coarse
- *Texture:* textural information, where available
- *Detailed information:* any information regarding e.g. lesser occurring minerals
- *Notes:* any information that does not fit into any other columns
- *Average schistosity:* in degrees, where available
- *Logged by:* name of core logger

In addition, a *lithology* column was added later, during the simplifications. This is the main column read by Leapfrog Geo.

The degree of detail in the core logs vary by the different loggers, and there are instances where the entries are rather extensive with regards to information about a given section of rock. As far as possible, the first word, or words in each entry has been interpreted and thus defined as the main lithology. Some entries contain no information regarding the rock type, only a colour or texture reference. These entries are set as *NA*. As an additional note, it should be mentioned that less ten 10 m of the total logged length of all drillholes, is classified as *core loss.*

The main difficulty in digitising the core logs has been the 'greenstone conundrum'. Greenstone is by far the most abundant lithology in the Hessjø deposit, but the different loggers are not in agreement regarding the various types of greenstone, as well as the difference between greenstone and greenschist.

In his thesis, Bakke (1975) separates between *dark greenstone*, *quartzitic dark greenstone, dark greenschist, pillow lava,* and *light, partially porphyritic greenstone.* In his logging of drillhole 312 however, he separates between *greenstone, greenschist, dark greenstone, dark greenschist,* and *light greenstone* (only one entry). There is no referral to pillow lava in Bakke's core log, even though he has marked a rather large area as pillow lava in his geological map (Figure 6). Johannessen separates between *greenstone* and *dark greenstone* (one entry). Both NN-1 and NN-2 separates between *greenstone* and *greenschist,* in addition, NN-1 has one entry termed *pillow lava.* However, all the loggers remark on the colour (light/dark) to a greater or lesser extent after defining the main rock type, though not all entries contain colour specifications, and are thus left with only 'greenstone'. Also, NN-1 separates between dark greenstone and light greenstone quite clearly in his summaries (Table 8). The differences in the definition of greenstone has turned out to cause particular difficulties in modelling of the host rock geology, as discussed in chapter 3.2.2.

NN-1 often uses abbreviations in his core logs, and it is assumed that 'gr. st.' and 'gr.' are abbreviations for greenstone (*grønnstein* in Norwegian).

Another inconsistency between the various core logs, is the definition of the felsic volcanic rocks. According to Bakke (1975) *quartz keratophyre* makes up approximately 2% of the area around the Hessjø deposit, however, he has no entry in the core log of drillhole 312 that is defined as such, as is also the case for drillhole 322 logged by NN-2, though as previously mentioned, only the immediate area around the mineralisation is logged. Johannessen uses the term quartz keratophyre, while NN-1 uses only *keratophyre*, as well as *keratophyre-like* and *feldspar-rich rock*, with no additional information regarding textures, colours, grain size etc. It is assumed that they are indeed talking about the same rock type, though by definition keratophyre and quartz keratophyre are not the same rock. Schermerhorn (1973) distinguishes between keratophyre and two types of quartz keratophyre, one with and one without phenocrysts. Keratophyre is defined as an intermediate rock, while the quartz keratophyres are felsic rocks, though all are leucocratic sodic albite-phyric volcanics. According to Bakke (1975), quartz keratophyre has a mineral composition of 45% quartz and 45% 'sludgy' feldspar in one thin section, but in another thin section it is difficult to distinguish between quartz and feldspar. It is a general characteristic of the core logs to not distinguish between quartz and feldspar, which often occurs as lesser minerals, only separating them with a forward slash. Slagstad (2003, p.169) notes that "the term quartz keratophyre has traditionally been used in the Nordic countries to describe a metamorphosed, felsic extrusive rock, corresponding to rhyolite, dacite, or rhyodacite according to IUGS terminology".

Bakke and Johannesen uses the term *porphyry* (Norwegian: porfyr), while NN-1 uses the term *porphyrite* (Norwegian: porfyritt). According to Store Norske Leksikon (SNL; Great Norwegian Encyclopaedia) *porfyr* refers to an igneous rock containing phenocrysts of typically quartz or feldspar in a fine-grained matrix (SNL, 2016), while *porfyritt* is an older term for porphyritic rocks with phenocrysts of plagioclase (SNL, 2015). Valid for all core log entries is that that the

type of phenocrysts in the rocks are rarely defined, the same also applies to other textural notations like banding. It is assumed that the core loggers are referring to the same type of rock, hereby noted only as *porphyry*.

Even if it does not specifically say in the original core logs, the textural attributes *porphyritic* and *schistose* have been added to the rock types where this is a defining trait. *Porphyritic* has been added to all sections defined as *porphyry* or *porphyrite*, while *schistose* has been added to all sections defined as *chlorite schist, greenschist, phyllite,* or any other rock type normally defined as schistose.

As the majority of the drillholes do not have available core logs, the sections analysed for Cu and Zn, available in the assay data, were added into the lithology file as *mineralisation*.

#### 3.1.3.2 Simplifications

To be able to use the core log data to create a sensible 3D geological model, simplifications are necessary. In addition, Leapfrog Geo does not accept special characters like forward slashes, quotation marks, and hyphens. These had to be removed prior to import.

To begin with, the following adjustments were made to the logged lithologies and implemented in a new column, *lithology,* as mentioned in the beginning of chapter 3.1.3.1.

- Rock type entries containing '-like', e.g. 'keratophyre-like, are replaced by the given lithology without the '-like'.
- Where the main lithology is defined by two rock types separated by a forward slash, the rock type mentioned first in the core log is set as the main type, unless additional entry information indicates otherwise.
- Where the core logger has set a question mark behind the main rock type, the question mark is removed.
- Where a greenstone entry also has a colour entry, the colour (light/dark) is added to the defining rock type, e.g. 'greenstone' that is dark is set as 'dark greenstone'.
- When the core logger has set quotation marks around the rock type, the marks are simply removed.
- Entries marked as any type of sulfide or oxide minerals, or as ore (*malm* in Norwegian), is simply termed *mineralisation,* i.e. same as for the assayed sections converted to lithology.

In addition, feldspar-rich rock, keratophyre, and quartz keratophyre are all compiled into a collective lithology denoted *felsic volcanics*. USGS (2014) defines a felsic volcanic rock as "a light-colored, fine-grained or aphanitic extrusive or hypabyssal rock, with or without phenocrysts and composed chiefly of quartz and feldspar".

The complete digitised file containing all data from the core logs is available in the appendix.

Further simplifications have been deemed necessary after the commencement of the geometric modelling in Leapfrog Geo. These are discussed in chapter 3.2.

### 3.1.4 Downhole survey data

Only measurements from drillholes 306 and 308-315 (drilled in 1974 and 1975) are present in the report by Gvein (1976), and out of these nine drillholes, number 312-315 are drilled on lens A. This causes substantial difficulties for the modelling of the Hessjø deposit, as all the drillholes show significant deviation from the original path (e.g. Gvein (1976)). It is known, however, that drillholes 229 and 237-244 were surveyed by A/S Terratest in 1971 (six of these intersect lens A) (Gvein, 1976), and Eriksen & Pettersen (1972) explicitly states that drillholes with lengths of more than 150 m have been surveyed by A/S Terratest using a magnetic three-component method. For lens A, ten drillholes are shorter than 150 m. The report containing the downhole survey measurements was owned by A/S Røros Kobberverk, but a copy was sent to A/S Sydvaranger the 30th of May 1974 (Valseth & Bakken, 1974). It has not been possible to find this report. Whether or not drillholes drilled in 1976/1977 were surveyed is not known.

#### 3.1.4.1 Drillhole deviation

Drillhole deviation is a common occurrence during longhole drilling, and the total hole deviation is a combination of errors in

- Collaring
- Alignment
- Trajectory deviation

Errors in collaring and alignment are mainly due to human factors and inaccuracies in drilling equipment and drill operating variables, while trajectory deviation is caused by the characteristics of the rock through which the hole is drilled (Singh et al., 1998).

In un-fissured and homogenous rock with a drillhole alignment deviating from vertical, the drilling will only be affected by gravitation. Any layered or fissured rock will cause the drillhole to deviate. Depending on the initial alignment relative to the rocks, the drillhole will either deviate towards becoming perpendicular to, or level towards, the layering or fissuring, where the former occurs more commonly (Olsen, 2002).

For the Hessjø deposit, the drillholes are generally aligned such that the paths deviate towards becoming perpendicular to the layering (see Figure 7).

#### 3.1.4.2 Estimation of missing survey data

When viewing the non-adjusted drillholedata in Leapfrog Geo, it is generally easy to see the difference between the surveyed drillholes (no. 312-315) and the non-surveyed drillholes. The non-surveyed drillholes continues along the initial dip and azimuth angle in a straight line, while the surveyed drillholes show a clear curvature. Trying to establish a good geometrical model

without survey data for so many drillholes will result in major flaws in the model. To get a viable geometrical model, it is therefore necessary to find an approximation of the curvature of the drillhole paths that can be applied to the drillholes that are missing survey data. However, any general approximation for the deviation will inherently be flawed, because the deviation varies from drillhole to drillhole.

Some information regarding the non-surveyed drillholes does exist, at least for the vertical component of the deviation. The paths of drillholes 312, 240, 237 and 232 is drawn in on Figure 3, and the same goes for drillholes 244, 313, 311, and 243 on the geological profile shown in Figure 7. Drillholes 311 and 243 do not intersect lens A, while 312 and 313 have available survey measurements, and 232 is shorter than 150 m and has thus not been surveyed. That leaves drillholes 244, 240, and 237. Due to scanning and copying, the scale on Figure 3 is most likely distorted and uncorrect, but measuring the angles at which drillholes 237 and 240 intesect lens A will none-the-less give an indication to the deviation of the drillhole. For drillhole 244, the paper version of Figure 7 is available, and a measurement of the drillhole path will hopefully be somewhat more correct. The original paper version of Bakke's (1975) geological profile is in A2 format in a scale of 1:2000. Measurements using a ruler and calculating the angles gives the values provided in Table 9. Intersection depths are taken from tables containing chemical analysis in Rui (1990).

Table 9: Dip angles calculated from drillhole paths in Figure 3 and Figure 7 where drillhole traces intersect lens A.

| Drillhole no. | Calculated dip angle [º] | Intersection depth downhole [m] |
|---|---|---|
| 237 | 71 | 170 |
| 240 | 42 | 374 |
| 244 | 39.5 | 717 |

This method does, however, not give any indication to the horizontal deviation of the drillhole paths. For the remaining drillholes, a different approach was used, where the mean directional deviation was calculated from the surveyed drillholes and adapted for all other drillholes. The process is described in the following subchapter.

#### 3.1.4.2.1 Estimation of mean directional deviation

Downhole survey values for surveyed drillholes were used to calculate the rate of change in degrees per meter along the drillhole traces, both in the horizontal and vertical direction, using Microsoft Office Excel. The rate of change was determined both from the drillholes intersecting only lens A (no. 312-315), and from all surveyed drillholes intersecting lens A, B, and C (no.

306, 308-315), in an attempt to evaluate which set of drillholes gave the more correct deviational pattern for lens A drillholes.

The vertical rate of change was determined by taking the initial dip angle of the drillhole trace and subtracting the subsequent measured dip angle, then dividing by the drillhole length between the two dip angle measurements, and repeating the procedure for each measured section. The equivalent was done for the horizontal rate of change, using azimuth values. Thus, a positive value means that the drillhole trace deviates upwards in the vertical direction, and counter-clockwise (when viewed from above) in the horizontal direction. Descriptive statistics for the horizontal and vertical rate of change calculated for drillholes only intersecting lens A, and drillholes intersecting lens A, B, and C, are given in Table 10 and Table 11, respectively.

Even though the number of drillholes with available survey data is small, the drillholes in question are long, giving a total of 1560 meters of drillhole surveyed in connection to lens A, and 1340 meters in connection to lens B and C. All surveyed drillholes thus gives a total length of 2900 m.

While the mean horizontal rates of change are -0.043205706 degrees/m and 0.122395833 degrees/m for the two scenarios (Table 10 and Table 11), the standard deviation and range values raises questions concerning the applicability of the associated mean values. For rates of change calculated from drillholes 312-315, the standard deviation is more than 14 times larger than the mean value, with a range of 16.7, while for all surveyed drillholes the standard deviation is more than 32 times larger than the mean value, with a range of 18.1. When reviewing the surveyed drillholes in Leapfrog Geo, it seems arbitrary whether the drillholes deviates in a northerly or southerly direction. Adjusting for a horizontal deviation will therefore be disregarded.

Table 10: Descriptive statistics for the rate of change using drillholes intersecting lens A, B, and C. The vertical rate gives degrees per meter upwards, while the horizontal rate gives degrees per meter counter-clockwise.

| Drillholes 306, 308-315 | | |
|---|---|---|
| | Vertical rate of change | Horizontal rate of change |
| Mean | 0.105782998 | -0.043205706 |
| Standard Error | 0.008939659 | 0.114720638 |
| Median | 0.1 | 0 |
| Mode | 0.05 | 0 |
| Standard Deviation | 0.109122439 | 1.395636793 |
| Sample Variance | 0.011907707 | 1.947802058 |
| Range | 1 | 18.1 |
| Minimum | -0.2 | -3.9 |
| Maximum | 0.8 | 14.2 |
| Sum | 15.76166667 | -6.394444444 |
| Count | 148 | 148 |

Table 11: Descriptive statistics for the rate of change using drillholes intersecting lens A. The vertical rate gives degrees per meter upwards, while the horizontal rate gives degrees per meter counter-clockwise.

| Drillholes 312-315 | | |
|---|---|---|
| | Vertical rate of change | Horizontal rate of change |
| Mean | 0.07675 | 0.122395833 |
| Standard Error | 0.007743521 | 0.193876603 |
| Median | 0.075 | 0 |
| Mode | 0.1 | 0 |
| Standard Deviation | 0.069260155 | 1.734085054 |
| Sample Variance | 0.004796969 | 3.007050974 |
| Range | 0.425 | 16.7 |
| Minimum | -0.2 | -2.55 |
| Maximum | 0.225 | 14.2 |
| Sum | 6.14 | 9.791666667 |
| Count | 80 | 80 |

For the vertical rate of change, it becomes a question of whether to choose the mean calculated from all drillholes, or just those intersecting lens A. The latter shows a lower standard deviation and variance than the former, as well as lower range, thus giving cause to use the mean calculated only from drillholes 312-315. In addition, the longest drillholes intersecting lens B and C are several hundred meters shorter than the longest drillholes intersecting lens A. Using the measurements from drillholes drilled on lens B and C would skew the mean rate of change to mainly reflect the deviation behaviour as it occurs higher up in the stratigraphy.

Both mean values for the vertical rate of change were implemented into the non-surveyed drillholes, by taking the dip at the collar and substracting the mean rate of change times the depth of the drillhole where it intersects lens A. This however, caused the dip angles to become too low, and at times with negative values. One reason for this is that some of the non-surveyed drillholes are several hundred meters longer than the surveyed drillholes, while the longest surveyed drillhole is approximately 500 m long. Using a set rate of change as far down as the mineralised lens does not take into account that drillhole deviation tends to cease when the drilling trajectory has become perpendicular to the layering of the surrounding rock (see chapter 3.1.4.1).

According to Vokes (1983), the mixed, mafic volcanic rocks in the Hessjø area dips more or less steeply towards west, and $40^0$-$60^0$ around the mineralisations. Gvein (1976) notes that the rocks generally have a dip of $40^0$-$65^0$, with the main dip angle being approximately $50^0$. Lens A has a

dip of approximately 35⁰ at the surface, and around 50⁰ at depth. As the host rocks lie conformably around lens A (Figure 7), it is likely that the drillhole paths have stabilised at a dip of c. 50⁰. The minimum dip registered for the surveyed drillholes is 40.5⁰ in drillhole 311 (lens B), at a depth of 360 m. For lens A, the lowest dip value registered is 48.5⁰ in drillhole 312, at 500 m depth, i.e. the deepest survey value that is available. Thus, a dip angle of 48.5⁰ is set as the minimum possible value along the drillhole traces. The depth at which to set this angle was calculated using equation 3.1, where the denominator is the mean vertical rate of change calculated from downhole survey measurements from drillholes 312-135 (Table 11).

$$depth_{48.5^0} = \frac{collar\ dip - 48.5}{0.07675} \tag{3.1}$$

At drillhole depths below this value, the dip angle is set to a constant 48.5⁰. However, not all the drillholes with missing survey data are long enough to reach this value of dip, instead, the same mean rate of change was used to calculate an estimated dip at the bottom of said drillholes.

The survey table with the estimated deviational paths was imported into Leapfrog Geo, and visually it appears that the estimated drillhole paths correlate with the surveyed drillholes, in addition to what is known of the general trend of lens A.

#### 3.1.4.2.2 Additional adjustments

In his 1975 thesis, Bakke (p.48) makes an attempt to calculate the ore mineral content for the Hessjø deposit, and as a part of this calculation, he provides the elevation value of the intersection between the drillhole paths and the mineralisation, for drillholes 237-240, 242, 244, and 312-315. This provides information that was used to further adjust the drillhole paths with more appropriate downhole survey estimators. However, as downhole dips have already been estimated for drillholes 237, 240, and 244, using profile depictions (Table 9), and measured data is available for drillholes 312-315, only drillholes 238, 239, and 242 were subjected to further adjustment.

After import to Leapfrog Geo, the elevation of the intersections was checked, and adjusted downhole dip angles were implemented to approximate the values given by Bakke (1975). Elevation values and adjusted dip angles are given in Table 12.

Table 12: Elevation values used for adjusting downhole survey estimators. *In hole depth* denotes where the adjusted dip angle is implemented.

| Drillhole no. | Elevation of mineralisation [masl.] according to Bakke (1975) | Adjusted dip angle [⁰] | In hole depth [m] |
|---|---|---|---|
| 238 | 826.5 | 55 | 149.8 |

| | | | |
|---|---|---|---|
| 239 | 854.4 | 43 | 149.8 |
| 242 | 764.4 | 38 | 390 |

### 3.1.5 Assay data

A general analysis performed in 1971 by Boliden on samples from the upper part of lens A, revealed copper and zinc to be the possible valuable constituents, as the analysis showed a very low content of precious metals and lead (Gvein, 1976). However, the lower parts of the deposit have only been analysed for Cu, Zn, S, and Fe, rendering the content of any other elements in the lower parts unknown.

Chemical analysis has been performed on samples from 24 of the drillholes intersecting lens A, with respect to Cu, Zn, S, and Fe. No samples were analysed from drillholes 225 and 235 as these do not cut the mineralisation. All results from the chemical analysis are available in the report by Rui (1990). As the qualimetric modelling will focus on the potentially valuable constituents of the Hessjø deposit, only the analysis of Cu and Zn is reviewed here.

According to Bakke (1975), drillhole 312 has an extremely high Cu-content. Mineralogical investigations indicate that the high Cu-content is local and conditional to tectonic events, however, it still seems to have a certain extent, since the tectonic strain seems to have reached rather deep. Cu content in drillhole 312, as calculated by Bakke (p. 64-65), is 4.16% over 14.52 m, 4.72% over 12.79 m, and 9.76% over 4 m. Gvein (1976) concurs with this.

Bakke also notes that the Cu and Zn content varies greatly across drillholes, as well as within each drillhole. The Hessjø deposit has been thoroughly investigated with regards to an iron ore potential, but Bakke comments that lens A would give 500 000 tons of pure magnetite, where 400 000 tons occurs as massive magnetite ore.

The assay data for the Hessjø deposit is not without issues. Firstly, there is no record of what methods were used to perform the chemical analysis, or who performed them, and thus there is no information regarding the uncertainties and errors of the data. As Røros Kobberverk was the main owner of the Hessjø deposit when the drillings were conducted, it can be assumed that they were responsible for, at least most of the analytical investigations. As the company went bankrupt in 1977 (Gvein, 2010), and since automated quantitative methods for chemical analysis were not widespread until the 1980s, it can be deduced that classical methods for analysis were used. According to Kolthoff & Sandell (1952), iodometry was the main method for determining quantitative values of copper in ores.

A second issue is that several of the samples contain zero-values. Through chemical analysis, it is not possible to conclusively determine when a sample value is absolute zero, such a value would rather be below the limit of detection. Out of the 214 core samples chemically analysed, 210 were sampled for Cu, with 7 values set as zero; 208 were sampled for Zn, with 44 values set as zero. The lowest non-zero value registered for any of the elements is 0.01%. See Table 13 for summary.

Table 13: Summary of sample characteristics for Cu and Zn. Table based on data from Rui (1990).

| | Cu | Zn |
|---|---|---|
| Total no. of samples | 210 | 208 |
| No. of zero value samples | 7 | 44 |
| Percentage of zero values | 3.33% | 21.15% |
| No. of lowest value samples (0.01%) | 8 | 7 |
| Highest value registered | 11.41% | 12.75% |

Frequency plots, including zero-values, of Cu and Zn are provided in Figure 40 and Figure 41. A discussion regarding how the handle the zero-values in connection to the qualimetric modelling, is presented in the following chapter.

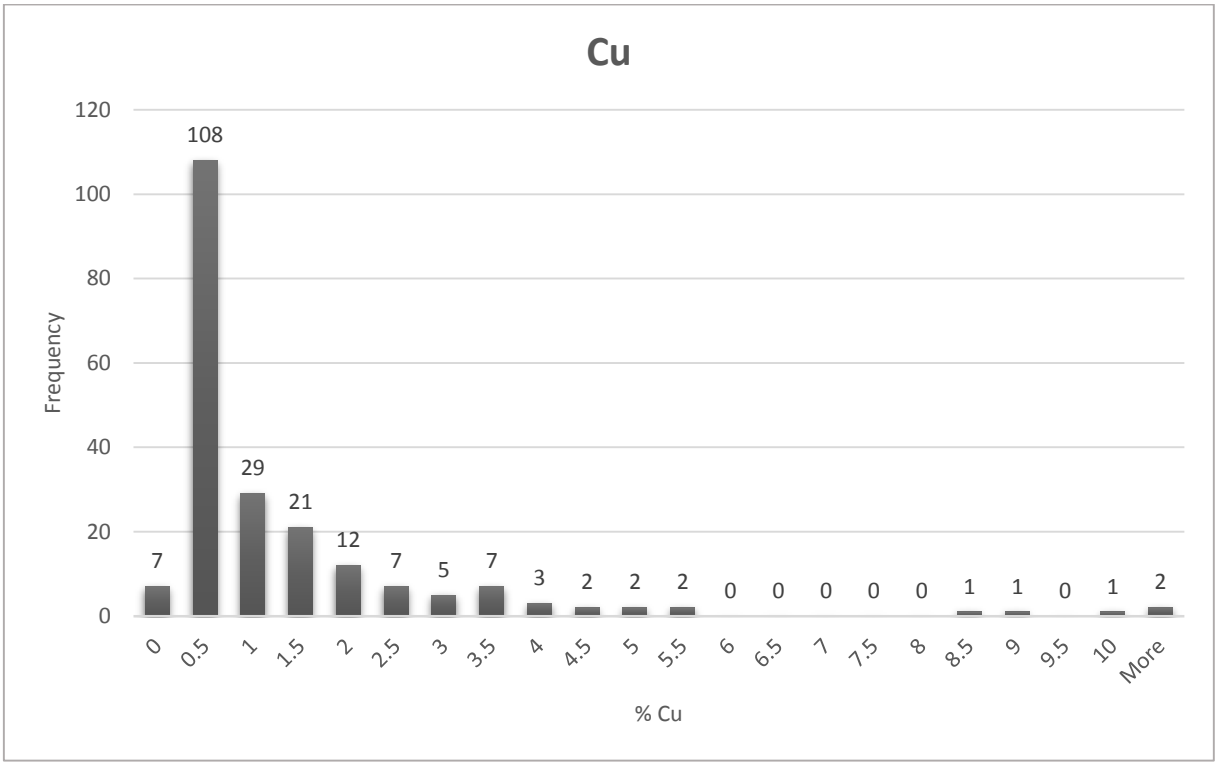


Figure 40: Frequency plot of copper samples from lens A in the Hessjø deposit.

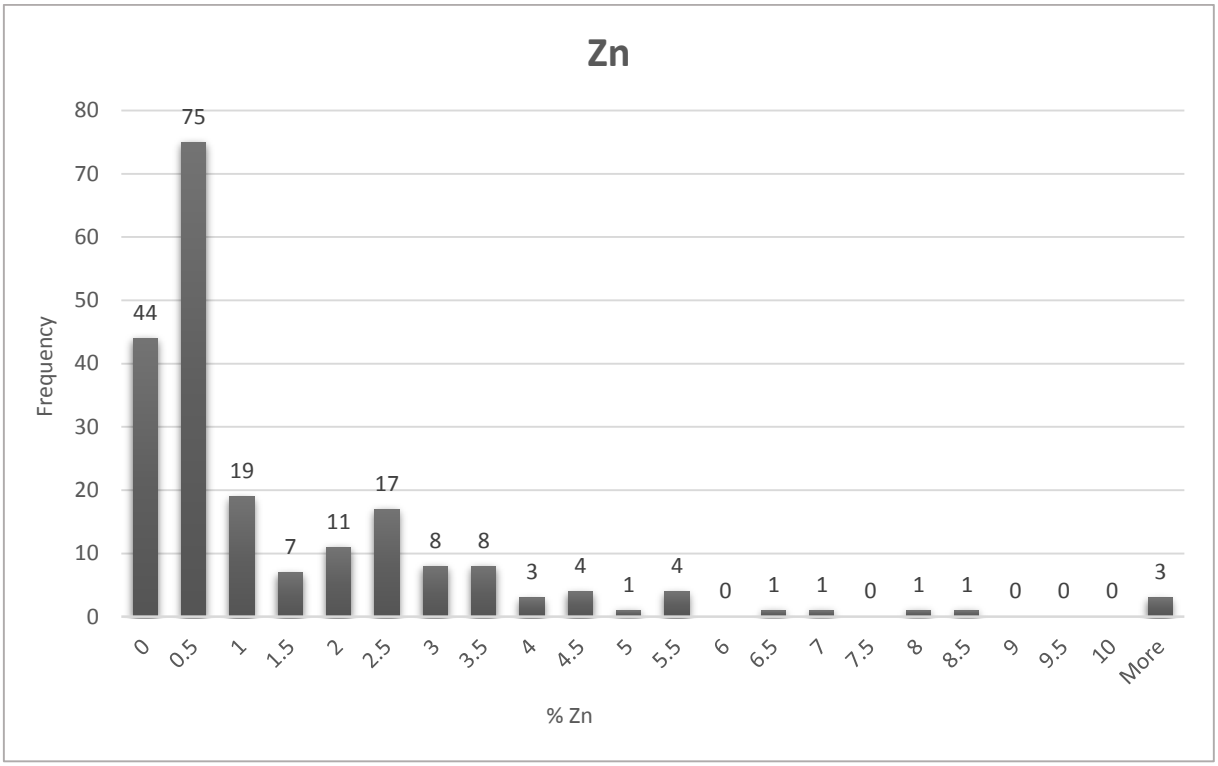


Figure 41: Frequency plot of zinc samples from lens A in the Hessjø deposit.

#### 3.1.5.1 Adjusting for sample values below the detection limit

Due to limitations if chemical analysis procedures, small concentrations cannot be precisely measured. These concentrations are said to be below the limit of detection (LOD) (Croghan & Egeghy, 2003). According to Taylor (1987), the limit of detection is the level at which a measurement has a 95% probability of being different than zero. Even though values near the LOD are statistically different from zero, they are, in general, less accurate and less relible than values much larger than the LOD. LOQ (the limit of quantification) is a term often used by laboratories to indicate the smallest amount that can be considered reliably quantifiable. The distinction between LOD and LOQ is not always clear, but the LOQ is usually defined as some multiple of the LOD (generally three times the LOD) (Croghan & Egeghy, 2003).

It has been common practice in statistical analyses to censor and substitute values below the limit of detection with a constant value, either half the LOD, the LOD divided by the square root of two, or zero, although the choice of the substitution fraction is largely arbitrary (Hewett & Ganser, 2007; Croghan & Egeghy, 2003) Effectively, this substitution method results in two distributions: a uniform distribution for the values below the LOD, and the true distribution. Depending on the percentage of values below the LOD, this can produce questionable descriptive statistics (Croghan & Egeghy, 2003).

Hewett & Ganser (2007) point out that there are numerous recommendations against the use of simple substitution using the LOD value, but the practice continuous to occur based on the

justification that such a practice is conservative as LOD substitution tends to result in a "conservative" or positive bias for the mean, and a negative bias for the variability. As the sample size increases, the bias asymptotically approaches a fixed value. Helsel (2010) also advocates avoiding the use of substitution in statistical procedures on low-level data, calling the problem *invasive data,* because "substituted values possess a pattern that is alien to the pattern of the original data" (p.258). He does, however, accept the use of substitution when estimating the mean for data with one censoring threshold.

There are various other methods for dealing with values at or below the LOD. For example, Hewett & Ganser (2007) performed a study to compare the performance of several methods for statistically analysing censored data sets, where the methods examined were variations on the maximum likelihood estimation (MLE) and log-probit regression methods, non-parametric (NP) quantile methods for the 95$^{th}$ percentile and the non-parametric Kaplan-Meier method. Their conclusion was that "no single method was unequivocally superior across all scenarios, although nearly all of the methods excelled in one or more scenarios" (p.611). Common for all the methods they examined, is that they require substantial calculations and various computer software.

Even though using substitution is not recommended, it is however, the least time-consuming method, and does not require any additional computer software, which is probably one of the reasons it is still a commonly used method. The United States Environmental Protection Agency (EPA, 2006) offers the following general recommendations:

- If the percent censored is <15%, use substitution with zero, LOD/2, or the LOD, or use the MLE method.
- For 15-50% censored, use the MLE method.
- For 50-90% censored, calculate the NP exceedance fraction for the limit.

For Cu, 3.33% of the sample values are registered as zero (Table 13), thus giving cause to use substitution. For Zn 21.15% of the samples are zero-values. However, due to lack of time and sufficient knowledge of the other methods for dealing with censored data, substitution will be used for Zn as well. Thus, for the purpose of this thesis, qualimetric modelling of the Cu and Zn content in lens A of the Hessjø deposit will be performed using substitution with half the lowest value registered in the assay data. As mentioned in the previous chapter, the lowest registered value, for both Cu and Zn, is 0.01%, giving a half value of 0.005%. However, the question remains whether the lowest, non-zero value registered in the Hessjø deposit assay data, is a LOD or LOQ value, if any of them.

## 3.2 Geometric modelling

The 3D geological modelling was conducted using Leapfrog Geo version 3.0.1. The newest user manual corresponds to version 2.1 (ARANZ Geo, 2014), with additional updates available online (ARANZ Geo, 2016).

After importing the collar, survey, lithology, and assay tables, the modelling commenced with the generation of the lens A mineralisation, before continuing on to modelling the host rock geology.

### 3.2.1 Lens A

The 3D geometric model of lens A was modelled by taking the *mineralisation* lithology in the lithology .csv-file and using the *New Vein* function in Leapfrog Geo to generate a volume based on the mineralisation contacts. However, as this function by default generates a plate-like volume, the margins of the lens needed to be restricted in the northern and southern directions. Aided by the geological map shown in Figure 6, polylines were drawn along the outcropping lens boundaries and draped on the topography, thus creating the upper restrictions for the lens.

Further, the model volume was edited using curved polylines for the hanging wall and footwall, starting at the top of the lens and editing in sections along the main axis of the lens. Tangent discs were added to each polyline to define the angle at which the curved polylines were implemented onto the lens volume (Figure 42), thus taking into account the apparent 'kink' in the lens geometry, where the dip changes from c. $35^0$ to c. $45^0$ (chapter 2.1.1.2.1). This change in dip is exhibited as more of a fold than a kink in the geometric model, had the two sections of curved polylines used to define the change been spaced closer together, a more distinct kink might have been visible. The change in dip is located between the fourth and fifth polyline section in Figure 42, counting from above.

The assay data for zinc and copper was added to the scene while editing the lens volume, providing visual aid to appropriately restrict the edges.

Even though geophysical measurements downhole in drillhole 318 indicate that the conductive zone continues deeper than the drillhole-lens intersection (Logn, 1976, as cited in Vokes, 1983), the geometric model of lens A terminates just below the 318 drillhole-lens intersection as there is no more drillhole data beyond this point.

As mentioned in chapter 3.1.2 and visualised in Figure 38, drillhole 319 causes what appears to be an anomaly by making a downwards bulge in the lens volume. Without any further information regarding the positioning of drillhole 319, the bulge will be left as it is.

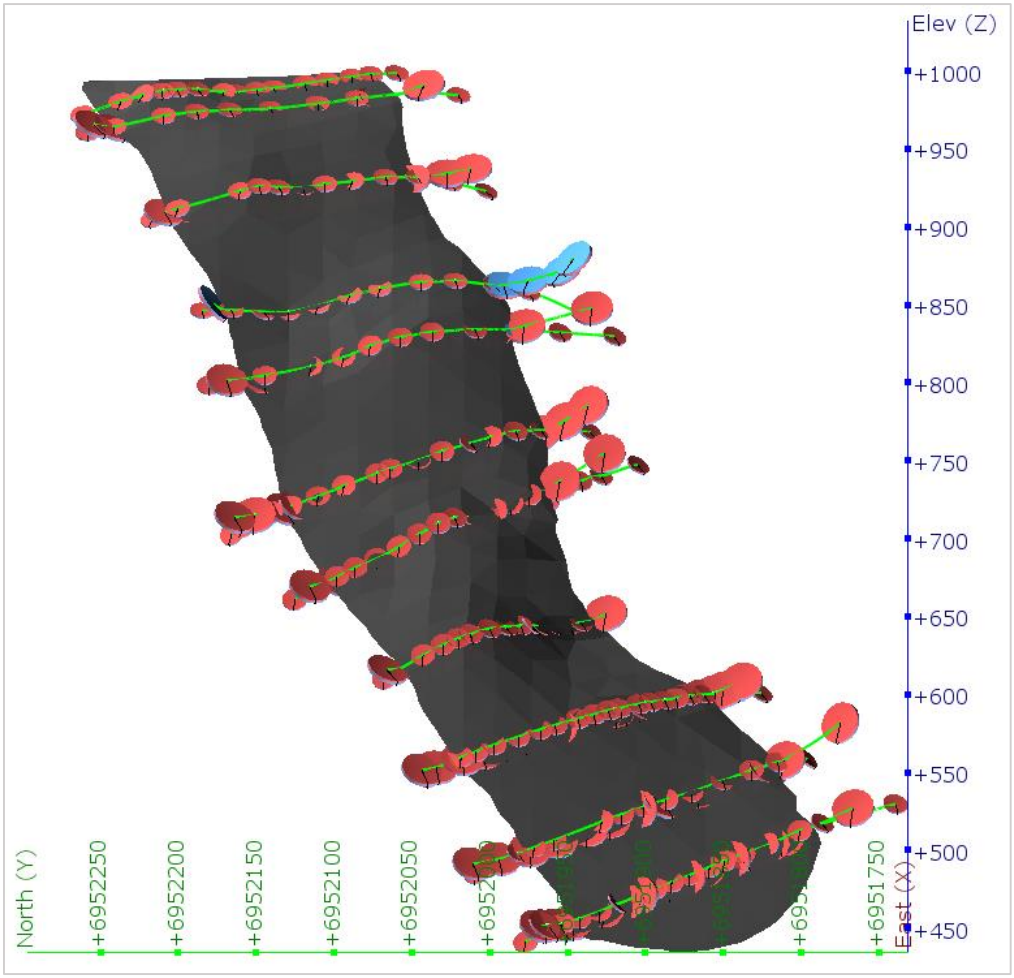


Figure 42: Curved polylines (green) with tangent discs defining the angle of the polylines, used to restrict the northerly and southerly extents of lens A. View from east, plunge zero.

The geophysical map by Singsaas (1975) (Figure 2) was applied as a means to control and validate the shape, direction of main axis, and horizontal extents, of the model. Viewing the map and model simultaneously from above gave indications leading to subsequent adjustments of the curved polylines (Figure 43). The maximum distance the model is extrapolated beyond drillholes is c. 130 m (south-westerly lower edge).

What this model does not take into account, is the apparent presence of intertwining between the host rocks and the mineralisation, especially along the edges, as shown in Figure 8. This might, however, be possible to model, given time and expertise.

The quality of the geometric model is discussed in chapter 5.1.

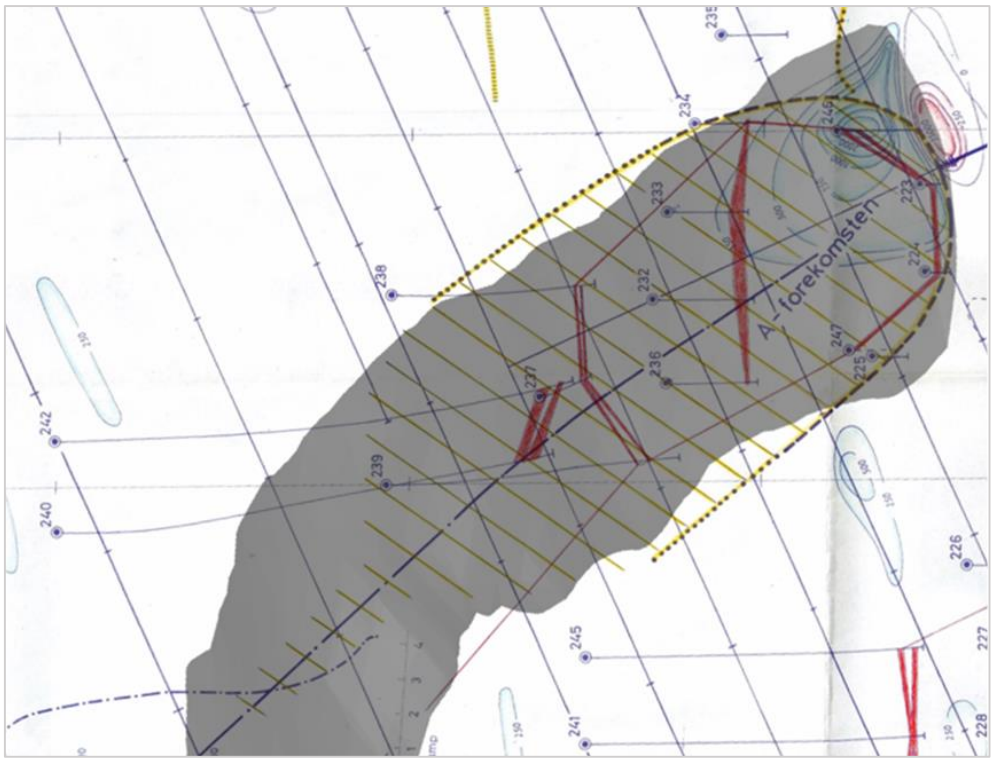


Figure 43: Extract of geophysical map given by Singsaas (1975), seen directly above final version of geometric model of lens A. Yellow markings indicate the extent of lens A based on geophysical investigations, while red indicates where drillholes have intersected the mineralisation.

### 3.2.2 Host rock geology

Modelling of the host rock geology turned out to be far more complicated than first envisioned. The main problems were caused by the lack of downhole lithology data around the upper half of the mineralised lens, as well as the inconsistencies between lithological definitions across drillholes.

After the lithology is imported into Leapfrog Geo, it is possible to both split and group the various lithologies. Having the visual aid of being able to view the drillholes with associated rock types in 3D will normally indicate the general trend of lithological contacts that can be modelled, and give indications as to which lithologies would be logical to group or split into separate units. For the Hessjø deposit geology, no apparent trends were visible from the drillhole data, with the exception of the overlying soil, and the contact between the Gula Group and Fundsjø Group rocks.

The various greenstone types represent the majority of the geology, and though Bakke (1975) has displayed the different types and the contacts between them in his geological profile (Figure 7), the same contacts were not easily distinguished when looking at the drillhole lithologies. Figure 44 shows the various greenstones as they have been logged in drillholes, along with Bakke's geological profile georeferenced in the background. Even though it might be possible to see a

trend of the light greenstones corresponding to Bakke's equivalent unit of light, partly porphyritic greenstone and pillow lava (light green) in the background, the drilhole lithologies are too inconsistent to be able to construct a viable contact.

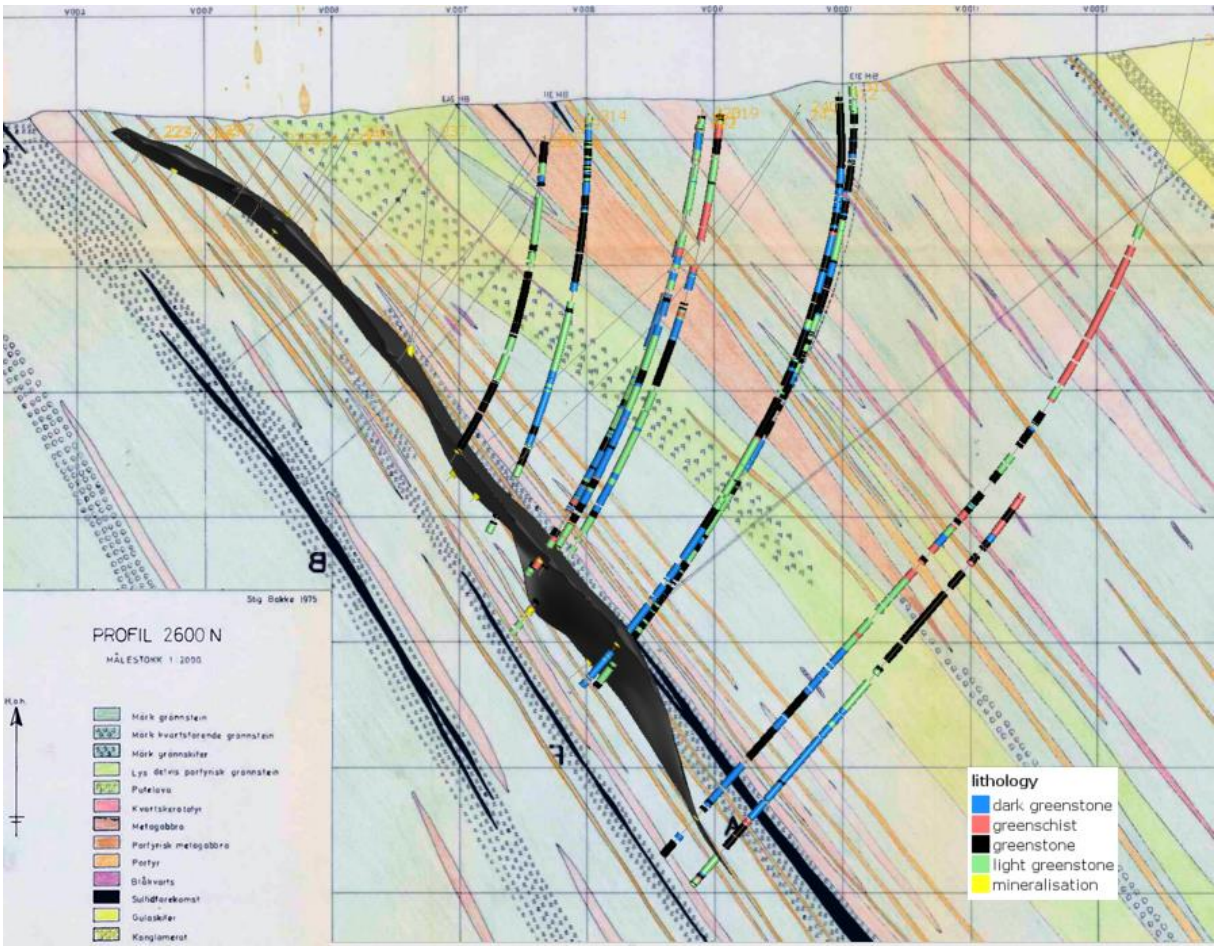


Figure 44: Screen clipping from Leapfrog Geo showing the various greenstone types as logged in drillholes, Bakke's (1975) geological profile (inverted) in background. View towards south.

Attempts were made to model the host rock geology using the core logged drillholes. However, as Leapfrog Geo by default models the lithological contacts based only on drillhole data, the resulting volumes were concentrated around the drillholes, and did not take into account that the geological units apparently lie conformably along the mineralised lens. There are various ways of modelling lithological contacts in Leapfrog, and attempts were made setting the contacts as vein, deposit, and intrusion, none of which gave satisfactory results. The only exception was the overlying soil layer, as it was possible to model this as an erosional contact, and further editing the contact with polylines as the initial output volume was too thick towards the boundaries set to incorporate the geological model.

When simplifying and grouping the lithological units to the extreme extent shown in Table 14, it was possible to define some of the contacts using only curved polylines.

Grouping the gabbroic and porphyritic rocks together is not without cause. Reviewing the detailed information in the core logs from drillholes 313-315, logged by Johannessen, the sections termed *metagabbro* appear to be a variety of porphyritic greenstone. In addition, Bakke (1975), in his descriptions of the geology of the Hessjø area, mentions what he has called *porphyritic metagabbro,* and *porphyry* as two of the defining lithologies, where the porphyries are characterised by a fine-grained, gabbroic matrix.

Table 14: Simplified lithological groups used in Leapfrog Geo.

| Simplified group | Original lithology |
|---|---|
| | dark greenstone |
| | light greenstone |
| | greenstone |
| | pillow lava |
| | greenschist |
| | chlorite schist |
| | chlorite |
| | breccia |
| Gabbros and porphyries | gabbro |
| | metagabbro |
| | porphyry |
| | metadiorite |
| Gula sediments | conglomerate |
| | graphite |
| | phyllite |
| | schist |
| Mineralisation | mineralisation |
| Soil | soil |
| Felsic rocks | felsic volcanics |
| | agglomerate |
| | quartz |
| | quartzite |
| Unassigned | blue quartz |
| | calcite |
| | clay gouge |
| | core loss |
| | garbenschiefer |
| | NA |

In terms of resource classification and initial evaluation of the ore potential of the Hessjø deposit, detailed information regarding the host rocks is not deemed of great importance. Thus, only a

few selected geological contacts were modelled to exemplify what is possible to model from the available data.

The contacts modelled using curved polylines are the Gula - Fundsjø Group contact, as well as the larger slice of porphyritic metagabbro (light brown) lying adjacent to the light greenstone unit (light green) in Figure 44, on the geological profile in the background. When viewing the simplified lithology in the drillholes in Leapfrog Geo, it is possible to discern the intimation of said slice of porphyritic metagabbro. In addition, several of the greenstone units logged in the given area are porphyritic. The geological profile in combination with the drillhole data was then used to guide the alignment and positioning of the curved polylines. As lens A is modelled as a vein, it has been set to cut through all other lithologies, with the exception of the soil layer.

The results of the geometric modelling are presented in chapter 4.1.

## 3.3 Qualimetric modelling

*Qualimetry* concerns various methods of quantification of the quality of any product, object, or process (Nazarov & Krushnyak, 2006). For the Hessjø deposit, the 3D qualimetric modelling includes the use of the interpolant function in Leapfrog Geo to generate grade shells and cut-off scenarios using the geometric model of lens A in combination with assay data of copper and zinc. As mentioned in chapter 3.1.5.1, zero-values in the assay data will be substituted by half the lowest value registered, i.e. 0.01%, giving a substitution value of 0.005%.

Ideally, a variography analysis of the assay data should be performed prior to any qualimetric evaluation, so as to be able to approximate the interpolant function parameters in Leapfrog to the semivariogram parameters. No variography analysis has been performed for the Hessjø assay data, due to insufficient time, knowledge, and availability of suitable computer software.

The results from the qualimetric modelling are provided in chapter 0.

### 3.3.1 Numeric interpolants

In Leapfrog Geo, a *numeric interpolant* describes a physical quantity that various continuously in space (ARANZ Geo, 2014). Numeric interpolant models were constructed for both copper and zinc, based on assay data.

#### 3.3.1.1 Copper

The values used for the qualimetric modelling of copper using a numeric interpolant are given in Figure 45.

The sill was set to the same value as the variance provided by Leapfrog, and the nugget to approximately 10% of the sill value (see chapter 2.2.2.2.3 for reasoning). As mentioned in chapter 3.1.5, anomalously high Cu-values occur in drillhole 312; the same is valid for drillehole 321. This gives reason for incorporating a nugget effect.

The alpha value is set to max, as this, in most cases, gives the most accurate results, and the dataset for the Hessjø deposit is not so large as to cause difficulties with the computational time and power. The accuracy is set to the lowest value in the dataset. The base range was set approximately twice the average distance between drillholes (chapter 4.3), as recommended in the Leapfrog Geo user manual if no variography analysis is available (see chapter 2.2.2.2.3).

Parameters). In addition, a search for feasibility studies of similar deposits was conducted, but finding studies on Cu-Zn VMS deposits proved to be difficult. However, the Phu Kham deposit in Laos, a distal aspect of a Cu-Au-system, uses a range of 250 m in their estimations (PanAust, 2014), while variography for the Rubtsovsk massive sulfide Cu-Pb-Zn deposit gives a range of 175 m for copper (Shatagin et al., 2007). A worked example from Edumine's online course in *Practical Geostatistics, Modeling and Spatial Analysis* (EduMine, 2010b), describes a high-grade Cu-Zn-sulfide deposit where a global semivariogram analysis of samples from chalcopyrite ore are

best represented by an exponential semivariogram model, with an apparent range of influence of 125 m, a nugget value of 0.24, and a sill value of 0.71.

Lastly, a structural trend based on a mesh extracted from the footwall points of the geometric model of the lens, was added to the interpolant.

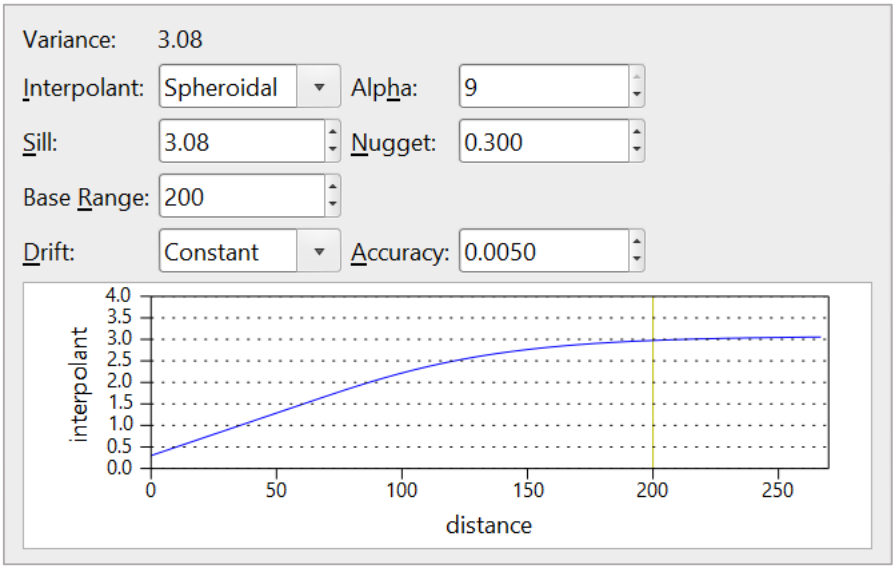


Figure 45: Interpolant values for Cu as used in Leapfrog Geo.

### 3.3.1.2 Zinc

The values used for the qualimetric modelling of zinc using a numeric interpolant is given in Figure 46.

The structural trend and sill, alpha, and accuracy values were set by the same standards as for the copper interpolant. The nugget value is also here set to approximately 10% of the sill value, as some drillholes, especially number 233, give anomalously high grades of zinc.

The base range was initially set to the same value as for copper, but through trial and error it was apparent that below a range of 300 m, the model shows significant variation. In an attempt to verify this, a search for variography analysis of zinc deposits was conducted, and it was found that for the sediment-hosted Citronen Fjord Zn-Pb deposit in Greenland, a range of 340 m for used for primary interpolation runs, even with a drilling pattern of 50 x 50 m (Ironbark Zinc, 2013). However, the worked example from Edumine's online course in *Practical Geostatistics, Modeling and Spatial Analysis* mentioned for copper (chapter 3.3.1.1), describing a high-grade Cu-Zn-sulfide deposit, gives spherical semivariogram model for massive black ore (>10% sphalerite), with a range of influence of 239 m, a nugget value of 0.2, and a sill value of 1.22 (EduMine, 2010c). Setting a base range of 300 m is therefore within reason.

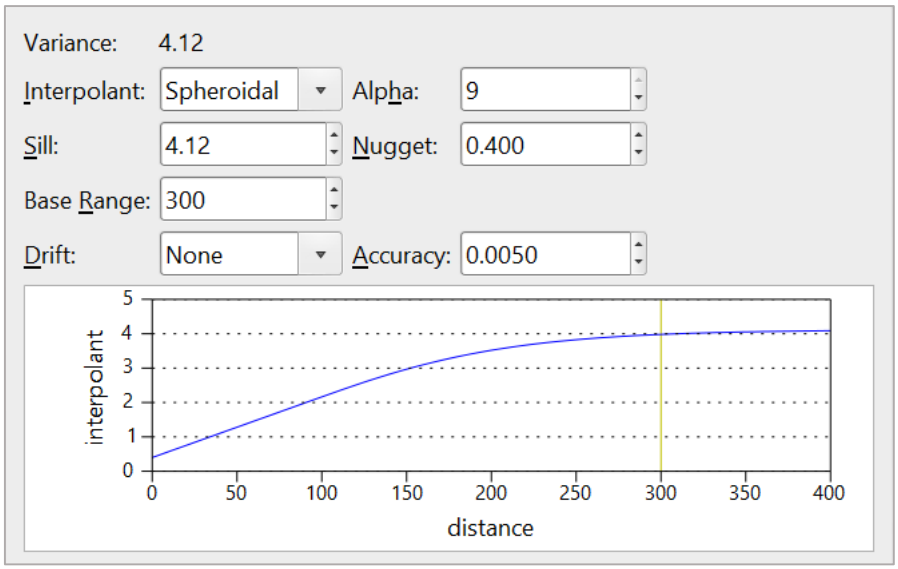


Figure 46: Interpolant values for Zn as used in Leapfrog Geo.

### 3.3.2 Indicator interpolants

In addition to the main interpolation model, scenarios for various cut-off grades were made, using the *indicator interpolant* function in Leapfrog Geo. This provides basic statistics for the above and below cut-off values, as well as a visual model.

#### 3.3.2.1 Copper

For copper, two scenarios were made, one for a cut-off value of 0.5%, and one for 1%. The interpolant values used are presented in Figure 47 and Figure 48. The parameter values are set by the same standards as for the main copper interpolant model, except for the nugget value, which is set to zero to be able to view the entire range of data.

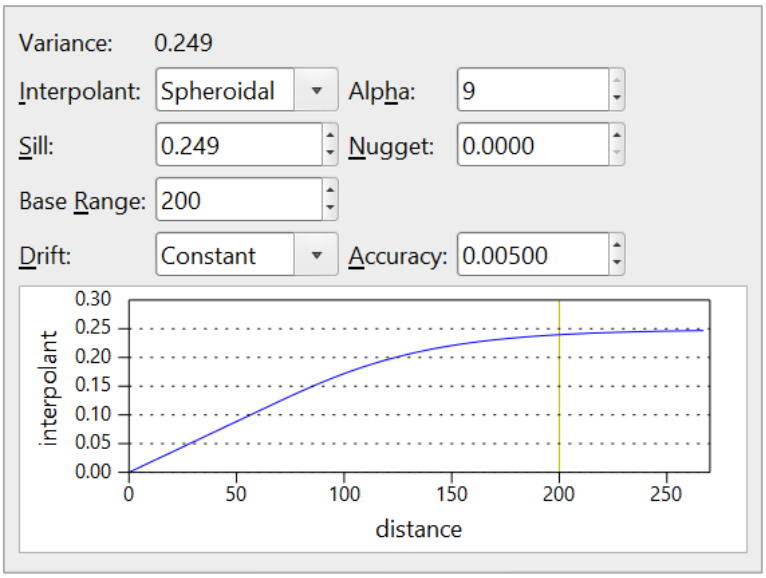


Figure 47: Indicator interpolant values used for a 0.5% cut-off value for Cu.

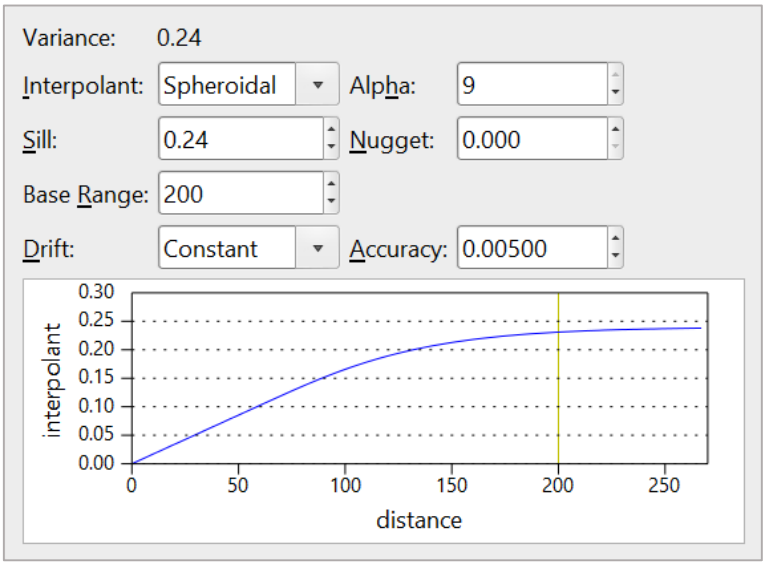


Figure 48: Indicator interpolant values used for a 1% cut-off value for Cu.

#### 3.3.2.2 Zinc

Same as for copper, indicator interpolants for zinc were constructed, here using cut-off values of 1% and 3%. Interpolant values are given in Figure 49 and Figure 50. The parameter values are set by the same standards as for the main zinc interpolant model, except for the nugget value, which is set to zero to be able to view the entire range of data.

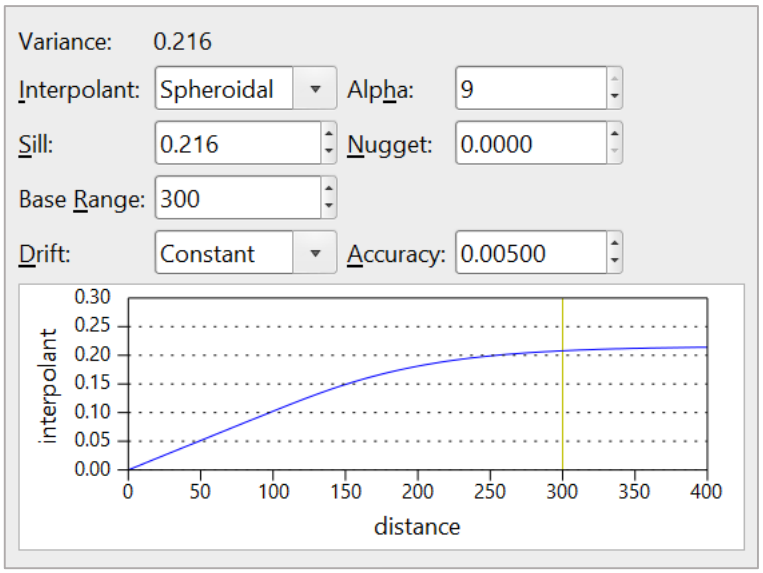


Figure 49: Indicator interpolant values used for a 1% cut-off value for Zn.

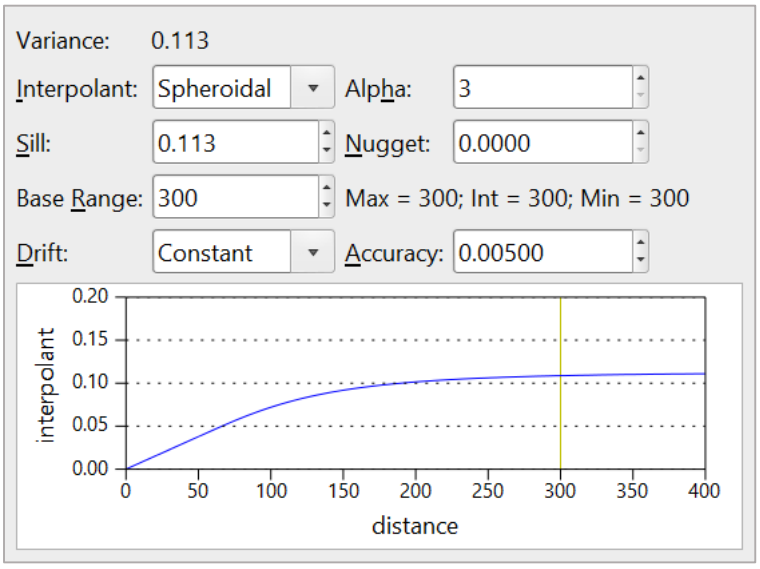


Figure 50: Indicator interpolant values used for a 3% cut-off value for Zn.

### 3.3.3 Block modelling

Two block models were constructed, one for copper and one for zinc. The models were evaluated on the numeric interpolant models and the geometric model of lens A. 2 x 2 x 2 m blocks were used.

Results from the qualimetric modelling of lens A in the Hessjø deposit are presented in chapter 0.

# 4 Results

The following subchapters present results from the geometric and qualimetric modelling of lens A in the Hessjø deposit. All models are generated using Leapfrog Geo, and all applicable statistics are also extracted from the same software.

A copy of all the files comprising the work done in Leapfrog Geo, in addition to separate versions of the .csv-files, will be available as a digital appendix.

## 4.1 Geometric model

The results from the geometric modelling of the Hessjø deposit are primarily presented using three vertical cross sections (plunge 90º), as visualised in Figure 52, Figure 53, and Figure 54. Drillholes displayed in the cross sections occur within a 15 m distance of each cross section. Placements of the cross sections relative to lens A are given in Figure 51.

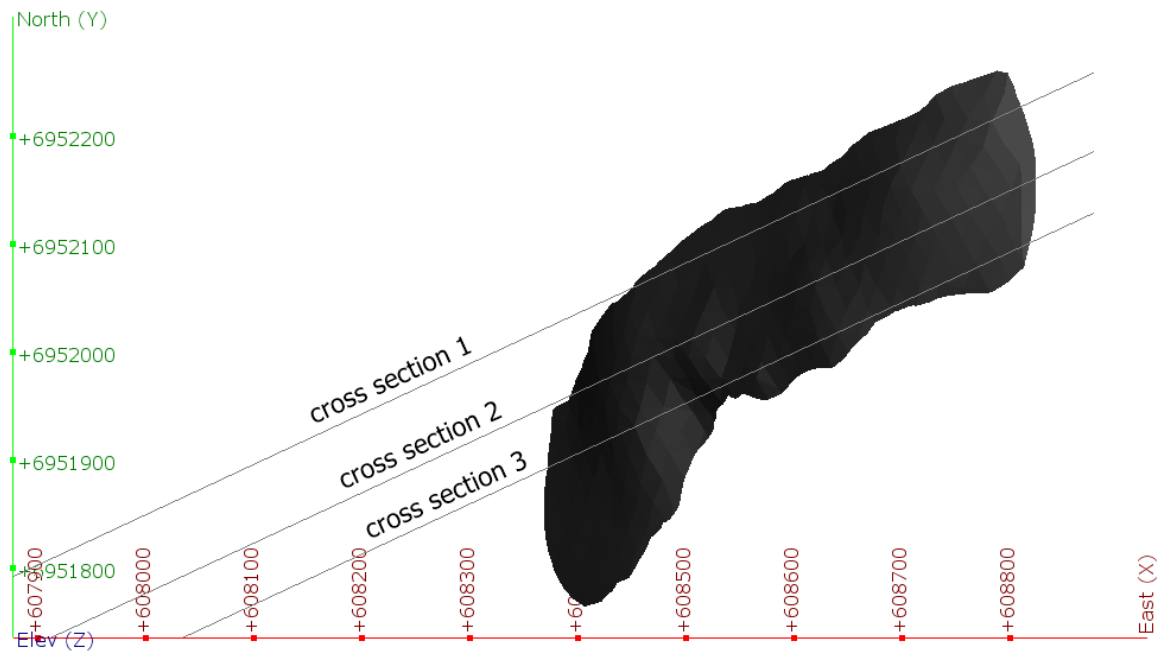


Figure 51: Placements of cross sections given in Figure 52 (cross section 1), Figure 53 (cross section 2), Figure 54 (cross section 3) relative to lens A. View from above.

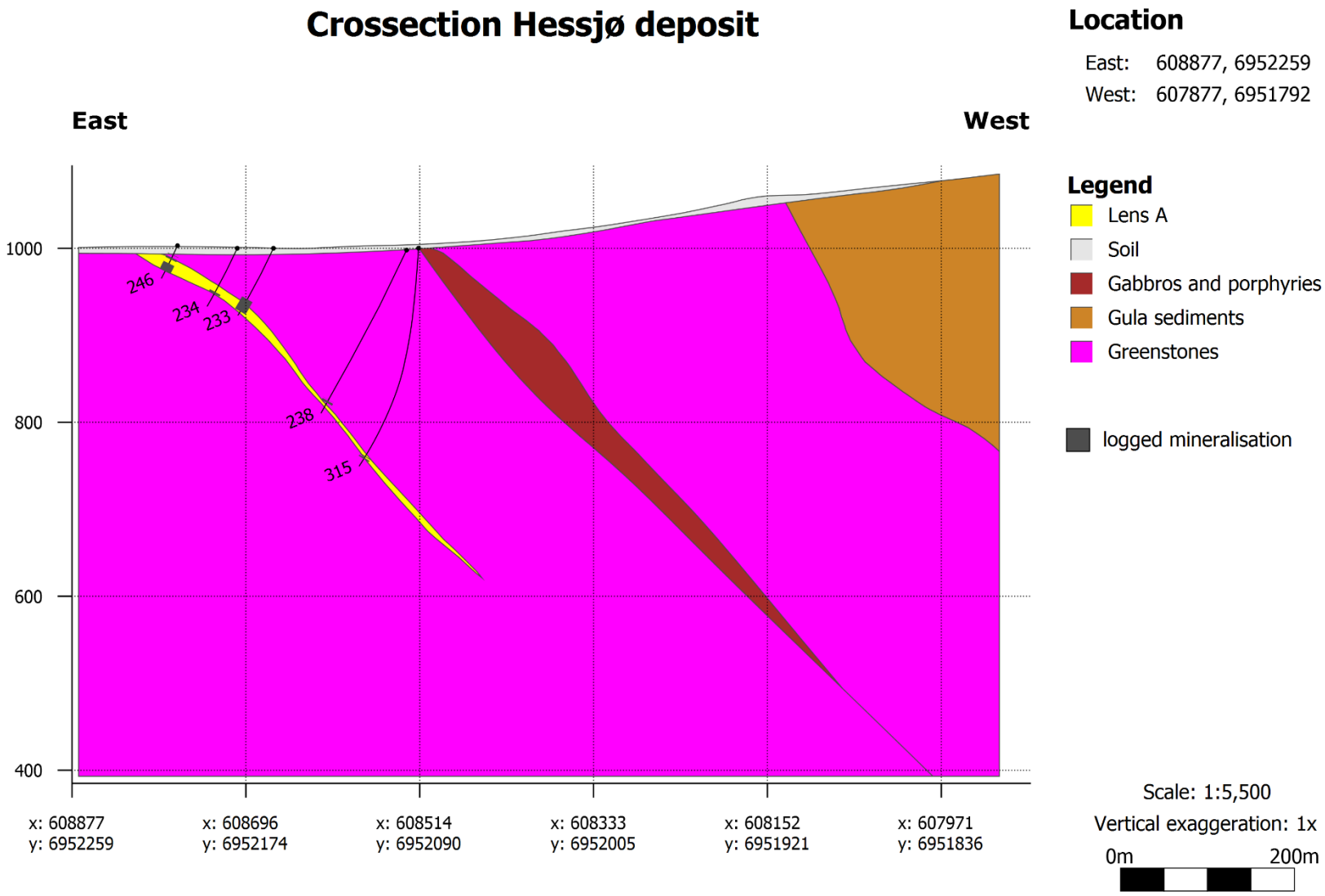


Figure 52: Cross section 1 from geometric model of the Hessjø deposit, northern end of mineralisation.

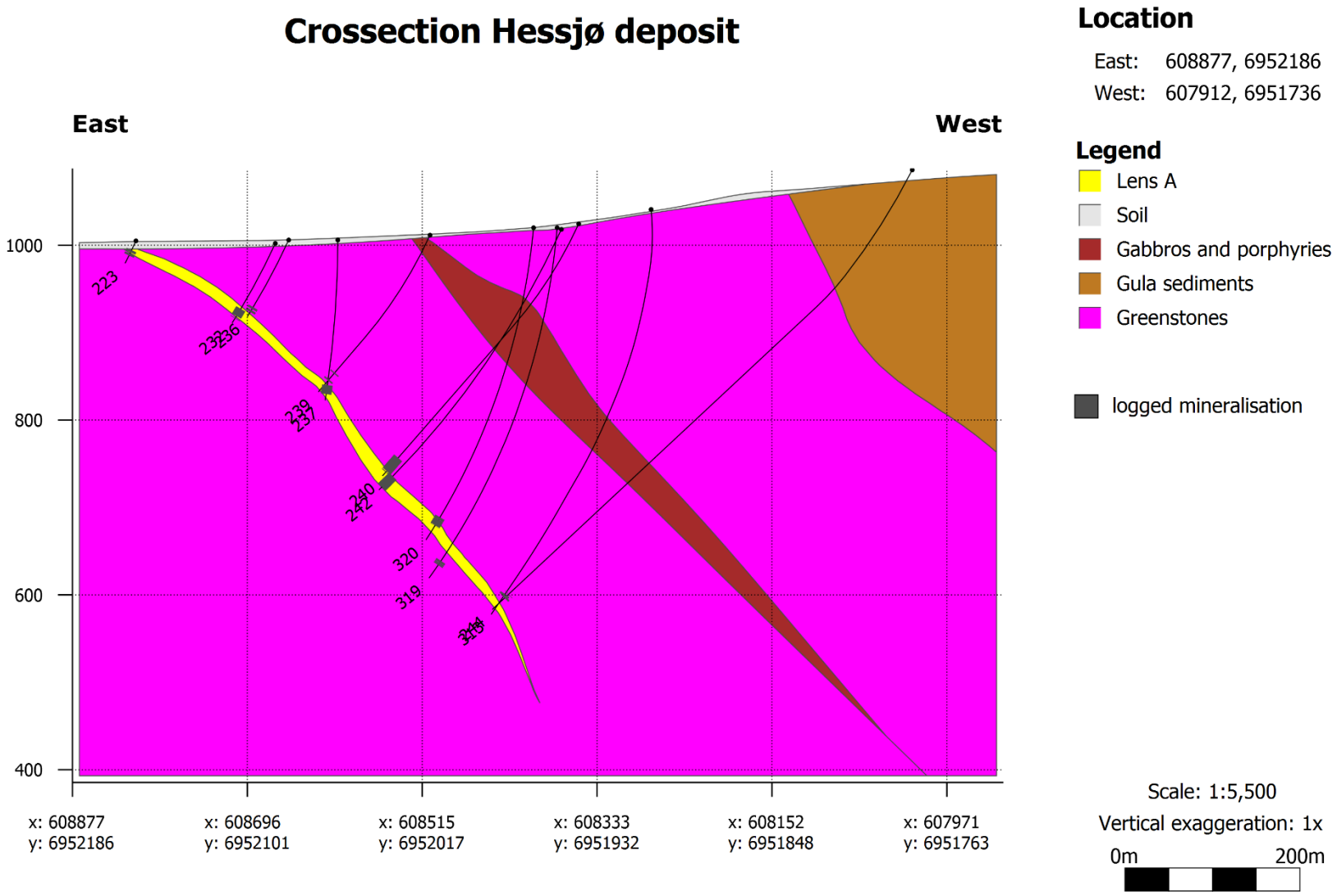


Figure 53: Cross section 2 from geometric model of the Hessjø deposit, central part of mineralisation. The two drillholes crossing at the lower end of lens A are no. 313 (eastern path) and no. 244 (western path).

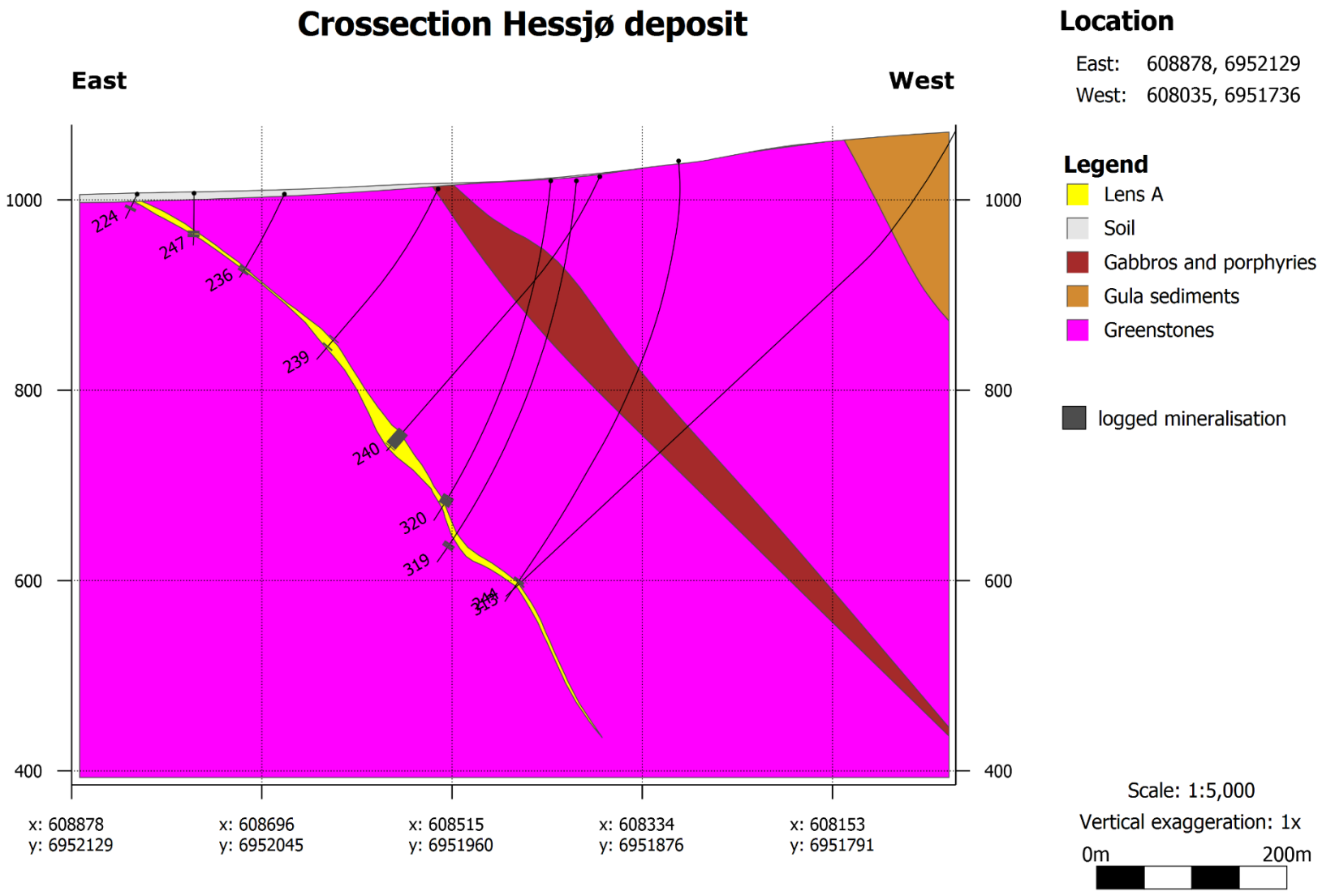


Figure 54: Cross section 3 from geometric model of the Hessjø deposit, southern end of mineralisation. The two drillholes crossing at the lower end of the lens are no. 313 (eastern path) and no. 244 (western path).

The black area located below and to the left of 'Lens A (model)' text in Figure 55 shows the positioning of the modelled lens relative to the geological profile constructed by Bakke (1975).

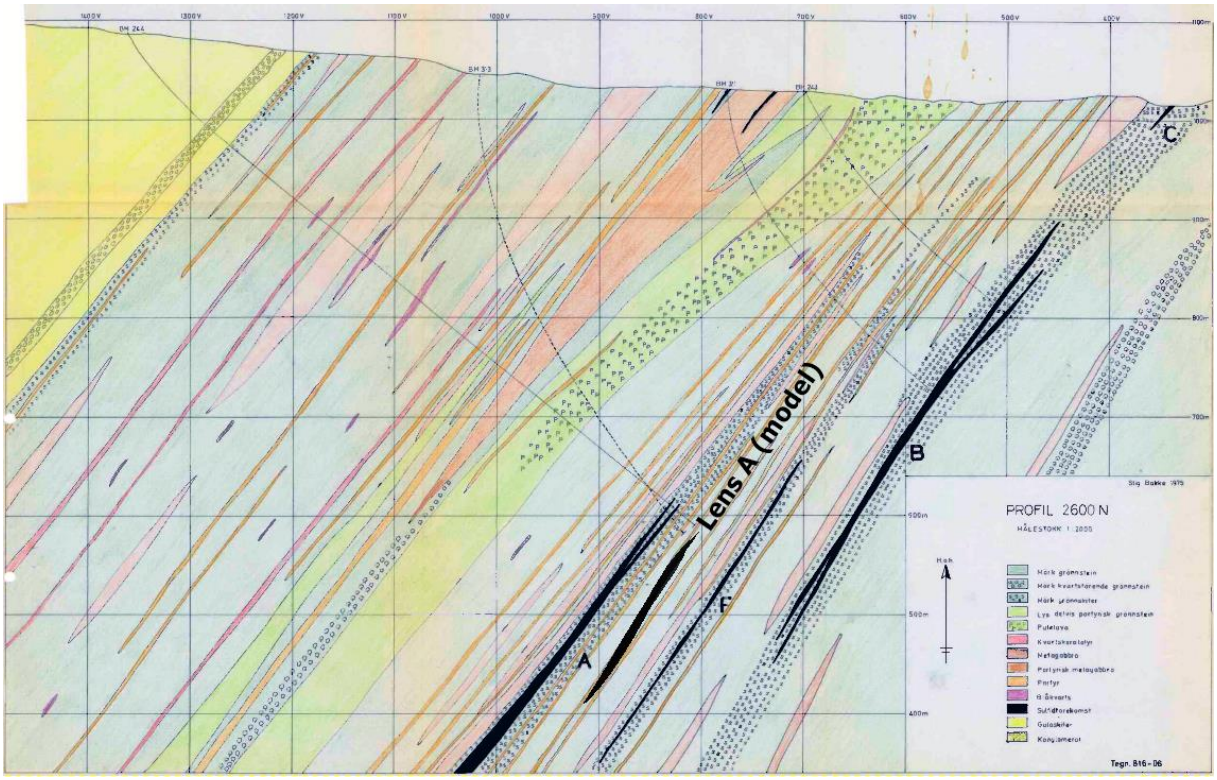


Figure 55: Screen clipping from Leapfrog Geo with geological profile georeferenced and imported into software. Figure shows model of lens A relative to the placement of lens A in geological profile by Bakke (1975). Positioning of profile is given in Figure 6, unmodified version of geological profile is shown in Figure 7.

## 4.2 Qualimetric models

Leapfrog Geo only supports exports of cross sections, screen clippings of the qualimetric models are provided instead, so as to be able to view the entire mineralised lens in 3D.

### 4.2.1 Numeric interpolants

Qualimetric models generated using the numeric interpolant function in Leapfrog Geo, describing the distribution of copper and zinc in lens A of the Hessjø deposit, are presented in the following subchapters.

#### 4.2.1.1 Copper

Statistics for the numeric interpolant model of copper are presented in Table 15, while a visualisation of the physical model is displayed in Figure 56.

Table 15: Statistics for numeric interpolant model of copper, given in grade intervals.

| *Cu* | | | |
|---|---|---|---|
| Interval [%] | Interval volume [$m^3$] | Approx. mean value [%] | No. of units |
| < 0.1 | 13551.35 | 0.1 | 1355.13 |
| 0.1-0.5 | 278144.8 | 0.3 | 83443.4 |
| 0.5-1.0 | 431649.5 | 0.75 | 323737. |
| 1.0-1.5 | 161671 | 1.25 | 202088. |
| 1.5-2.0 | 54205.75 | 1.75 | 94860.0 |
| 2.0-2.5 | 31055.7 | 2.25 | 69875.3 |
| > 2.5 | 22827.27 | 2.5 | 57068.1 |
| | | | |
| | | Approx. total: | 832,428 |

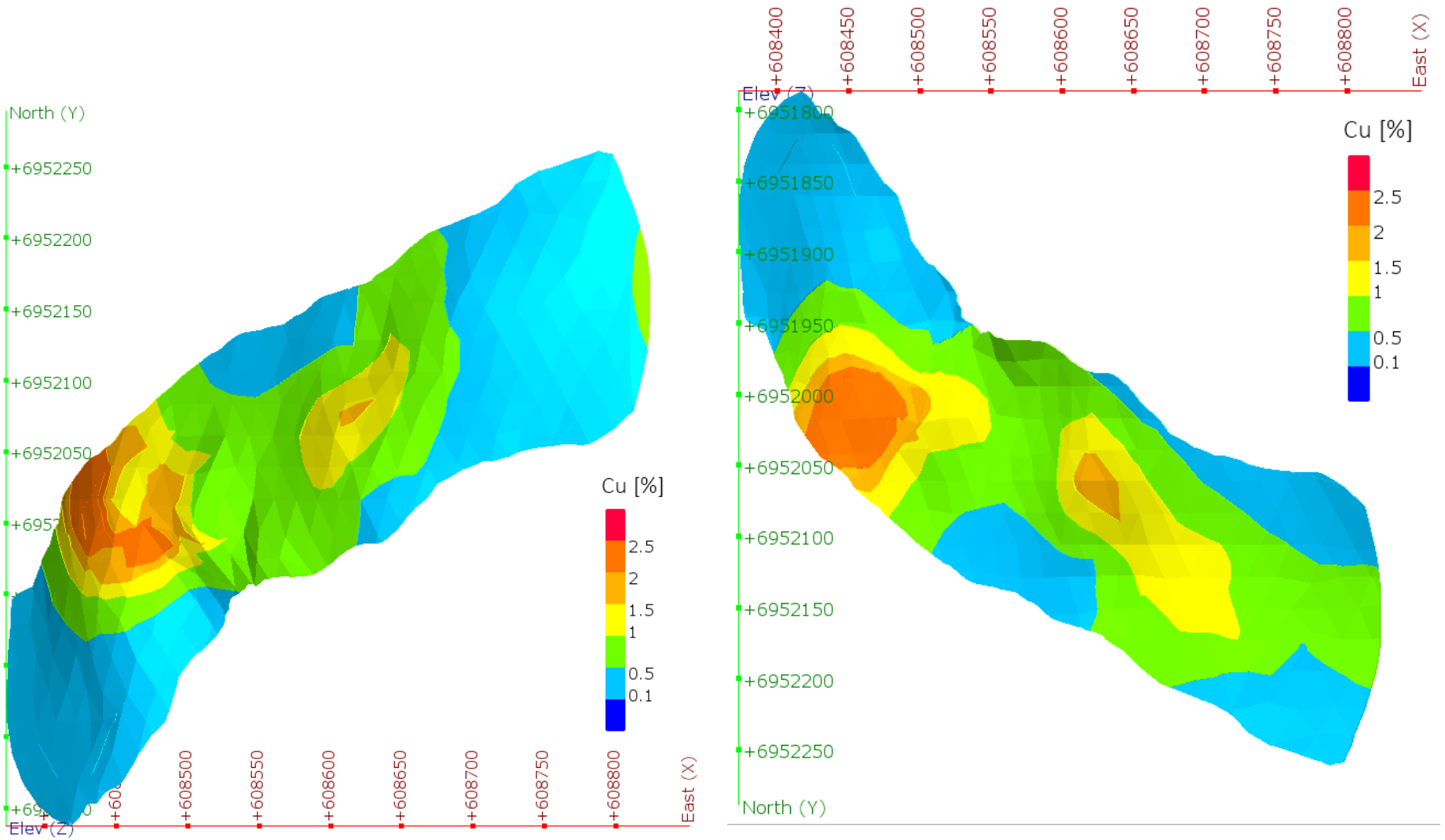


Figure 56: Qualimetric model of copper grades in lens A, generated by numeric interpolant in Leapfrog Geo. View from above (left) and below (right). North is upwards in the figure on the left side, and downwards in the figure on the right side.

#### 4.2.1.2 Zinc

Statistics for the numeric interpolant model of zinc are presented in Table 16, while a visualisation of the physical model is displayed in Figure 57.

Table 16: Statistics for numeric interpolant model of zinc, given in grade intervals.

| *Zn* | | | |
|---|---|---|---|
| Interval [%] | Interval volume [m³] | Approx. mean value [%] | No. of units |
| < 0.1 | 22788.59 | 0.1 | 2278.859 |
| 0.1-0.5 | 233009.5 | 0.3 | 69902.86 |
| 0.5-1.0 | 259256.1 | 0.75 | 194442.1 |
| 1.0-1.5 | 184924.1 | 1.25 | 231155.1 |
| 1.5-2.0 | 110224.4 | 1.75 | 192892.7 |
| 2.0-2.5 | 67044.6 | 2.25 | 150850.3 |
| > 2.5 | 115858 | 2.5 | 289645 |
| | | | |
| | | Approx. total: | 1,131,167 |

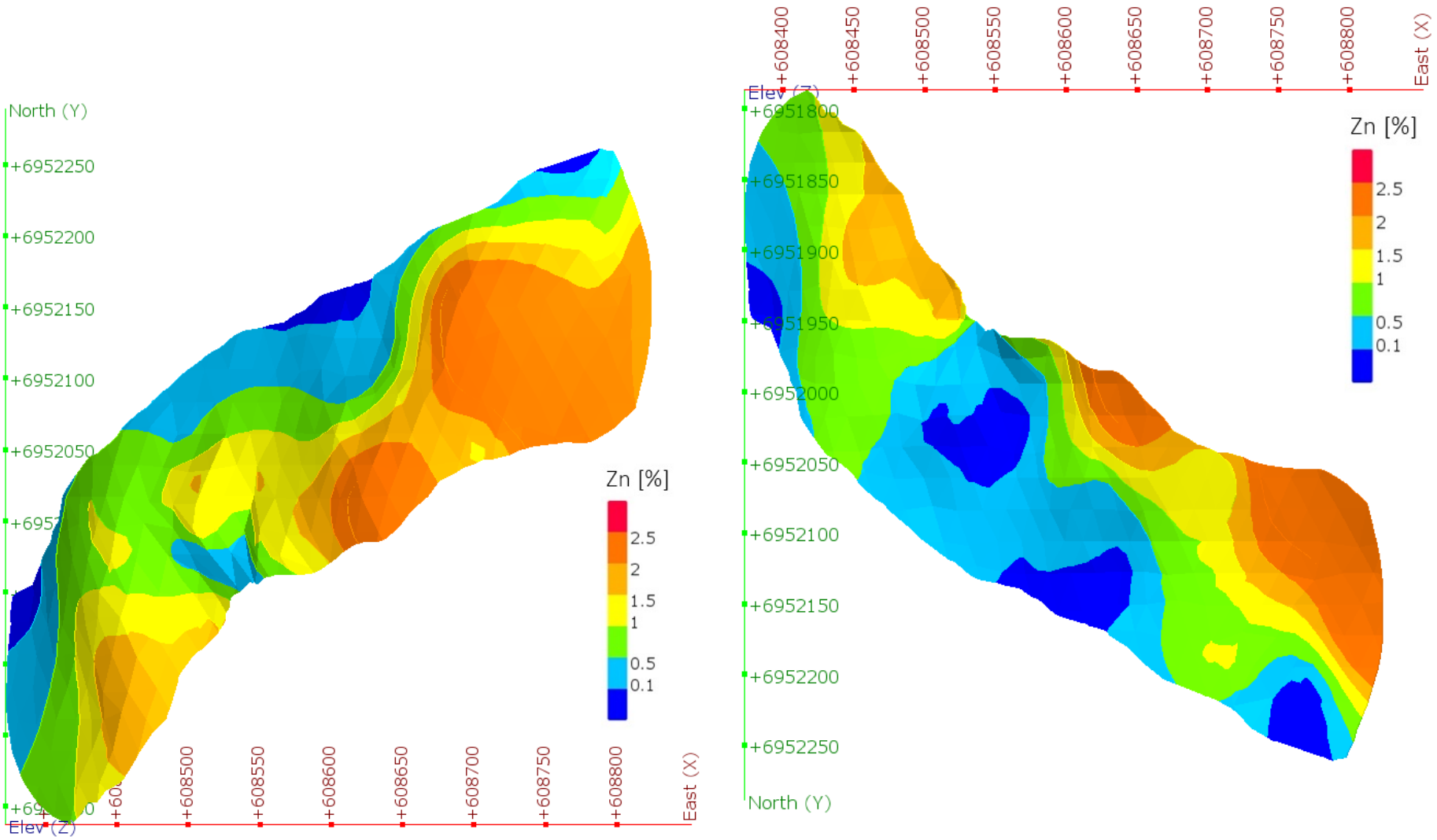


Figure 57: Qualimetric model of zinc grades in lens A, generated by numeric interpolant in Leapfrog Geo. View from above (left) and below (right). North is upwards in the figure on the left side, and downwards in the figure on the right side.

### 4.2.2 Indicator interpolants

Qualimetric models generated using the indicator interpolant function in Leapfrog Geo, describing various cut-off scenarios for copper and zinc in lens A of the Hessjø deposit, are presented in the following subchapters.

#### 4.2.2.1 Copper

Statistics for the indicator interpolants of copper cut-off grades are presented in Table 17 and Table 18. Visualisations of the physical models are displayed in Figure 58 and Figure 59.

Table 17: Statistics for indicator interpolant model of Cu at a cut-off value of 0.5%.

| *Cu: cut-off at 0.5%* | | |
|---|---|---|
| **Indicator statistics** | | |
| Total number of samples | 148 | |
| | | |
| | **≥ cut-off** | **< cut-off** |
| Number of points | 81 | 67 |
| Percentage | 54.73% | 45.27% |
| Mean value | 2.29779 | 0.155176 |
| Minimum value | 0.5 | 0.005 |
| Maximum value | 11.41 | 0 |
| Standard deviation | 2.25899 | 0.138498 |
| Coefficient of variance | 0.983115 | 0.892523 |
| Variance | 5.10305 | 0.0191818 |
| | | |
| **Output volume statistics** | | |
| Resolution | 5 | |
| Iso-value | 0.1 | |
| | | |
| | **Inside** | **Outside** |
| **≥ cut-off:** | | |
| Number of samples | 81 | 0 |
| Percentage | 54.73% | 0.00% |
| **< cut-off:** | | |
| Number of samples | 36 | 33 |
| Percentage | 24.32% | 22.30% |
| | | |
| **All points:** | | |
| Mean value | 1.72069 | 0.105557 |
| Minimum value | 0.01 | 0.005 |
| Maximum value | 11.41 | 0.4286 |
| Standard deviation | 2.13698 | 0.109921 |

| | | |
|---|---|---|
| Coefficient of variance | 1.24193 | 1.04135 |
| Variance | 4.56668 | 0.0120827 |
| Volume | 815,730 | 177,375 |
| Number of parts | 4 | 11 |

Table 18: Statistics for indicator interpolant model of Cu at a cut-off value of 1%.

| *Cu: cut-off at 1%* | | |
|---|---|---|
| **Indicator statistics** | | |
| Total number of samples | 148 | |
| | | |
| | **≥ cut-off** | **< cut-off** |
| Number of points | 58 | 90 |
| Percentage | 39.19% | 60.81% |
| Mean value | 2.91728 | 0.303504 |
| Minimum value | 1.0088 | 0.005 |
| Maximum value | 11.41 | 1 |
| Standard deviation | 2.40175 | 0.287595 |
| Coefficient of variance | 0.823283 | 0.94758 |
| Variance | 5.76839 | 0.0827107 |
| | | |
| **Output volume statistics** | | |
| Resolution | 5 | |
| Iso-value | 0.1 | |
| | | |
| | **Inside** | **Outside** |
| **≥ cut-off:** | | |
| Number of samples | 58 | 0 |
| Percentage | 39.19% | 0.00% |
| **< cut-off:** | | |
| Number of samples | 29 | 61 |
| Percentage | 19.59% | 41.22% |
| | | |
| **All points:** | | |
| Mean value | 2.08193 | 0.252289 |
| Minimum value | 0.015 | 0.005 |
| Maximum value | 11.41 | 0.954 |
| Standard deviation | 2.29621 | 0.263023 |
| Coefficient of variance | 1.10292 | 1.04255 |
| Variance | 5.27256 | 0.0691813 |
| Volume | 644,386 | 348,718 |
| Number of parts | 5 | 11 |

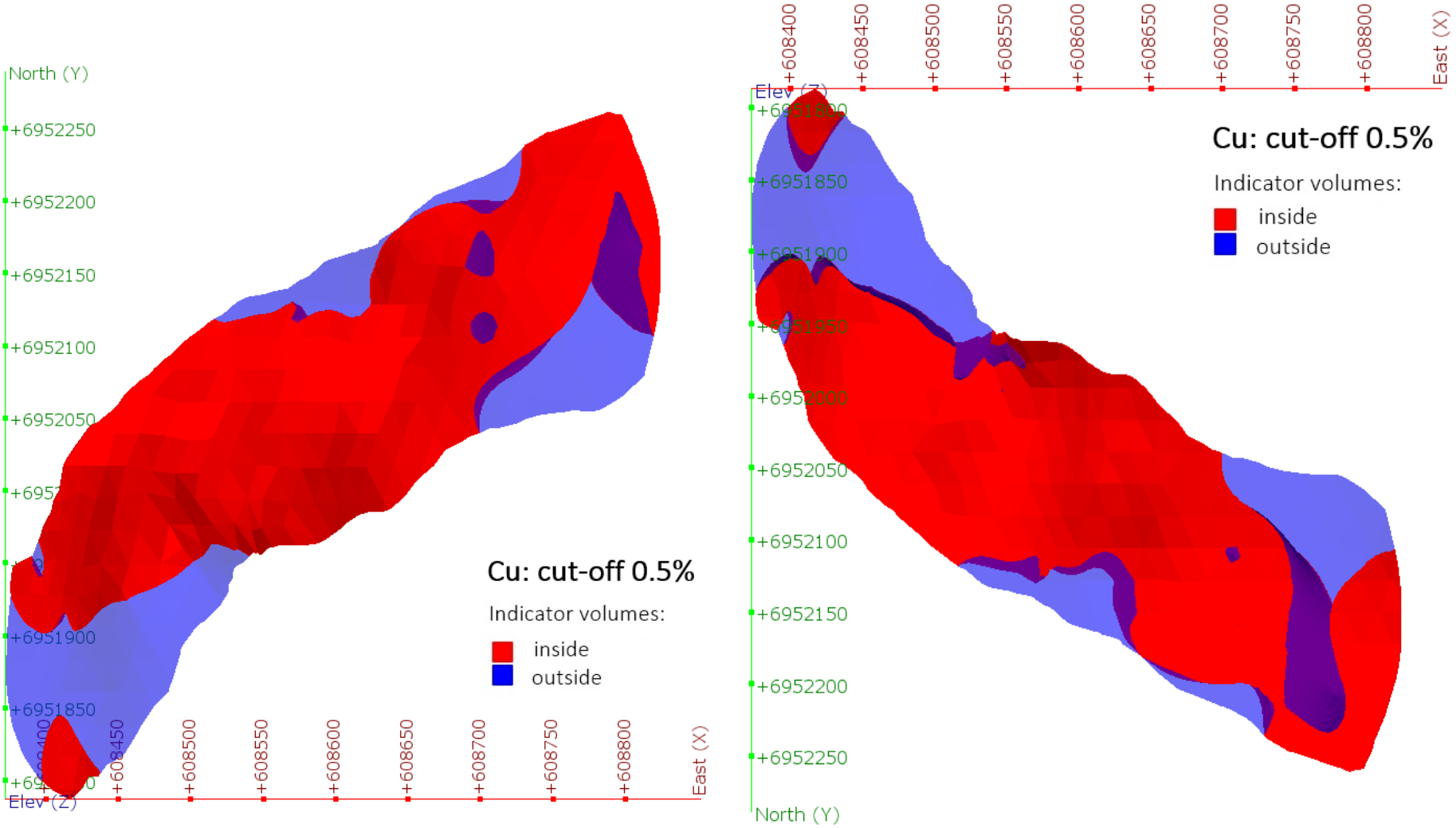


Figure 58: Qualimetric model of zinc at cut-off of 0.5%. Inside (red) indicates grades above cut-off. View from above (left) and below (right). North is upwards in the figure on the left side, and downwards in the figure on the right side.

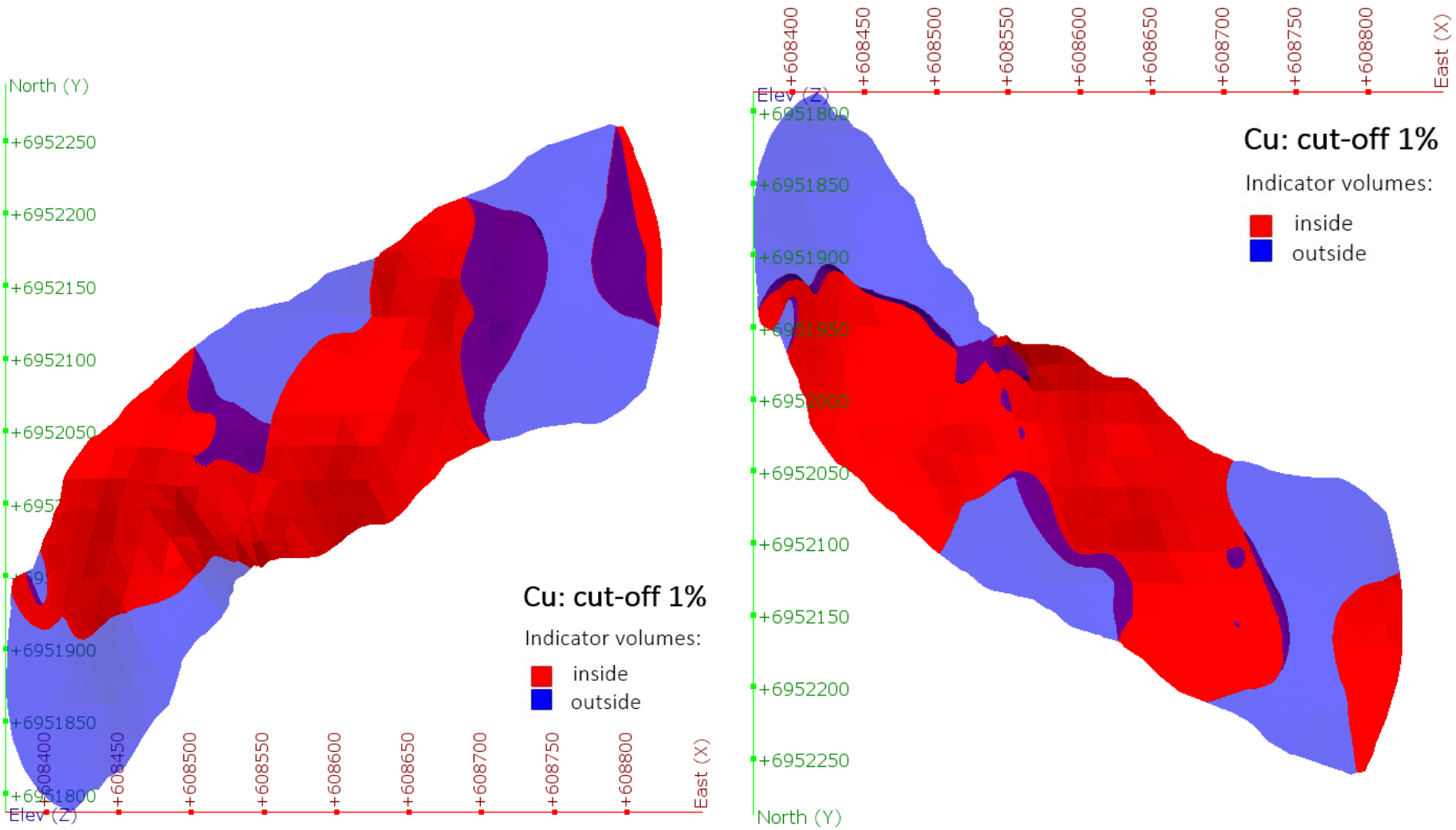


Figure 59: Qualimetric model of copper at cut-off of 1%. Inside (red) indicates grades above cut-off. View from above (left) and below (right). North is upwards in the figure on the left side, and downwards in the figure on the right side.

#### 4.2.2.2 Zinc

Statistics for the indicator interpolants of zinc cut-off grades are presented in Table 19 and Table 20. Visualisations of the physical models are displayed in Figure 60 and Figure 61.

Table 19: Statistics for indicator interpolant model of Zn at a cut-off value of 1%.

| *Zn: cut-off at 1%* | | |
|---|---|---|
| **Indicator statistics** | | |
| Total number of samples | 148 | |
| | | |
| | **≥ cut-off** | **< cut-off** |
| Number of points | 46 | 102 |
| Percentage | 31.08% | 68.92% |
| Mean value | 3.5 | 0.165837 |
| Minimum value | 1.01 | 0.005 |
| Maximum value | 12.75 | 1 |
| Standard deviation | 2.72983 | 0.237828 |
| Coefficient of variance | 0.779952 | 1.43411 |
| Variance | 7.45197 | 0.056562 |
| | | |
| **Output volume statistics** | | |
| Resolution | 5 | |
| Iso-value | 0.1 | |
| | | |
| | **Inside** | **Outside** |
| **≥ cut-off** | | |
| Number of samples | 46 | 0 |
| Percentage | 31.08% | 0.00% |
| **< cut-off** | | |
| Number of samples | 23 | 79 |
| Percentage | 15.54% | 53.38% |
| | | |
| **All points:** | | |
| Mean value | 2.40287 | 0.153385 |
| Minimum value | 0.005 | 0.005 |
| Maximum value | 12.75 | 0.955 |
| Standard deviation | 2.72023 | 0.226166 |
| Coefficient of variance | 1.13208 | 1.4745 |
| Variance | 7.39963 | 0.0511511 |
| Volume | 768,117 | 224,987 |
| Number of parts | 2 | 6 |

Table 20: Statistics for indicator interpolant model of Zn at a cut-off value of 3%.

| *Zn: cut-off at 3%* | | |
|---|---|---|
| **Indicator statistics** | | |
| **Total number of samples** | 148 | |
| | | |
| | **≥ cut-off** | **< cut-off** |
| Number of points | 19 | 129 |
| Percentage | 12.84% | 87.16% |
| Mean value | 5.75239 | 0.531936 |
| Minimum value | 3 | 0.005 |
| Maximum value | 12.75 | 3 |
| Standard deviation | 3.01398 | 0.772869 |
| Coefficient of variance | 0.523953 | 1.45294 |
| Variance | 9.08408 | 0.597326 |
| | | |
| **Output volume statistics** | | |
| Resolution | 5 | |
| Iso-value | 0.2 | |
| | | |
| | **Inside** | **Outside** |
| **≥ cut-off** | | |
| Number of samples | 18 | 1 |
| Percentage | 12.16% | 0.68% |
| **< cut-off** | | |
| Number of samples | 18 | 111 |
| Percentage | 12.16% | 75.00% |
| | | |
| **All points:** | | |
| Mean value | 3.6107 | 0.427948 |
| Minimum value | 0.005 | 0.005 |
| Maximum value | 12.75 | 7.65 |
| Standard deviation | 3.0328 | 0.915597 |
| Coefficient of variance | 0.83995 | 2.13951 |
| Variance | 9.1979 | 0.838317 |
| Volume | 288,934 | 704,170 |
| Number of parts | 3 | 3 |

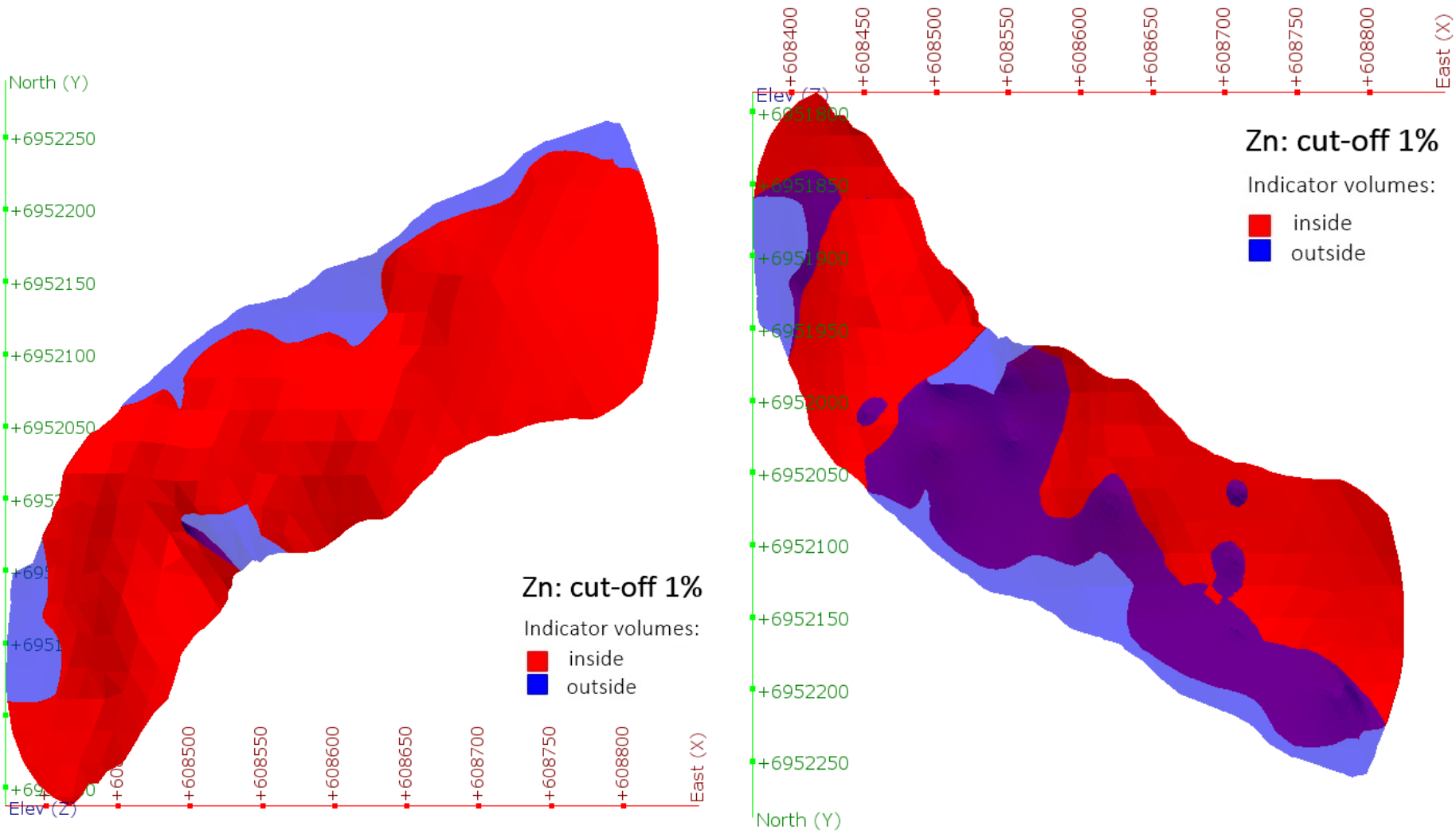


Figure 60: Qualimetric model of zinc at cut-off of 1%. Inside (red) indicates grades above cut-off. View from above (left) and below (right). North is upwards in the figure on the left side, and downwards in the figure on the right side.

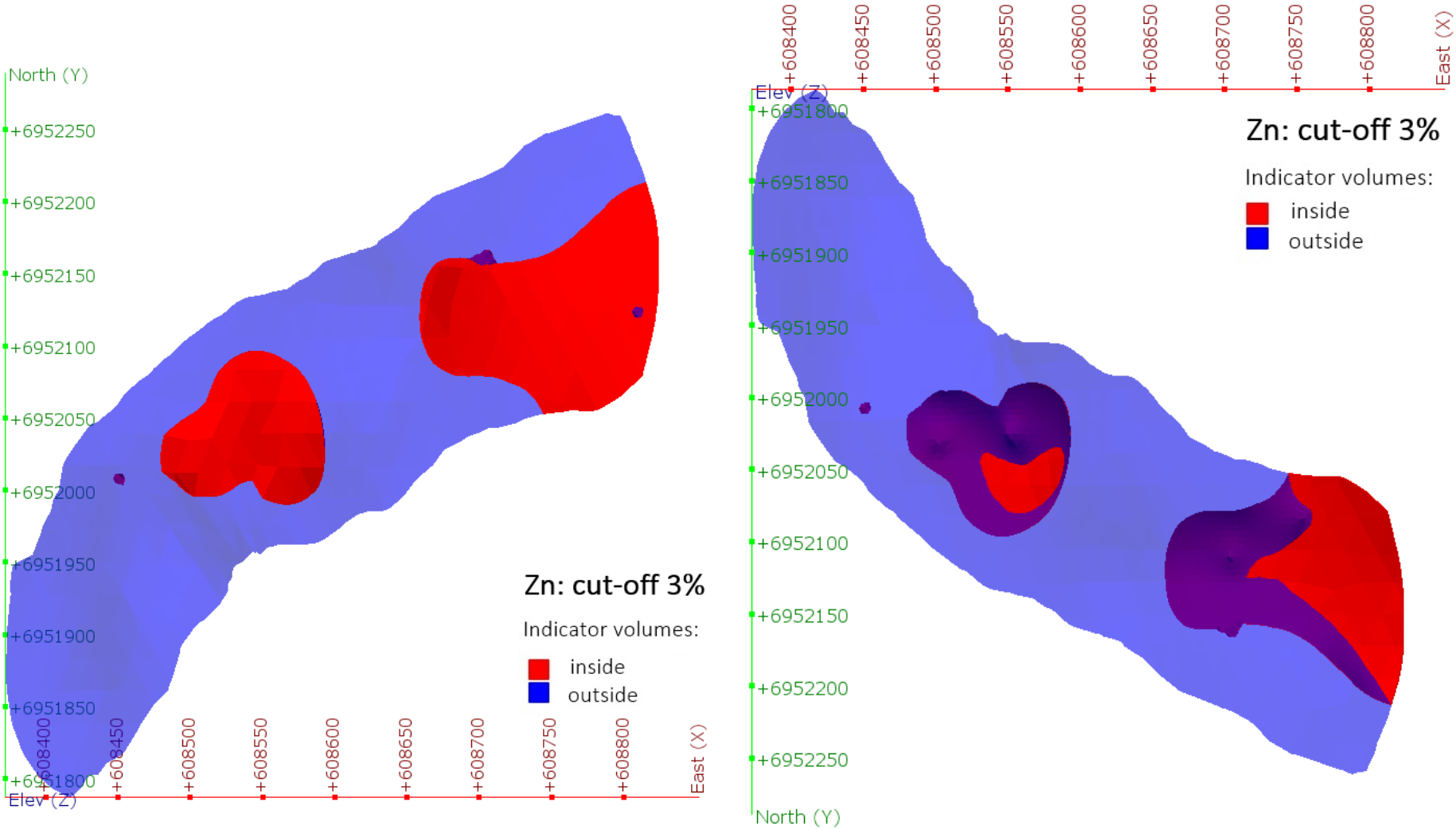


Figure 61: Qualimetric model of zinc at cut-off of 3%. Inside (red) indicates grades above cut-off. View from above (left) and below (right). North is upwards in the figure on the left side, and downwards in the figure on the right side.

### 4.2.3 Block models

The block model of lens A evaluated on Cu and Zn consists of 125 817 blocks, the results are presented in the following subchapters.

#### 4.2.3.1 Copper

Summary statistics for the block model of copper are presented in Table 21, while a visualisation of the physical model is displayed in Figure 62.

Table 21: Statistics for block modelling of copper grades [%].

| *Statistics block model Cu* | |
|---|---|
| Minimum | 0.0145896 |
| Lower quartile | 0.441948 |
| Median | 0.762865 |
| Upper quartile | 1.11646 |
| Maximum | 6.96685 |
| | |
| Mean value | 0.917695 |
| Standard deviation | 0.72309 |
| Variance | 0.52286 |

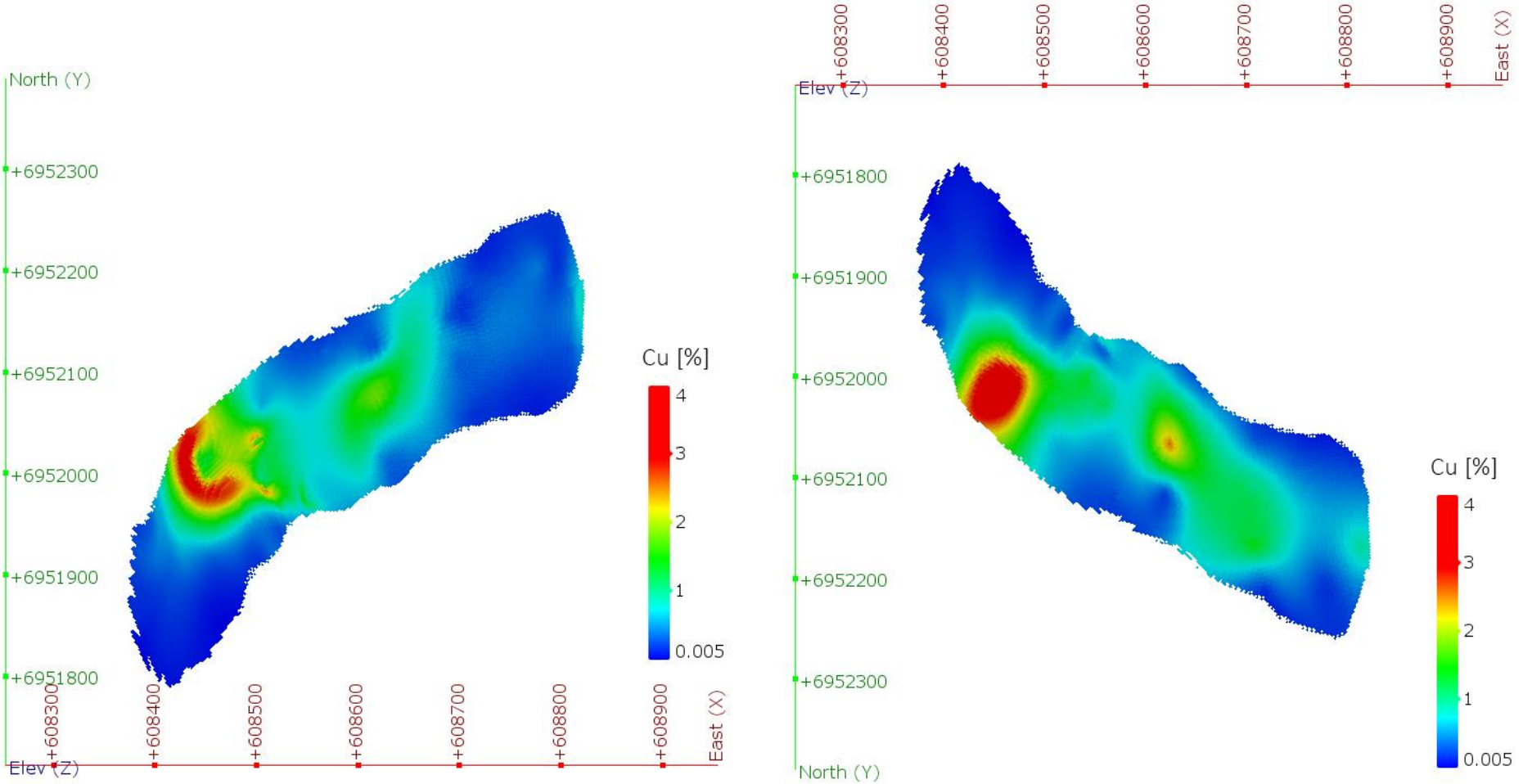


Figure 62: Block model of copper grades in lens A. View from above (left) and below (right). North is upwards in the figure on the left side, and downwards in the figure on the right side.

#### 4.2.3.2 Zinc

Summary statistics for the block model of zinc are presented in Table 22, while a visualisation of the physical model is displayed in Figure 63.

Table 22: Statistics for block modelling of zinc grades [%].

| *Statistics block model Zn* | |
|---|---|
| Minimum | 0 |
| Lower quartile | 0.47615 |
| Median | 0.96496 |
| Upper quartile | 1.68272 |
| Maximum | 5.29772 |
| | |
| Mean value | 1.19366 |
| Standard deviation | 0.904835 |
| Variance | 0.818726 |

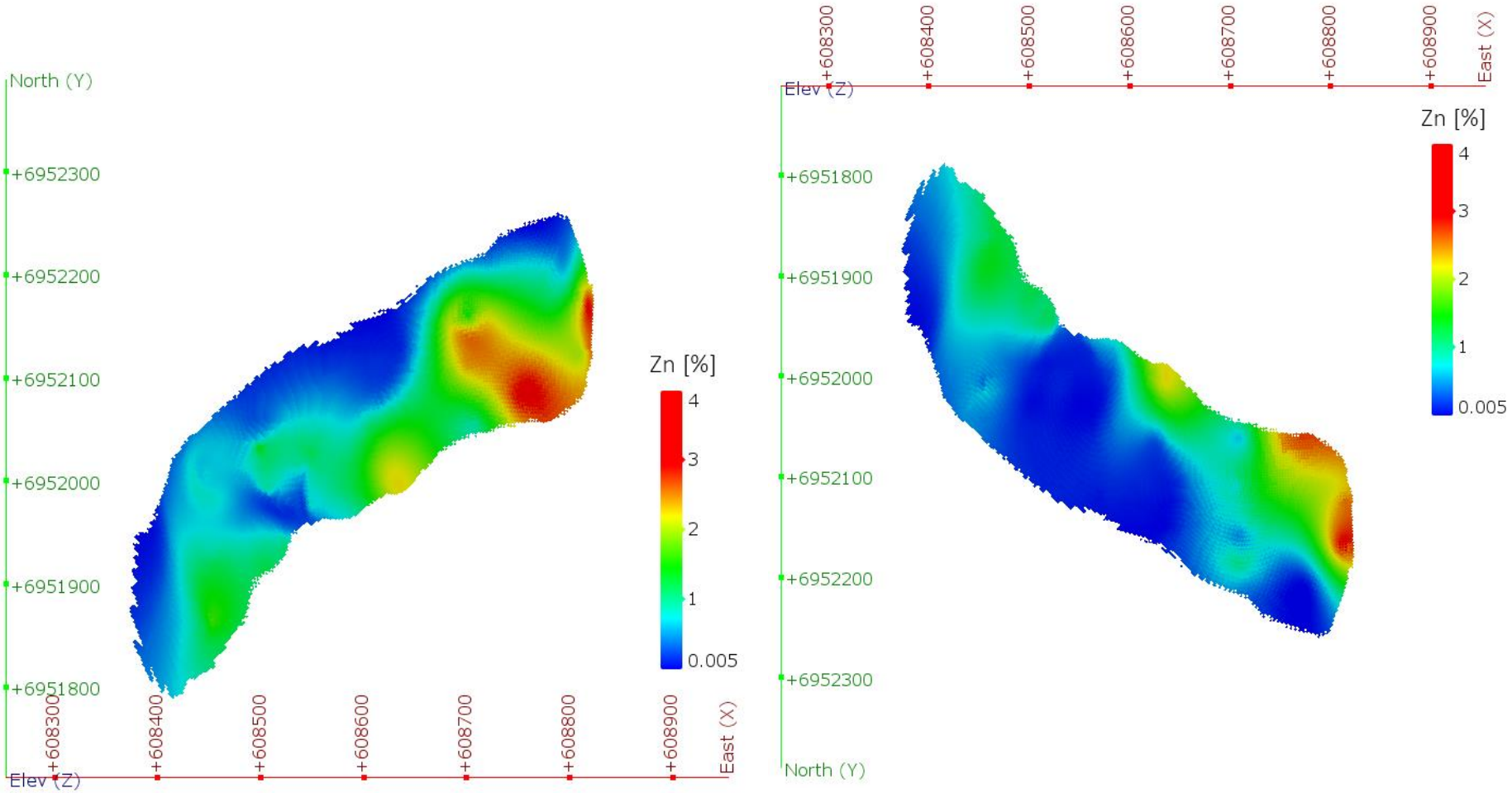


Figure 63: Block model of zinc grades in lens A. View from above (left) and below (right). North is upwards in the figure on the left side, and downwards in the figure on the right side.

## 4.3 Drillhole spacing

The drillhole spacing for lens A in the Hessjø deposit was approximated to be 40 to 80 m perpendicular to the main axis of the lens, and 60 to 250 m along axis. Figure 64 shows the distribution of the drillholes.

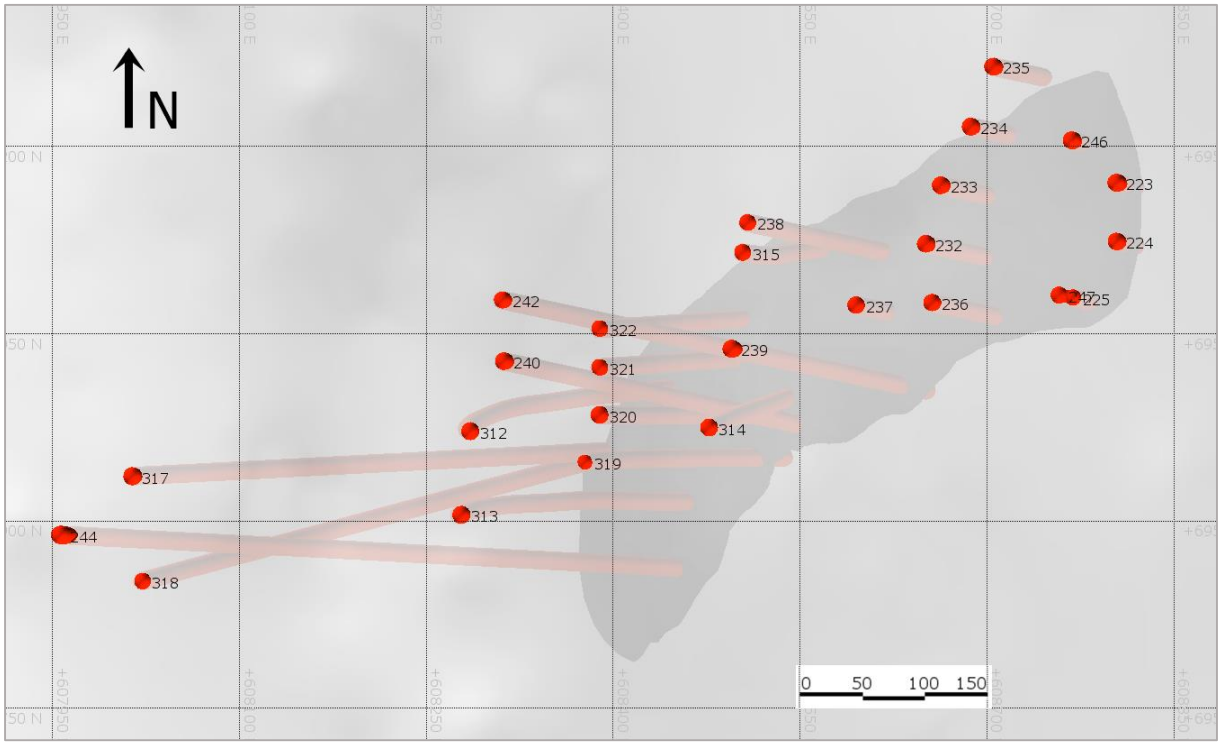


Figure 64: The distribution of drillholes on lens A of the Hessjø deposit. The drillholes are set to show with a diameter of 15 m for visualisation purposes. Grey overlay is the topography, outline of modelled lens in the background. Scale in meters, view from above.

# 5 Discussion

In the following subchapters, a discussion regarding the results and quality of the geometric and qualimetric modelling is presented, in addition to an attempt to indicate what resource classification category the Hessjø deposit would fall under. As the data used in the 3D-modelling was continuously evaluated prior to the commencement of the modelling, the discussion is concentrated around the results from the 3D-modelling, and the resource classification.

## 5.1 Geometric modelling

Through the process of modelling the Hessjø deposit, it became clear that the drillhole data quality is inadequate as discussed earlier, and the resulting model can only be regarded as a highly simplified interpretation.

The quality of the data used to model lens A has several issues, and as can be seen in Figure 55, the model of lens A does not match the placement of the lens given by Bakke (1975) in his geological profile. There are numerous reasons that can explain why this has occurred:

- No estimation of the horizontal deviation of the non-surveyed drillholes was applied, providing a low confidence in the lateral placement of the modelled lens.
- The positioning of drillhole 319 is incorrect, there is however no way of saying how incorrect given the current available data.
- There are uncertainties regarding the positioning of all collar points.
- The vertical deviation of the drillholes are only based on mean estimate, with the exception of some drillhole paths, where the deviation was estimated using profile maps.
- The lateral extent of the model is based mainly on visual interpretation using assay data and a geophysical map.
- Bakke's geological profile is in itself only an interpretation based on sparsely outcropping surface geology and drillhole data.

As for modelling of the host rock geology, an extreme simplification of the lithology was the only option to be able to model the lithological contacts. It is however, important to bear in mind the following factors that affected this simplification:

- There is only a small number of core logs available (9 complete, 1 partial), even though they are from long drillholes.
- Four different people logged the cores.
- The geology is characterised by many transitional forms between the various rock types.

This extreme simplification of the lithology leads to an array of possible interpretations of the host rock stratification and geometry, significantly lowering the quality of the resulting model.

## 5.2 Qualimetric modelling

According to the results from the qualimetric modelling (Figure 56 and Figure 62), copper appears to be enriched in the central part of the mineralised lens. The footwall shows a slightly more wide-spread distribution of higher Cu-grades than the hanging wall. As mentioned in chapter 2.1.1.2.2, Gvein (1976) stipulates that the copper rich portions of the mineralisation are situated in the footwall, and along the north edge of the lens. While the former seems to correlate with the qualimetric modelling, the latter is not immediately visible in the models.

Regarding zinc, the qualimetric models shown in Figure 57 and Figure 63, display a clear visulation of Zn-enrichment along the south edge of the lens, and there is also a slight indication of a more wide-spread zinc distribution in the hanging wall. This concurs with Gvein's (1976) conclusions as given in chapter 2.1.1.2.2.

The alignment of the zinc and copper rich areas towards the southern and northern edges, respectively, indicate that the deposit has been rotated and deformed during subsequent deformational and metamorphic events.

From the block models, the mean content of copper and zinc is estimated to be 0.92% and 1.19%, respectively. By applying a cut-off of 0.5% to copper, the inside indicator volume is reduced by c. 20% compared to the total volume of the lens, while a 1% cut-off reduces the inside indicator volume by over 40%. For zinc, a cut-off of 1% reduces the inside volume by more than 50%, and a cut-off of 3% reduces the inside volume by as much as c. 75%. This shows that, even though zinc has a higher mean content, it is more sensitive to cut-off. This is likely caused by the fact that the zinc samples display a wider range of content than copper, with a maximum value of 12.75% for zinc, and 11.41% for copper. In addition, the number of samples originally registered as zero is much higher for zinc (44), than for copper (7), thus indicating that the mean zinc content for the lens a whole, which is higher than that of copper, is highly influenced by the few, but high sample values. The mean grade contents from the block modelling are also substantially lower than the historical estimates shown in Table 2. A value of 0.005% was substituted for the zero-values in the assay data, and, if assuming that the historical estimates disregarded and did not apply the zero-value samples, this could be one explanation for why the estimated mean grades are lower than the historical estimates.

However, as no variography of the assay data was performed, and the methodology concerning the acquisition of the data from chemical analysis is unknown, the estimates from the qualimetric modelling should be reviewed with caution.

## 5.3 Resource classification

The drillhole spacing applied in the Hessjø deposit might be adequate compared to other copper deposits as those presented in chapter 2.3.2, but the uncertainties concerning the positioning of

not only the collar points, but also the downhole trajectories, significantly lower the quality of any estimates based on drillhole data. The general geometry of lens A is well known through thorough geophysical investigations, and shows that is ruler-shaped, probably continues towards depth, and lies separately from the other mineralised lenses as a massive mineralisation. However, the wide variation in thickness, together with the tapering and pinching along the edges (as shown in Figure 8), indicates an irregularity that would lower the confidence in grade continuity. Another issue is the lack of knowledge regarding the methods used in data acquisition, especially for the chemical analysis of copper and zinc. Confidence in the quality of the assay data is a key point in resource estimation, and as the historical estimates, along with the results from the qualimetric modelling presented here have shown, the estimated values of grades and tonnages vary greatly.

As for classification of the Hessjø deposit within the classification scheme defined by JORC, it is deemed highly unlikely that lens A could be classified as anything higher than an Exploration Target or an Inferred Resource. The amount of data available is quite high, but the question is whether the quality of the data is within reach of the Inferred category.

Factors that lower the grade of quality of the Hessjø data are:

- No variography analysis has been performed
- Absent and uncertain downhole surveys
- Uncertainties regarding correct positioning of collar data
- Absent core logs and discrepancies between core loggers' definition of rock types
- Absent information regarding data acquisition procedures
- Uncertainties regarding the geometric irregularities of the lens relative to the host rocks

Factors that heighten the grade of quality of the Hessjø data are:

- Confidence in geological continuity, based both on drillings and on geophysical investigations
- Very high percentage of core recovery in the logged drillholes (less than 10 m total)

According to JORC (2012, p.13), the intention of the Inferred Category is as follows:

> *The Inferred category is intended to cover situations where a mineral concentration or occurrence has been identified and limited measurements and sampling completed, but where the data are insufficient to allow the geological and grade continuity to be confidently interpreted.*

It is thus not impossible that the Hessjø deposit could be classified as an Inferred Resource. A definite answer can however, only be given by a Competent Person, as defined by JORC, through a complete evaluation of the data available.

# 6 Conclusion

It can be inferred that lens A of the Hessjø deposit is a Cu-Zn VMS-type deposit, of a likely bimodal-mafic subclassification. The lens was probably deposited relatively proximal to the vent, and it is likely that the metals were derived by leaching of the more than 2 km thick mafic volcanic sequence underlying the Hessjø deposit. Zonation patterns in the lens indicate that the current hanging wall and footwall are in concurrence with the original depositional stratigraphy, with a Zn-enrichment in the hanging wall and along the southern edges, and a Cu-enrichment in the footwall and central (northern) part of the lens. The lens shows several signs of deformation and metamorphism, including a rotation of the lens body, metamorphism of the surrounding host rocks into an upper greenschist-facies, porphyroblastic growth of pyrite grains, and injection of softer sulfide minerals into the more refractory minerals. In addition, the rocks in the Hessjø area display a directional schistosity and signs of folding.

The Hessjø deposit is located within the Fundsjø Group in the Trondheim Nappe Complex. It has been proposed that the Fundsjø Group was deposited in an immature arc/marginal basin setting.

Much of the data available for the Hessjø deposit is deemed to be of low quality in terms of resource classification, as many of the drillholes lack downhole survey measurements and core logs, and there are uncertainties surrounding the correct positioning of the collar points. In addition, records describing the methods and equipment used in data acquisition have not been found, if they so exist. In light of these factors, it is unlikely that lens A in the Hessjø deposit could be classified as anything higher than an Exploration Target or Inferred Resource with regards to JORC standards.

The geometric modelling of the Hessjø deposit turned out to be more complicated than first envisioned. As mentioned above, the quality of the data is questionable, and the resulting model can only be interpreted as a crude simplification of reality, especially with regards to the host rock geology.

The results from the qualimetric modelling of lens A showed that, when applying various cut-off values, the output volumes of especially zinc, are significantly lowered. The block modelling provided mean grade estimates of copper and zinc at values of 0.92% and 1.19%, respectively. This is significantly lower than the historical estimates. However, in regards to the quality of the data used, these estimates should be reviewed with caution.

## 6.1 Suggestions for further work

In light of the quality of the data inherent to the Hessjø deposit, the following recommendations and suggestions for further work are made:

- Variography analysis of the assay data
- Downhole surveying of the drillholes that are missing survey data

- Re-registration of the collar positions
- Lithological logging of the cores that are available at the Løkken storage facility
- Modelling of lens A in a greater detail, for example with respect to Bakke's (1975) indications of cross-section geometry
- Modelling of the host rock geology in greater detail
- Digitising of core logs inherent to lens B and C, and subsequent geometric and qualimetric modelling of these lenses, to see if they can shed light upon the interpretation made for lens A
- Performing an extended element analysis on samples from cores stored at Løkken, especially as no analysis for precious metals has been conducted towards the deeper end of lens A.

# 7 References


Altona Mining, 2014. *JORC 2012 Resource Estimate for the Little Eva Deposit.* [Online] Altona Mining Limited Available at: http://www.altonamining.com/static/uploads/documents/AOH0585_-_JORC_2012_Resource_Estimate_for_the_Little_Eva_Deposit.pdf [Accessed 4th April 2016].

Anon., 1985. *Hersjøfeltet, malmundersøkelser og muligheter for gruvedrift - BV 3850.* Killingdal Grubeselskap A/S, Bergvesenet.

ARANZ Geo, 2014. *User Manual for Leapfrog Geo version 2.1.* [Online] Available at: http://help.leapfrog3d.com/Geo/2.1/en-GB/LeapfrogGeoUserManual.pdf [Accessed 25th March 2015].

ARANZ Geo, 2016. *What's New in Leapfrog Geo 3.0.* [Online] Available at: http://help.leapfrog3d.com/Geo/3.0/en-GB/Content/new.htm [Accessed 20th March 2016].

ARANZ Geo, n.d. *The Leapfrog engine.* [Online] Available at: http://www.leapfrog3d.com/about-us/technology [Accessed 12th June 2016].

Argosy Minerals, 2015. *Maiden JORC Resource for Wee MacGregor Project.* [Online] Argosy Minerals Limited Available at: http://www.argosyminerals.com.au/IRM/PDF/1711/MAIDENJORCRESOURCEFORWEEMACGREGORPROJECT [Accessed 4th April 2016].

Bakke, S., 1975. *En malmgeologisk undersøkelse av området ved Hersjø Gruber i Ålen - Hovedoppgave i malmgeologi.* Trondheim: NTH - Bergavdelingen NTNU.

Barrie, C.D., Cook, N.J. & Boyle, A.P., 2010. Textural variation in the pyrite-rich ore deposits of the Røros district, Trondheim Region, Norway: implications for pyrite deformation mechanisms. *Mineralium Deposita*, 45(1), pp.51-68. Available at: http://link.springer.com/article/10.1007/s00126-009-0261-3 [Accessed 3rd February 2016].

Barrie, C.T. & Hannington, M.D., 1999. Classification of Volcanic-Associated Massive Sulfide Deposits. *Reviews in Economic Geology*, 8, Available at: https://www.segweb.org/store_info/REV/REV-08-Additional-Product-Info.pdf [Accessed 9th April 2016].

Barton, P.B. & Bethke, P.M., 1987. Chalcopyrite disease in sphalerite: pathology and epidemiology. *American Mineralogist*, 72(5-6), pp.451-67.

Beatson, R.K., Cherrie, J.B. & Mouat, C.T., 1999. Fast fitting of radial basis functions: Methods based on preconditioned GMRES iteration. *Advances in Computational Mathematics*, 11, pp.253-70. Available at: http://download.springer.com/static/pdf/294/art%253A10.1023%252FA%253A1018932227617.pdf?originUrl=http%3A%2F%2Flink.springer.com%2Farticle%2F10.1023%2FA%3A101893

2227617&token2=exp=1465743729~acl=%2Fstatic%2Fpdf%2F294%2Fart%25253A10.1023%25252FA%25253A1018 [Accessed 12th June 2016].

Bjerkgård, T., 2007. *The Hersjø ore deposit, evaluation of ore potential.* [report] Trondheim: Norges Geologiske Undersøkelse Available at: http://www.ngu.no/upload/Publikasjoner/Rapporter/2007/2007_023.pdf [Accessed 17th March 2015].

Bjerkgård, T., 2012. *N022 Folldal-Meråker Cu-Zn (pp. 81-85).* [Online] Espoo: Geological Survey of Finland Available at: http://tupa.gtk.fi/julkaisu/specialpaper/sp_053.pdf [Accessed 10th February 2016].

Bjerkgård, T., 2015. *Subject heading: Rapport om avviksmålinger fra 1971.* [e-mail] Message from Terje.Bjerkgard@ngu.no to s.norsett@gmail.com, sent May 5th 2015 [Accessed 27th June 2016].

Bjerkgård, T. & Bjørlykke, A., 1994. Geology of the Folldal area. *NGU Bulletin 426*, pp.53-75. Available at: http://www.ngu.no/FileArchive/NGUPublikasjoner/Bulletin426_53-75.pdf [Accessed 3rd April 2016].

Bjerkgård, T. & Bjørlykke, A., 1996. Sulfide Deposits in Folldal, Southern Trondheim Region Caledonides, Norway: Source of Metals and Wall-Rock Alterations Related to Host Rocks. *Economic Geology*, 91, pp.676-96. Available at: http://economicgeology.org/content/91/4/676.full.pdf+html [Accessed 3rd February 2016].

Bjørlykke, A., Vokes, F.M., Birkeland, A. & Thorpe, R.I., 1993. Lead Isotope Systematics of Strata-Bound Sulfide Deposits in the Caledonides of Norway. *Economic Geology*, 88, pp.397-417. Available at: http://economicgeology.org/content/88/2/397.full.pdf+html [Accessed 3rd February 2016].

Box, G.E.P., 1987. *Empirical model-building and response surfaces.* New York: Wiley.

Caravel Minerals, 2016. *Calingiri Maiden JORC Resource.* [report] Caravel Minerals Available at: http://www.csaglobal.com/wp-content/uploads/2016/04/Caravel-Resources-4-April-2016.pdf [Accessed 15th June 2016].

Corfu, F., Andersen, T.B. & Gasser, D., 2014. The Scandinavian Caledonides: main features, conceptual advances and critical questions. Geological Society Special Publication 390. In F. Corfu, D. Gasser & D.M. Chew, eds. *New Perspectives on the Caledonides of Scandinavia and Related Areas.* London: The Geological Society of London. pp.9-44.

Cowan, E.J. et al., 2003. Practical Implicit Geological Modelling. In Dominy, S., ed. *5th International Mining Geology Conference.* Bendigo, Victoria, 2003. The Australasian Institute of Mining and Meallurgy.

Craig, J.R. & Vaughan, D.J., 1994. *Ore Microscopy and Ore Petrography.* 2nd ed. New York: John Wiley & Sons, Inc. Available at:

http://www.minsocam.org/msa/OpenAccess_publications/Craig_Vaughan/#contents [accessed 20th June 2016].

Craig, J.R. & Vokes, F.M., 1992. Ore mineralogy of the Appalachian-Caledonian stratabound sulfide deposits. *Ore Geology Reviews*, pp.77-123. Available at: http://www.sciencedirect.com/science/article/pii/0169136892900078 [Accessed 3rd February 2016].

Craig, J.R. & Vokes, F.M., 1993. The metamorphism of pyrite and pyritic ores: an overview. *Mineralogical Magazine*, 57, pp.3-18. Available at: http://www.minersoc.org/pages/Archive-MM/Volume_57/57-386-3.pdf [Accessed 5th April 2016].

Croghan, C.W. & Egeghy, P.P., 2003. Methods of Dealing with Values Below the Limit of Detection using SAS. St. Petersburg, Florida, 2003. Presentation at Southeastern SAS User Group; Sept 22-24.

Doman, R.C. & Alper, A.M., 1983. Refractory minerals. In K. Frye, ed. *The Encyclopedia of Mineralogy*. 1st ed. New York: Springer US. pp.441-45. Part of the series Encyclopedia of Earth Science.

Edumine/Clark & Harper, 2014. *Online course. Practical Geostatistics 2000 - 2: Spatial Statistics, Part 2 - The Semi-Variogram.* [Online] Available at: http://www.edumine.com/xutility/html/template.htm?category=xcourse&course=xpg2000-2&session=doc0100.xml&level=text&lang=EN [Accessed 10th April 2016].

EduMine, 2010a. *Practical Geostatistics, Modeling and Spatial Analysis: Part 3: Basic Concepts and Theory of Geostatistics.* [online course] Available at: http://www.edumine.com/xutility/html/template.htm?category=xcourse&course=xgeostats&session=doc0100.xml&level=text&lang=EN [Accessed 15th June 2016].

EduMine, 2010b. *Practical Geostatistics, Modeling and Spatial Analysis: Figure 21.* [online course] Available at: http://www.edumine.com/xcourse/xgeostats/docs/wrkx03/xm0312d.xml#lock [Accessed 15th April 2016].

EduMine, 2010c. *Practical Geostatistics, Modeling and Spatial Analysis: Figure 19.* [online course] Available at: http://www.edumine.com/xcourse/xgeostats/docs/wrkx03/xm0312b.xml#lock [Accessed 15th April 2016].

Eilu, P., 2012. Introduction. In P. Eilu, ed. *Mineral deposits and metallogeny of Fennoscandia.* Espoo: Geological Survey of Finland. pp.6-12.

Eilu, P. et al., 2009. *Metallogenic Map of the Fennoscandian Shield.* [Online] Available at: http://tupa.gtk.fi/kartta/erikoiskartta/ek_080_300dpi.pdf [Accessed 10th February 2016].

Ellefmo, S. & Larsen, E., 2013. *Innføring i geostatistikk.* Trondheim: NTNU - Institutt for geologi og bergteknikk.

EPA, 2006. *Data Quality Assessment: Statistical Methods for Practitioners, EPA QA/G-9.* [Online] Washington DC: United States Environmental Protection Agency. Available at: http://nepis.epa.gov/Exe/ZyPDF.cgi/900B0D00.PDF?Dockey=900B0D00.PDF [Accessed 16th June 2016].

Eriksen, K.R. & Pettersen, Ø., 1972. *Ad. BVIL - Utvalg: "Undersøkelsesboring of prøvetaking", Besvarelse på spørreskjema.* Røros: A/S Røros Kobberverk. Letter archived at Røros Museum.

ESRI, 2016. *ArcMap - How Kriging works.* [Online] Available at: http://desktop.arcgis.com/en/arcmap/10.3/tools/3d-analyst-toolbox/how-kriging-works.htm [Accessed 14th June 2016].

Fox, J.S., Farquhar, R., Rui, I. & Cook, N., 1988. Genesis of basalt-hosted massive sulphide deposits from the Trondheim and Sulitjelma districts, Norway: ore lead isotopic considerations. *Mineralium Deposita*, 23(4), pp.276-85. Available at: http://link.springer.com/article/10.1007/BF00206408 [Accessed 3rd February 2016].

Franklin, J.M., Gibson, H.L., Jonasson, I.R. & Galley, A.G., 2005. Volcanogenic Massive Sulfide Deposits. *Economic Geology 100th Anniversary Volume*, 100, pp.523-60.

Franklin, J.M., Lydon, J.W. & Sangster, D.F., 1981. Volcanic-Associated Massive Sulfide Deposits. *Economic Geology 75th Anniversary Volume*, 75, pp.485-627.

Goovaerts, P., 1997. *Geostatistics for Natural Resources Evaluation.* New York, Oxford: Oxford University Press.

Grenne, T., 1988. Marginal basin type metavolcanites of the Hersjø Formation, eastern Trondheim district, Central Norwegian Caledonides. *NGU Bulletin 412*, pp.29-42. Available at: http://www.ngu.no/filearchive/NGUPublikasjoner/Bulletin412_29-42.pdf [Accessed 3rd February 2016].

Grenne, T. et al., 1995. The sequential development of magmatic and ore-forming processes in the Fundsjo Group, Meraker district, Central Norway. *NGU Bulletin 427*, Available at: http://www.ngu.no/FileArchive/NGUPublikasjoner/Bulletin427_108-111.pdf [Accessed 3rd April 2016].

Grenne, T., Ihlen, P.M. & Vokes, F.M., 1999. Scandinavian Caledonide Metallogeny in a plate tectonic perspective. *Mineralium Deposita*, 34(5), pp.422-71. Available at: http://link.springer.com/article/10.1007/s001260050215 [Accessed 3rd February 2016].

Grenne, T. & Lagerblad, B., 1985. The Fundsjø Group, central Norway - a Lower Palaeozoic island arc sequence: geochemistry and regional implications. In D.G. Gee & B.A. Sturt, eds. *The Caledonide Orogen - Scandinavia and Related Areas. Part 2.* John Wiley & Sons. pp.743-60.

Gvein, Ø., 1976. *Sulfidmalmfeltet Hersjø V. Holtålen, Sør-Trøndelag. BV5549.* [report] Lysaker: A/S Sydvaranger Available at: http://www.ngu.no/FileArchive/BVrapporter/BV5549.pdf [Accessed 24th March 2015].

Gvein, Ø., 2010. *Røros Kobberverk*. [Online] Store Norske Leksikon Available at: https://snl.no/R%C3%B8ros_Kobberverk [Accessed 28th June 2016].

Hannington, M.D., 2014. 13.18 Volcanogenic Massive Sulfide Deposits. In H. Holland & K. Turekian, eds. *Treatise on Geochemistry*. 2nd ed. Amsterdam: Elsevier. pp.463-88.

Hardy, R.L., 1971. Multiquadric equations of topography and other irregular surfaces. *Journal of Geophysical Research*, 76(8), pp.1905-15. Available at: http://onlinelibrary.wiley.com/doi/10.1029/JB076i008p01905/epdf [Accessed 12th June 2016].

Helsel, D., 2010. Much Ado About Next to Nothing: Incorporating nondetects in science. *Annals of occupational hygiene*, 54(3), pp.257-62. Available at: http://annhyg.oxfordjournals.org/content/54/3/257.full.pdf+html [Accessed 19th April 2016].

Hessjøgruva AS, 2013. *Hessjøgruva AS*. [Online] Available at: http://hessjogruva.no/ [Accessed 19th March 2015].

Hewett, P. & Ganser, G.H., 2007. A Comparison of Several Methods for Analyzing. *The Annals of Occupational Hygiene*, 51(7), pp.611-32. Available at: http://annhyg.oxfordjournals.org/content/51/7/611.full.pdf [Accessed 19th April 2016].

Ihlen, P.M., Grenne, T. & Vokes, F.M., 1997. Metallogenic evolution of the Scandinavian Caledonides. *Transactions of the Institution of Mining and Metallurgy. Section B. Applied earth science*, 106, pp.B194-203.

Ironbark Zinc, 2013. *Citronen Zinc-Lead Project: Feasibility Study*. [Online] Ironbark Zinc Limited Available at: http://ironbark.gl/wp-content/uploads/2013/11/Citronen-Feasibility-Study.pdf [Accessed 22nd June 2016].

JORC, 2012. *The JORC Code: Australasian Code for Reporting of Exploration Results, Mineral Resources and Ore Reserves*. [Online] Australasian Joint Ore Reserves Committee (JORC) Available at: http://www.jorc.org/docs/JORC_code_2012.pdf [Accessed 27th March 2015].

Journel, A.G., 1989. Fundamentals of Geostatistics in Five Lessons. In Crawford, M.L. & Padovani, E., eds. *Short Course Presented at the 28th International Geological Congress*. Washington D.C., 1989. American Geophysical Union.

Kartverket, n.d. *Gamle Norgeskart*. [Online] Available at: http://gammel.norgeskart.no/adaptive2/default.aspx?gui=1&lang=2 [Accessed 25th June 2015].

Kolthoff, I.M. & Sandell, E.B., 1952. *Textbook of Quantitative Inorganic Analysis*. 3rd ed. New York: The Macmillan Company.

Lane/ARANZ Geo, 2013. *Leapfrog blog - Predictions at locations where there are no measurements*. [Online] Available at: http://blog.leapfrog3d.com/2013/11/19/the-connection-between-radial-basis-functions-rbfs-and-kriging/ [Accessed 10th April 2016].

Lydon, J.W., 1984. Ore Deposit Models - 8. Volcanogenic Massive Sulphide Deposits Part I: A Descriptive Model. *Geoscience Canada*, 11(4), pp.195-202. Available at: https://journals.lib.unb.ca/index.php/GC/article/view/3396/3910 [Accessed 22nd June 2016].

McLennan/ARANZ Geo, 2013. *Leapfrog Blog*. [Online] Available at: http://blog.leapfrog3d.com/2013/07/26/interpolant-functions-in-leapfrog-geo/ [Accessed 10th April 2016].

Mineralogy Database, n.d.-a. *Glossary - Metabasite*. [Online] Available at: http://www.mindat.org/glossary/metabasite [Accessed 15th April 2016].

Mineralogy Database, n.d.-b. *Glossary - Definition of nugget effect*. [Online] Available at: http://www.mindat.org/glossary/nugget_effect [Accessed 11th June 2016].

Nazarov, N.G. & Krushnyak, N.T., 2006. What is measured in qualimetry? *Measurement Techniques*, 49(3), pp.238-43. Available at: http://link.springer.com/article/10.1007/s11018-006-0097-5 [Accessed 29th June 2016].

NGU, 1980. Hersjøfeltet, Ålen. In *Teknisk Rapport nr. 45 (BVLI): Geofysikk i malmleting B. 2.* Trondheim: Bergverkenes landssammenslutnings industrigruppe. pp.313-15.

NGU, 2007. *Forekomstområde 1644-005, Hessjøgruva*. [Online] Available at: http://aps.ngu.no/pls/oradb/minres_deposit_fakta.Main?p_objid=4391&p_spraak=N [Accessed 24. april 2015].

NGU, 2008. *NGU Report 2008.064. A tectonostratigraphic transect across the central Scandinavian Caledonides, Storlien-Trondheim-Lepsøy. Part II: Excursion guide in Norway*. [report] Trondheim: NGU Available at: http://www.ngu.no/upload/publikasjoner/rapporter/2008/2008_064.pdf [Accessed 14th April 2016].

NGU, 2009. *Berggrunn*. [Online] Available at: http://geo.ngu.no/kart/berggrunn/?lang=Norsk&Box=-214586:6452754:1270610:7939800&map=Berggrunn.N250.med.lineamenter [Accessed 22. juni 2015].

NGU, 2011. *Mineral resources*. [Online] Available at: http://geo.ngu.no/kart/mineralressurser/?map=Metals%3A.Metals.Commodities&lang=English [Accessed 25. juni 2015].

Nilsen, O., 1988. The Tectonostratigraphic Setting of Stratabound Sulphide Deposits in the southern Trondheim Region, Central Norwegian Caledonides. *NGU Bulletin*, 412, pp.55-66. Available at: http://www.ngu.no/filearchive/NGUPublikasjoner/Bulletin412_55-66.pdf [Accessed 7th June 2016].

Nørsett, S., 2015. *Behov for, krav til og digitalisering av geodata som inngår i 3D-modellering av geologiske forekomster*. Trondheim: NTNU - Institutt for Geologi og Bergteknikk.

Nussir, n.d. *Nussir*. [Online] Available at: http://www.nussir.no/en_projec_ulvery.php [Accessed 30th June 2016].

Nussir, n.d. *Nussir*. [Online] Available at: http://www.nussir.no/en_projec_nussir.php [Accessed 30th June 2016].

Olsen, V., 2002. Fjellsprengningsteknikk - Boring i fjell. In A. Bruland, ed. *Kompendium i anleggsteknikk - del 1*. Trondheim: Institutt for bygg, anlegg og transport, NTNU. p.chapter II.5.

PanAust, 2014. *2014 Mineral Resource and Ore Reserve Statement*. [report] PanAust Limited Available at: http://www.panaust.com.au/sites/default/files/asx/2014%20Mineral%20Resource%20and%20Ore%20Reserve%20Statements.pdf [Accessed 15th June 2016].

Pettersen, Ø., 2011. Malmleting ved Røros Kobberverk - og litt om Hersjøfeltet. *Fjell-folk Røros*, 36, pp.36-42.

Robb, L., 2005. *Introduction to ore-forming processes*. Blackwell Publishing.

Roberts, D. & Gee, D.G., 1985. An introduction to the structure of the Scandinavian Caledonides. In D.G. Gee & B.A. Sturt, eds. *The Caledonide Orogen - Scandinavia and Related Areas, Part 1*. John Wiley & Sons. pp.55-68.

Røsholt, B. & Wilberg, R., 2001. *Exploration in Tydal area, and Fløttum Mine in Gauldal and Vingelen Mine in Tolga, Røros, Norway, BV4810*. [report] Tydal, Tolga: Bergvesenet/Crew Norway AS Available at: http://www.ngu.no/FileArchive/BVrapporter/BV4810.pdf [Accessed 8th June 2016].

Rui, I., 1990. *Hersjøfeltet. BV4151*. Trondheim: Bergvesenet/Direktoratet for Mineralforvaltning.

Schermerhorn, L.J.G., 1973. What is keratophyre? *Lithos*, 6(1), pp.1-11. Available at: http://ac.els-cdn.com/0024493773900765/1-s2.0-0024493773900765-main.pdf?_tid=f37037a8-3cfb-11e6-8687-00000aacb35d&acdnat=1467096530_0eea68c609f576b0b82f97d9abf9c255 [Accessed 4th February 2016].

Shatagin, N.N., Jafar, S. & Chekalin, B.M., 2007. Variography of Ores from the Rubtsovsk Massive-Sulfide Copper–Lead–Zinc Deposit (Altai Territory). *Moscow University Geology Bulletin*, 62(6), pp.376-82. Available at: http://link.springer.com/article/10.3103%2FS0145875207060026 [Accessed 22nd June 2016].

Singh, S.P., Ladouceur, M. & Rouhi, F., 1998. Sources, implications and control of blasthole deviation. In Singhal, R.K., ed. *Mine Planning and Equipment Selection 1998*. Calgary, 1998. A. A. Balkema.

Singsaas, P., 1975. *Turammålinger Hersjøfeltet. NGU Rapport nr. 1305.* Trondheim: Norges Geologiske Undersøkelse.

Singsaas, P., 1976. *Turammålinger Hersjøfeltet. NGU rapport nr. 1392.* Trondheim: Norges Geologiske Undersøkelse.

Singsaas, P. & Brækken, H., 1949. *Geofysisk undersøkelse 1. Hessdalen Grube 2. Storvoll Grube 3. Rogn- gruben 4. From-gruben 5. Harsjø Grube Vest.* [report] Norges Geologiske Undersøkelse: Norges Geologiske Undersøkelse Available at: http://aps.ngu.no/pls/oradb/rf.Visdok?c_dokid=0000028967 [Accessed 26th March 2015].

Slagstad, T., 2003. Geochemistry of trondhjemites and mafic rocks in the Bymarka ophiolite fragment, Trondheim, Norway: Petrogenesis and tectonic implications. *Norwegian Journal of Geology*, 83, pp.167-85. Available at: http://foreninger.uio.no/ngf/ngt/pdfs/NJG_83_167-185.pdf [Accessed 3rd February 2016].

Sletten, A., 2015. *subject heading: Ressursklassifisering.* [e-mail] Message sent from audun.sletten@gmail.com to s.norsett@gmail.com, June 17th 2016 [Accessed 30th June 2016].

SNL, 2015. *porfyritt.* [Online] Available at: https://snl.no/porfyritt [Accessed 12th November 2015].

SNL, 2016. *porfyr.* [Online] Available at: https://snl.no/porfyr [Accessed 26th June 2016].

Spragg/ARANZ Geo, 2013. *Leapfrog interpolation basics.* [Online] Available at: http://blog.leapfrog3d.com/2013/05/08/leapfrog-interpolation-basics/ [Accessed 9th April 2016].

Stephenson, P., 2005. *Resource/Reserve Reporting Standards for Minerals - Presentation to the International Accounting Standards Board in London by video link from Melbourne.* [Online] Crirsco Available at: http://www.crirsco.com/crirsco_presentation_to_iasb.pdf [Accessed 4th April 2016].

Taylor, J.K., 1987. *Quality Assurance of Chemical Measurements.* 17th ed. Boca Raton, Florida: Lewis Publishers. Available at: https://books.google.no/books?id=7NyDzQBp-b4C&printsec=frontcover#v=onepage&q&f=false [accessed 16th June 2016].

Tessem, S., 1985. *Hersjøforekomsten - Betenkning vedrørende undersøkelse of drift, BV3952.* Røros: A/S Killingdal Grubeselskap/Bergvesenet.

Trochu, F., 1993. A Contouring Program Based on Dual Kriging Interpolation. *Engineering with Computers*, 9, pp.160-77. Available at: http://download.springer.com/static/pdf/976/art%253A10.1007%252FBF01206346.pdf?originUrl=http%3A%2F%2Flink.springer.com%2Farticle%2F10.1007%2FBF01206346&token2=exp=1465894693~acl=%2Fstatic%2Fpdf%2F976%2Fart%25253A10.1007%25252FBF01206346.pdf%3ForiginUrl%3 [Accessed 14th June 2016].

USGS, 2014. *Felsic volcanic rock.* [Online] Available at: http://mrdata.usgs.gov/geology/state/sgmc-lith.php?text=felsic+volcanic+rock [Accessed 8th April 2016].

Valseth, F. & Bakken, R.E., 1974. *brev til A/S Sydvaranger.* Røros: A/S Røros Kobberverk. Letter archived at Røros Museum.

Venture X Resources, 2010. *Pilbara VMS Copper Project Robust and Profitable: Scoping Study.* [Online] Venture X Resources Limited Available at: http://www.venturexresources.com/investorrelations/Released/Pilbara%20VMS%20Scoping%20Study%20-%2026-11-10.pdf [Accessed 4th April 2016].

Vokes, F.M., 1983. *Hersjø Vest malmfelt. BV1993.* Holtålen: NTH/Killingdal Grubeselskap A/S Bergvesenet.

Zhang, Y., 2011. *Geofaculty University of Wyoming.* [Online] Available at: http://geofaculty.uwyo.edu/yzhang/files/Geosta1.pdf [Accessed 10th April 2016].